Ontwerpen van samenstellingsvariabelen en verwerkingscondities
voor gecontroleerde thermische geleiding van thermoplastische composieten

Designing the Formulation Variables and Processing Conditions
for Controlling Thermal Conductivity of Thermoplastic Composites

Tom Wieme

Promotoren: prof. dr. ing. L. Cardon, prof. dr. ir. D. R. D'hooge
Proefschrift ingediend tot het behalen van de graad van
Doctor in de industriële wetenschappen: chemie

UNIVERSITEIT
GENT

Vakgroep Materialen, Textiel en Chemische Proceskunde
Voorzitter: prof. dr. P. Kiekens
Faculteit Ingenieurswetenschappen en Architectuur
Academiejaar 2019 - 2020

ISBN 978-94-6355-346-9
NUR 971
Wettelijk depot: D/2020/10.500/23

PROMOTORS

prof. dr. ing. L. Cardon
Ghent University
Faculty of Engineering and Architecture
Department of Materials, Textiles and Chemical Engineering

prof. dr. ir. D. R. D'hooge
Ghent University
Faculty of Engineering and Architecture
Department of Materials, Textiles and Chemical Engineering

EXAMINATION COMMITTEE

Prof F. De Turck	(Chair)	Ghent University, Belgium
Prof. L. Cardon	(Promotor)	Ghent University, Belgium
Prof D. D'hooge	(Promotor)	Ghent University, Belgium
Prof. G. Pinter		Montanuniversität Leoben, Austria
Prof. M. De Paepe		Ghent University, Belgium
Prof. P. Van Steenberge		Ghent University, Belgium
Prof. P. Cornillie		Ghent University, Belgium

RESEARCH INSTITUTE

Ghent University
Department of Materials, Textiles and Chemical Engineering
Tech Lane Ghent Science Park/Campus A
Technologiepark Zwijnaarde 130
B-9052 Gent
Tom.Wieme@ugent.be

List of Publications

Full research articles included in Web of Science

T. Wieme, D. Tang, L. Delva, D.R. D'hooge, L. Cardon 'The relevance of material and processing parameters on the thermal conductivity of thermoplastic composites' *Polym. Eng. Sci.* **2018**, 58, 466 (SCI-IF 2016: 1.449; Special Issue)

L. Duan, M. Spoerk, T. Wieme, P. Cornillie, H. Xia, J. Zang, L. Cardon, D.R. D'hooge 'Designing formulation variables for extrusion-based manufacturing of carbon black conductive polymer composites for piezoresistive sensing' *Compos. Sci. Technol.* **2019** , 171, 78 (SCI-IF 2018: 6.309)

T. Wieme, L. Duan, N. Mys, L. Cardon, D.R. D'hooge 'Effect of matrix and graphite filler on thermal conductivity of industrially feasible injection molded thermoplastic composites' *Polymers* **2019**, 11, 87 (SCI-IF 2017: 2.935; invited)

T. Wieme, B. Augustyns, L. Duan, L. Cardon 'Increased through-plane thermal conductivity of injection molded thermoplastic composites by manipulation of filler orientation' *Plast. Rubber Compos* **2020** (SCI-IF 2018: 1.202)

S. Petersmann, F. Arbeiter, M. Feuchter, T. Wieme, P. Erdely, M. Spoerk 'Process-induced orientations in material extrusion-based additive manufacturing of polypropylene' (to be submitted in 2020)

Patent Applications

L. Cardon, D.R. D'hooge, T. Wieme 'Technology for conductivity' in preparation

Extended abstracts

T. Wieme, B. Augustyns, L. Duan, D.R. D'hooge, L. Cardon Increased thermal conductivity of thermoplastic composites by manipulation of filler orientation: 8th International Conference on Polymers and Moulds Innovations Guimarães, Portugal, 19-21 September **2018**, oral presentation

S. Boden, T. Wieme, M. Erkoç, L. Cardon Thermal behaviour of hydrid injection moulds for short production series 8th International Conference on Polymers and Moulds Innovations Guimarães, Portugal, 19-21 September, **2018**, oral presentation

N. Mys, L. Delva, M. Kuzmanovic, T. Wieme, K. Ragaert Functional evaluation of compatibilization systems for recycled PP-PET blends 8th International Conference on Polymers and Moulds Innovations Guimarães, Portugal, 19-21 September, **2018**, oral presentation

J. Schalnat, A. Krairi, T. Wieme, W. Van Paepegem Experimental characterization of thermoplastics for use in heat exchangers ICEM 2018, Brussels, Belgium, 1 July-7July, **2018** oral presentation

Abstracts

L. Duan, M. Spoerk, T. Wieme, P. Cornillie, H. Xia, J. Zang, L. Cardon, D.R. Dhooge Morphology control of thermoplastic polyurethane-olefin block copolymer-carbon black blends for enhanced piezoresistive sensing at both low and high strains Spring ACS National Meeting & Exposition; Florida, USA, 31-4 March - April, **2019** oral presentation

W. Van De Steene, S. Boden, T. Wieme, L. Cardon Experimental and numerical optimization of processing parameters for hybrid injection moulds International SimaTec User meeting 2019, Essen, Germany, 25-26 March, **2019** oral presentation

Expression of gratitude

Around the same time that I started my PhD here at CPMT, I've decided to buy an old-timer car as a full rebuild project. Admittedly, there seems to be a lot of similarities between this rebuild-project and my PhD. Both are projects that are impossible to do completely on your own, so I have plenty of people to thank.

I'd like to thank my promotor, prof. Ludwig Cardon, and co-promotor, prof. Dagmar D'hooge, for steering me and my PhD in the right direction, while still giving me the freedom to explore new and unfamiliar roads. I really appreciate the opportunities you've given me, sharing your enthusiasm for some of my ideas and the fact that you always had me covered when I put myself in a tricky situation. Thank you for your valuable feedback, patience and providing me with the equipment I needed.

A great share of my gratitude goes towards the incredibly fine-tuned engine that is the CPMT research group. I'd like to thank Karen, Laurens, Maja, Nicolas, Sara, Willem, Lingyan, Veerle, Mustafa, Kurt, Marcel and prof. Kim Ragaert for welcoming and accepting me to be part of the group. Furthermore, I'd like to thank Astrid, Andrea, Daniel, Dahang, Ellen, Flavio, Gianni, Ellen, Martin, Ruben, Rudinei, Stefaan, Sisi, Amir, Kerstin, Ruben, Marie and Tom, whom all of which became vital parts of this well-oiled machine. A special thanks goes to Willem, for sharing my pain on the bumpy road towards the end of a PhD.

As a long road might get monotonous after a while, turning on the radio having a passenger to talk to helps to smoothen the ride. That is why I'd like to thank Lingyan Duan, Nicolas Mys, Martin Spörk, Ellen Fernandez and Tom Van Waelegem for sharing the office with me. I'm incredibly grateful for always having someone around to talk to and, from time to time, sing along with.

EXPRESSION OF GRATITUDE

A special word of gratitude should be directed to the people who make sure that the engine keeps on running. Thank you, Mustafa Erkoç, Stefaan Van Biervliet and Marcel Moerman, for showing me all kinds of tips and tricks on how to tame the machinery I worked with, and helping me out when I was stranded along an empty road with a broken car. An incredible amount of gratitude towards Veerle as well, for helping me out with the paper work and administrative tasks that I showed up with, sometimes later than I should.

I'd like to thank Kurt Van Houtte, who somehow managed to provide me with almost any spare part I needed during my journey. If not in stock, he was always happy to make it out of thin air with a little help of a 3D printer.

Though often discouraged to use in large quantities to avoid damage, it is a well-known fact that adding octane booster can significantly improve car performance. Thank you, prof. Kim Ragaert, for providing me with sometime harsh but certainly valuable feedback. It helped both me and my scientific work to be boosted to a higher and hopefully respectable level.

Often forgotten or underestimated is the chemistry that goes into a car. Without the right fuel, oil, coolant and what not, a car is sure to break down in no-time. Hence, I'd like to show my deepest appreciation towards Maarten Delahaye, Nicolas Mys, Rudinei Fiorio and Laurens Delva for their help in the last chapter on chemical functionalization of the carbon nanotubes. Without your help and insights, I'd never gotten this far.

I'd like to thank everyone in the Compohex project for providing a frame to work on. I hope that I've shown to be an added value to the project, despites my fair share mistakes. I'd like to acknowledge VLAIO SBO for their financial support on the

Compohex project. A special thanks to Joanna Schalnat, for supplying me with sufficient snacks along the road, and making sure that I took a coffee break from time to time.

I'd like to thank the member of the examination committee; prof. F. De Turck, prof. G. Pinter, prof. M. De Paepe, prof. P. Van Steenberge and prof. P. Cornillie. Thanks to their close inspection and valuable feedback on my thesis, I was able to polish it so it can shine when it's ready to hit the roads.

A good cooling is a necessity for a car, to prevent is from overheating. For that, I'd like to thank all my friends for their support and helping me cool down in the weekends, take my mind of the sometimes frustrating topic of thermal conductivity. More specifically, I'd like to thank 'de grasmaaierclub', my close group of friends who took me on adventures that were even more random and exciting than our name. Furthermore, I'd like to thank everyone from the scouts Zingem, as they've been part of my life since I was only six. My friends from my years as a student, both in chemistry as in engineering, deserve a thank you as well, for helping me struggle through those sometimes rough years.

Finally, I'd like to thank my family for their constant support and unconditional love. Thank you Bart, Wouter and Leentje for being amazing siblings, and thank you for picking wonderful family in law to further brighten up our family events. A special thanks goes to my mom and dad. Even though they often admitted not understanding what it exactly was I was doing, they'd always showed interest and support. As any old-timer would soon turn into scrap without shelter, I'd like to thank you for providing me with it for years. Last but not least, I'd like to add a child seat to my car, for the cutest niece anyone can imagine. Welcome to the family, Eleonoor.

With this, I’d like to invite you to join along on this road trip through the vast lands of thermal conductivity. Buckle up, sit back and enjoy the ride.

Abstract

Improving the thermal conductivity of polymers could open a vast new market in heat management application, replacing the often heavy, expensive and corrosion vulnerable metals currently used. Increasing thermal conductivity of polymer composites has been a topic of research since the late 70's that showed revival in recent years. This PhD research reviews previous work on this subject, investigating the effect of filler type, shape and dispersion and their effect on the thermal conductivity of the final composite. This doctoral research focused strongly on the industrial feasibility. Current research focuses a lot on the lab-scale synthesis, with mixing and shaping techniques that are considerably less economically scalable, such as solvent mixing, compression molding and film casting. Conventional techniques, such as melt blending, extrusion and injection molding, can introduce extra complexities such as low dispersion and, most importantly, anisotropic properties. Measuring these anisotropic properties requires adapted equipment and failing to do so can often lead to wrong conclusions. Further research focuses on (semi)industrially-scaled implications of thermal conductivity. Transient plane source was employed as measurement device, as it is capable of measuring both in-plane and through-plane thermal conductivity in anisotropic samples.

Injection molding is generally considered the best option for manufacturing complex shapes in large quantities. Hence, this processing technique was employed for sample production. Different previous established theories were tested on a larger scale, closer to the industry rather than lab work. Graphite was chosen as a thermal conductive filler, due to the relatively high aspect ratio and good thermal conductivity and low price. Commercially available polymers were chosen as matrix material. First of all, the importance of the probing depth and the related skin-core effect, e.g. the

difference in filler orientation between the sample core and (near) surface, was highlighted. As the orientation of the fillers change deeper in the sample, the thermal conductivity changes accordingly. A representative measurement thus required to measure to half the sample thickness, or through the whole sample thickness. The effect of average molar mass on the thermal conductivity of the matrix was investigated but proved not to be relevant when comparing two commercial grade polystyrenes. While semi-crystalline polymers generally show higher thermal conductivity, increasing the crystallinity of a polymer does little to nothing that could prove industrially relevant to improve the thermal conductivity. The effect of moisture on the thermal conductivity, relevant for different practical applications, was found to be negligible as well. The thermal conductivity in the plane of the polymer proved a much higher value than through the plane. This is caused by the skin-core effect, where fillers orientated with the flow direction near the edges, and show a more random pattern towards the core of the sample. Cutting away the skin layers can drastically improve the through-plane thermal conductivity of an injection molded sample. In a last comparison, a graphite nanofiller was compared with the macro-sized filler. Comparison of these results showed a better TC for the macro-filler, but as mentioned before, the shape of the nanofiller was different than that of the macro-filler, making it hard to draw a straightforward conclusion.

The through-plane thermal conductivity is in many cases the important value to achieve better thermal management. However, due to the skin-core effect, the in-plane value is mostly dominant. Two economically easily applicable methods were addressed: the use of a foaming agent and the use of a two-phase polymer matrix. The filler in both cases was macro-scale graphite, the matrix used with the foaming agent was polyamide while the two-phase matrix consisted of 7-3 polypropylene-polyethylenterephthalat. The graphite was mixed in the two-phase matrix at a

temperature lower than that of the PET melting point to avoid the graphite migrating to the PET phase. A compatibilizer was added to control the size of the PET particles. Thermal conductivity measurements for the foaming agents showed an increase in through-plane thermal conductivity in exchange for a decreased in-plane thermal conductivity. SEM images confirmed the effect of the foaming agent disrupting the in-plane alignment of the thermal conductive filler. The two phase composite showed an increased through-plane thermal conductivity as well, but the mechanism was rather unclear. Strength of both composites decreased, as trapped air, weak interfaces and graphite as filler have no positive effect on mechanical properties.

Carbon nanotubes outperform nearly all materials when it comes to thermal conductivity, with a single-walled carbon nanotube achieving up to 2500 W m^{-1} K^{-1}. However, once embedded in a composite, a lot of these extraordinary properties are lost. Four different pathways were explored on the possibility to polymerize carbon nanotubes, in an effort to extrapolate the superior properties to macro scale. Polyurethane-based and epoxy based synthesis paths showed little result so far. The Bakelite doped with phenol produced a black solid mass, though it is possible the nanotubes are dispersed in the Bakelite matrix rather than part of the actual chemical structure. The second route in the polyamide-based material yielded a small, fiber-like sample. Unlike all the reactants involved in the synthesis, the reaction product was not dissolvable or dispersible in water nor ethanol. Besides that, the material was formed on the phase separation of the solvents of the reactants and, after drying, was capable of supporting its own weight; leading to the conclusion that the formed fiber is very likely the intended polymerized carbon nanotube. TGA analysis proved to be unreliable as analysis of identical materials showed large variations. DSC analysis showed unreliable results as well, due to the evaporation of the solvent during the scan. FTIR samples were pressed, but heavy contamination from an unknown source

overshadowed the spectra of the nanotubes. Improved analysis methods should further prove previous claims. More functionalization of the carbon nanotubes should improve dispersibility and reactivity, resulting in larger quantities of what could prove to be a valuable material for demanding, high-tech applications.

Samenvatting

Een verhoogde thermische geleidbaarheid van polymeren heeft veel potentieel om de huidige dure, zware en corrosiegevoelige metalen te vervangen in warmte-dispersie applicaties. Onderzoek naar thermische geleidbaarheid van polymeren dateert van de late jaren ’70, met recentelijk een oplevende interesse. Dit doctoraatsonderzoek bundelt eerder onderzoek naar het onderwerp met nadruk op onder andere het effect van type, vorm en dispersie van vulstoffen en hun effect op thermische geleidbaarheid van het composiet. In dit doctoraatsonderzoek werd vooral gekeken naar industriële relevantie. Huidig onderzoek focust zich vaak op labo-schaal testen en maakt gebruik van technieken die economisch moeilijk schaalbaar zijn, zoals mengen met behulp van solvent, vormpersen en filmgieten. Conventionele technieken zoals extrusie en spuitgieten kunnen extra complexiteiten zoals zwakke dispersie en, meer belangrijk, anisotropie introduceren in de resulterende materialen. Het meten van deze eigenschappen vereist aangepast apparatuur. Bij het gebruik van onaangepast apparatuur kan dit tot verkeerde conclusies leiden. Verder onderzoek legde nadruk op (semi)-industrieel gevormde teststukken en de invloed op warmtegeleiding. *Transient Plane Source* werd aangewend als meetmethode, gezien deze techniek in staat is zowel in het vlak als door het vlak de warmtegeleiding te bepalen van anisotrope specimina.

Spuitgieten wordt algemeen gezien als de beste optie voor het maken van complexe(re) vormen in grote hoeveelheden. Vandaar dat deze techniek werd aangewend voor het maken van de testspecimina. Verschillende eerder bestudeerde theorieën omtrent thermische geleiding werden opnieuw bekeken vanuit industriële productieschaal. Grafiet werd gekozen als thermisch geleidende vulstof omwille van de aspectratio, hoge thermische geleiding en relatief lage prijs. Verschillende

commercieel beschikbare polymeren werden als matrixmateriaal aangewend. Als eerste werd het belang van *probing depth*, gelinkt met het *skin core*-effect, uitgediept en verklaard. Gezien de orientatie van de vulstoffen afhangt van de diepte waarop gekeken wordt, zal ook de thermische geleiding variabel zijn met de opgemeten diepte. Een representatieve meting vereist dus een *probing depth* van de helft van het sample, of het volledige sample. Twee gelijkaardige polymeren met verschillende gemiddelde molaire massa werden vergeleken met elkaar op vlak van thermische geleiding, waaruit geconcludeerd kon worden dat het verschil niet relevant is. Semi-kristallijne polymeren vertonen over het algemeen een hogere thermische geleiding, maar het verhogen van de kristalliniteit van een polymeer op een industrieel haalbare manier toonde weinig effect te hebben op de warmtegeleiding. Eveneens bleek het effect van vocht op thermische geleiding, relevant voor verschillende praktische applicaties, verwaarloosbaar voor het geteste polymeer. De thermische geleidbaarheid van de composieten toonde een hogere geleiding in het vlak dan door het vlak. Dit wordt veroorzaakt door het *skin-core*-effect waarbij de vulstoffen zich aan de rand met de vloei gaan oriënteren, terwijl deze meer in het midden van het materiaal willekeuriger georiënteerd zullen zijn. Het wegnemen van deze toplaag kan de warmtegeleiding door het vlak van een spuitgietstuk drastisch verhogen. Als laatste werd ook gekeken naar koolstof nanovulstoffen vergeleken met macrovulstoffen. Een betere geleiding werd vastgesteld voor de macro-vulstoffen, maar zoals vermeld was de vorm van de nanovulstoffen anders dan die van de macrovulstof, waardoor een direct vergelijking moeilijk wordt.

In vele gevallen is de thermische geleiding door het vlak heen de belangrijkste waarde om betere prestaties bij warmteafvoer te verkrijgen. Door het skin-core effect is de waarde in het vlak steeds dominant. Twee industrieel gemakkelijk implementeerbare methoden werden bekeken: het gebruik van een schuimstof en het gebruik van een

twee fasen polymeermatrix. In beide gevallen was de vulstof een macro-grafiet. De matrix die gebruikt werd in combinatie met de schuimstof was een polyamide. De matrix van het twee-fasen systeem was een 7-3 verhouding van polypropyleen en polyethyleentereftalaat. In dit tweefasensysteem werd het grafiet tussen de matrix ingemengd op een temperatuur lager dan het smeltpunt van PET, om te voorkomen dat het grafiet zou migreren naar de PET fase. Een compatibilizer werd toegevoegd om de grootte van de PET partikels te controleren. Metingen op thermische geleidbaarheid bij de composieten met schuimvormer toonden een verhoogde thermische geleidbaarheid door het vlak, met een daling in het vlak. Microscoopbeelden konden bevestigen dat de schuimvormer de oriëntatie van de vulstoffen in het vlak kon tegengaan. Het composiet van het twee-fasen systeem toonde ook een verhoogde thermische geleidbaarheid door het vlak, maar het mechanisme was onduidelijk. De sterke van beide composieten daalde echter, gezien ingesloten lucht, zwakke interactie tussen twee fasen of grafiet als vulstof geen positieve effecten hebben op de mechanische eigenschappen.

Koolstof nanobuisjes zijn het summum van thermische geleidbaarheid, met waarden zo hoog als 2500 W m^{-1} K^{-1} voor een single-wall carbon nanotube. Echter, eens deze verwerkt worden tot een composiet gaan veel van de uitzonderlijke eigenschappen verloren. Vier verschillende manieren werden bekeken met als einddoel het polymeriseren van carbon nanotubes, met het idee de nano-eigenschappen naar macroschaal te krijgen. Polyurethaan en epoxy-gebaseerde methoden toonden weinig potentieel op dit moment. Uit de Bakeliet-methode, in aanwezigheid van fenol, werd een zwarte, vaste massa verkregen. De mogelijkheid bestaat echter dat het eerder gaat om nanotubes gedispergeerd in een Bakeliet-matrix, in plaats van de nanotubes die onderdeel uitmaken van de chemische structuur zelf. De polyamide-methode resulteerde in een klein, vezelachtige structuur. In tegenstelling tot alle reactanten

betrokken in de synthese was de vezel niet oplosbaar of dispergeerbaar in water of ethanol. Het product werd gevormd op de fasescheiding van de solventen waarin de reactanten verbleven en was na drogen sterk genoeg om zichtzelf te ondersteunen. Hieruit kan geconcludeerd worden dat het verkregen product hoogst waarschijnlijk het beoogde carbon nanotube polymeer is. Thermogravimetrische analyse bleek onbetrouwbaar voor de tussenproducten; verschillende testen op hetzelfde materiaal toonden sterk uiteenlopende resultaten. DSC toonde ook weinig betrouwbare data, dit door het verdampen van het solvent tijdens de meting. Plaatjes voor FTIR werden gemaakt met koolstof nanotubes uit verschillende reactiestappen. Echter, zware contaminatie van een onbekende bron overschaduwde het spectrum waardoor interpretatie moeilijk werd. Verdere analyse moet eerder gemaakte claims nog bewijzen. Een sterkere chemische functionalisering van de carbon nanotubes kan de dispersie en reactiviteit vermoedelijk verhogen. Dit kan resulteren in grotere hoeveelheden van wat mogelijks een waardevol materiaal kan zijn voor veeleisende high-tech toepassingen.

List of Symbols

Roman symbols

-C=O	Carbonyl group
-COOH	Carboxyl group
-OH	Hydroxyl group
C	Heat capacity per volume unit (MJ $m^{-3}K^{-1}$)
d_p	Probing depth (mm)
$D(\tau)$	Dimensionless time dependant function used in the TPS calculations
m%	Mass Percentage
vol%	Volume Percentage

Greek symbols

A	Temperature coefficient of resistivity
κ	Thermal diffusivity (m^2 s^{-1})
ΔH_{m}	Melt enthalpy (J g^{-1})
ΔH_{cc}	Cold crystallization enthalpy (J g^{-1})
$\Delta H_{\mathrm{m}}^{0}$	Theoretical melt enthalpy of 100% crystalline material (J g^{-1})

λ	Thermal conductivity (W $m^{-1}K^{-1}$)
Θ	Characteristic time (s)
x_c	Crystallinity of thepolymer (%)
δ	Thickness of insulating layer of a TPS sensor (μm)

Abbreviations

ABS	Acrylonitrile Butadiene Styrene
APTES	(3-aminopropyl)trioxysilane
AR	Aspect Ratio
ASTM	American Society for Testing and Materials
CNT	Carbon Nanotube
DBTDL	Dibutyltin dilaurate
DSC	Differential Scanning Calorimetry
FA	Foaming Agent
FTIR	Fourier-transform infrared spectroscopy
FWCNT	Few-walled carbon nanotubes
GNP	Graphene Nano Platelets
HATU	1-[Bis(dimethylamino)methylene]-1H-1,2,3-triazolo[4,5-b]pyridinium 3-oxide hexafluorophosphate; Hexafluorophosphate Azabenzotriazole Tetramethyl Uronium

hBN	Hexagonal Boron Nitride
HDPE	High Density Polyethylene
HVAC	Heating, Ventilation and Air Conditioning
ISO	International Organization for Standardization
LFA	Laser Flash Analysis
MDI	4,4’ Methylenebis(phenylisocyanate)
MWCNT	Multi-walled carbon nanotubes
N.A.	Nucleating Agent
PA6	Polyamide 6
PA6,6	Polyamide 6,6
PEEK	Polyetheretherketone
PET	Polyethylene Terephtalate
PLA	Polylactic Acid
PMMA	Poly(methyl metacrylate)
PP	Polypropylene
PPgMA	Polypropylene grafted with maleic anhydride
PS	Polystyrene
PUR	Polyurethane
PVC	Poly(vinyl chloride)
PVDF	Poly(vinylidene difluoride)

SEM	Scanning Electron Microscopy
SWCNT	Single-walled carbon nanotubes
TC	Thermal Conductivity
TGA	Thermogravimetric analysis
THF	Tetrahydrofuran
TPS	Transient Plane Source

TABLE OF CONTENTS

Chapter 1

The relevance of material and processing parameters on the thermal conductivity of thermoplastic composites: state-of-the-art, challenges and scope

1. 1. Introduction

Thermoplastic composites show great promise as an alternative for thermal management applications in the scope of the development of next-generation electronics and heat exchangers. Their low cost, reduced weight and corrosion resistance make them an attractive replacement for traditionally used metals, in case their thermal conductivity (TC) can be sufficiently increased by designing the material (*e.g.* filler type and shape) and processing (*e.g.* dispersion quality, mixing, and shaping) parameters. In the present contribution, the relevance of both type of parameters is discussed and guidelines are formulated for future research to increase the TC of thermoplastic polymer composites.

1. 2. State of the art

As electronics are becoming faster and smaller, the efficient transfer of waste heat becomes an important aspect to ensure a good performance and a longer lifetime. Lightweight, cheap, thermal conductive and electrical insulating polymer composites seem to be a promising material group for to resolve this challenge. In addition, manufacturers of *e.g.* heat exchangers for cars, heating, ventilation and air

conditioning (HVAC), and desalination are interested in a better chemical resistance and fouling resistance [1] and have highlighted a higher degree of freedom for the design of polymeric composite materials compared to traditionally used metals. The wide variety of available polymers offers the opportunity to select the (co)polymer (blend) with chemical and physical properties suiting the intended application. However, these polymers require a far more improved thermal conductivity (TC) in order to truly compete with metals. Table 1 shows the TC of several metals used in current heat exchangers which are clearly higher than the TC values for popular commodity and engineering plastics. Fortunately, the TC of polymeric materials can be increased by adding fillers with a high intrinsic TC. It should be stressed that TC is an anisotropic property, meaning that the TC of a material can depend on the direction in which it is measured. Hexagonal Boron Nitride (hBN), for example, consists of stacked sheets, each sheet being built of covalently bonded boron and nitrogen atoms in a hexagonal shape, resembling the structure of graphite. The TC in the plane of a sheet possesses a value of 600 W $m^{-1}K^{-1}$, while the through-plane value is 20 times lower [2]. Composites containing fillers with a high aspect ratio (AR), *i.e.* the ratio of the length of the filler to its cross-sectional diameter, can also have anisotropic properties if these fillers are not efficiently distributed. Figure 1 represents a section of an injection moulded sample containing fibrous fillers. Intuitively it can be understood that these fillers will mainly show orientation in the direction of the flow during the processing step, *i.e.* the flow direction. Perpendicular to the flow direction, through the thickness of the specimen, the through-plane or normal direction is defined. The direction perpendicular to both the flow and through-plane direction is known as the transverse direction [3]. The in-plane direction can be defined as the combination of the transverse and flow direction.

Table 1: TC of metals used in heat exchangers and TC of different polymers; room temperature. Polymers are considered to be homogenous.

Metal	**TC (W m^{-1} K^{-1})**
Aluminium	247 [4]
Copper	483 [4]
Titanium	19 [5]
Stainless steel 410	22 [5]
Alloy 600	15 [6]
Alloy 800	12 [6]
Hastelloy C	13 [5]
Polymer	**TC (W m^{-1} K^{-1})**
High density polyethylene (HDPE)	0,45-0,52 [7]
Polypropylene (PP)	0,14 [7]
Polystyrene (PS)	0,14 [7]
Polymethylmethacrylate (PMMA)	0,25 [7]
Nylon-6.6 (PA6,6)	0,25 [7]
Polyetheretherketone (PEEK)	0,25 [7]
Polyvinyl chloride (PVC)	0.17 [7]

Currently, main focus has been on the effect of the nature of the polymer matrix and the filler type, the filler shape, and filler quantity on the composite TC [1], [4], [7]–[11]. Hence, the relevance of the material properties as such has been the key research angle. However, limited focus has been put on their interplay with the processing

parameters, such as the differences induced by going from compression moulding to injection moulding processing. In the present work, first, a concise overview is given on the TC measuring techniques and the state-of-the-art related to the relation between the material properties and the TC. Next it is elaborated in detail how the processing method allows to further regulate the TC of the composites.

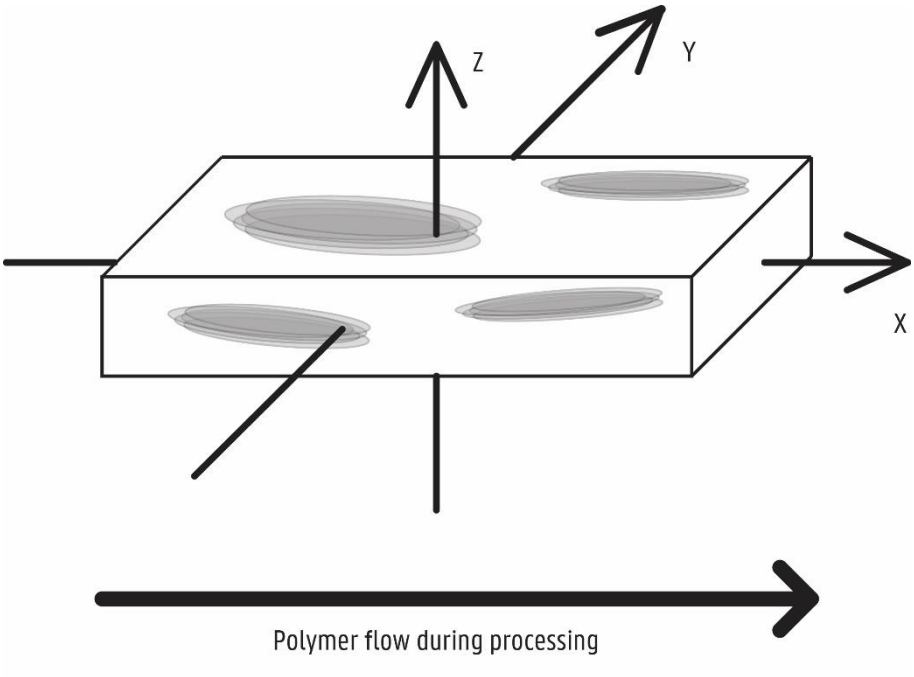

Figure 1: Different directions of a composite with plate-like fillers. The X arrow represents the direction of polymer flow during processing and thus the main direction of filler orientation, which is also known as the flow direction. The Z arrow represents the direction through the thickness of the specimen, better known as the through-plane direction. The Y arrow represents the direction perpendicular on the in-plane and through-plane direction and is referred to as the transverse direction.

1. 3. Measuring and predicting thermal conductivity

It should be emphasized that care should be taken with respect to the method of TC measurement. Some measurement methods tend to produce unreliable results upon their use to characterize anisotropic materials. TC measurement methods such as the Heat Flow Meter [12] and the Hot Wire [13] are not designed to measure the TCs of anisotropic materials and can reproduce results that are not representative. While Laser Flash Apparatus [14] (LFA) and Guarded Heat Flow [15] measure the through-plane TC rather than average (mean value of different direction) TC, the ASTM standards concluded that researchers should measure and interpret these results with care upon testing anisotropic materials. Recommended, as explained in Appendix A, is the use of the Transient Plane Source [16] method, standardized by ISO [17] for plastics, homogenous and anisotropic materials. The Transient Plane Source method is also able to measure the bulk, in-plane and through-plane TC. Important is that samples are placed and measured correctly to avoid in-plane TC being confused with through-plane TC and vice versa.

Numerous theoretical models exist for predicting the TC of a polymer-based composite material [18]. These theoretical models are yet not fully representative, since they assume for instance a continuous interface between the matrix and the filler, and a constant shape, size and spatial distribution of the filler material, or strongly depend on the orientation of the filler [18]. Higher filler loadings will result in a higher TC, but these loadings can pose a problem for processing [19] and the strength of the final composite [20], [21]. To better mathematically describe these aspects, an improved understanding of the relevance of the material and processing properties is thus needed, as covered in the next sections.

1. 4. Relevance of material properties

Since polymer materials have no free electrons, the heat is transported as phonons which can be seen as thermal energy waves moving in a lattice configuration [22]. An elaborate and detailed explanation on the mechanism of thermal conductivity has been described in-depth by Burger et al. [11]. From a certain amount of filler onwards, an "endless" interconnected network of filler is formed in the composite, which is called the percolation threshold. Unlike with electrical conductivity of polymer composites, the TC will not show a sharp increase at this point. From this point on however, the TC of the composite will start increasing more rapidly, since all the extra fillers added will thicken the existing network, easing the transport of heat waves [23]. But even upon blending in fillers, the resulting TC of the composite will still be low.

The main contributor to this behaviour is the interfacial resistance within the composite. This results in a weak transfer of heat flow due to different phonon spectra of the matrix and filler, with additionally a weak contact at the interfaces causing the phonons to scatter back [24]. Even above the percolation threshold and thus high filler loadings, the TC of the composite will come nowhere near the value of the pure filler [25]–[27]. This is because the particles that do have direct contact with one another interact only with weak dispersion forces, *i.e.* van der Waals forces and the small contact area between the filler particles also increases contact resistance [24]. For example, a single carbon nanotube is praised for its (theoretical) incredible TC of around 5800 W m^{-1} K^{-1} or even more, while a mat of several entangled nanotubes - shows a TC of no more than 35 W m^{-1} K^{-1} [18], [19].

1. 4. 1. Filler types

Popular fillers used for improving TC are the electrical conductive Carbon Nanotubes (CNTs), flake graphite, carbon fibres, and metal fillers like copper, silver, gold, and others. Since electrical conductivity is not allowed in electronic packaging, electrical insulating fillers with a high TC are applied. Boron Nitride (BN), Aluminium Nitride (AlN), Silicon Carbide (SiC) and some oxidized metals that can be used as fillers for electronic packaging purposes. For industrial scale applications, cost is always an important parameter. For this reason, different forms of graphite seem the best candidates for applications that allow electrical conductivity as well. Besides the cost, other factors like weight, corrosion resistance and aesthetics should also be considered when selecting the appropriate filler. BN could be considered as filler where the inherent black colour of graphite-based composite would be less desirable. A more in-depth discussion on thermal conductive fillers can be found in other papers [1], [4], [7], [8].

1. 4. 2. Filler shapes

It should be pointed out that the shape and size of fillers can have a more significant influence on the TC of the composite than the type of filler. While metals are sometimes described as bad fillers due to low TC of their composites compared with other fillers [28], it should be noted that in most of the reported experiments, the metals were powders, likely more or less spherical shaped, thus possessing a low AR. Nikhil et al. [29] showed that composites with gold nanofibers can display a TC of 5 W $m^{-1}K^{-1}$, even at filler amounts as low as 3 m%. Park et al. [30] indicated that by changing the shape of copper from sphere-like to flake-like an increase in TC can be noticed as well.

Bigg et al. [31] concluded in their study that spherical or isotropic irregular high TC fillers do not perform better once the TC of the filler reaches a value, which exceeds a factor 100 the TC of the matrix. For example, a spherical filler with a TC of 50 W $m^{-1} K^{-1}$ performs as well as a spherical filler with TC of 100 W $m^{-1} K^{-1}$ if the TC of the matrix is 0.5 W $m^{-1} K^{-1}$ or lower. This is however not the case for fillers with a higher aspect ratio, where the composite TC will increase with increasing TC of the filler material. In the same study, Bigg et al. [31] concluded that the increase in the composite TC with sphere-like fillers is limited to about 20 times the conductivity of the unfilled polymer. Since that would put a low limit on the maximum TC of thermoplastic-based composites, it is recommended to use fillers with a higher AR.

A large AR also means that less filler will be needed to form an endlessly interconnected filler network, resulting in a higher TC at lower loading levels. As explained further, orientation of the filler due to processing can destroy this percolation network. It is generally accepted that larger particles result in better TC, since they have less matrix-filler interfaces thus less thermal interfacial resistance [32]–[35]. Some researchers found a higher TC for smaller particles, ascribing this to the ability of small particles being able to form better networks [22], [36]. On the other hand, Burger et al. [11] claim that this improved thermal conductive network does not make up for the extra thermal interfaces created by the many small filler particles. Besides that it is non-trivial to compare different results, since next to the filler size plenty of other factors also have their influence on TC. Even the making of smaller filler particles could change the AR, the general shape or the surface chemistry depending on the method. This makes it challenging even to compare some results from the same study.

More generally accepted is that soft filler particles perform better than rigid ones, since deformation of these particles allows a larger contact area between the particles [37]. This explains why talc, possessing a low intrinsic TC (10 W $m^{-1} K^{-1}$ in-plane, 1.8 W $m^{-1} K^{-1}$ through-plane), still can achieve 2.5 W $m^{-1} K^{-1}$ in a polypropylene (PP)-talc 30 vol% blend [28].

1. 5. Relevance of processing parameters

The processing parameters for producing thermal conductive composites can have a huge effect on the TC which can be, as previously mentioned, an anisotropic property. In this section, the effect of different mixing and shaping methods on the TC is discussed. The most important parameters for TC affected by mixing and further processing are the dispersion quality of the filler in the matrix, which is influenced by the presence of compatibilizers or coupling agents, and the final orientation of the filler after all processing steps. Special focus is also on the relevance of disruptive alignment.

1. 5. 1. Dispersion quality

Dispersion quality as defined on the scale of the filler is a difficult subject when it comes to TC. Figure 2 shows three different cases, all with the same ‘amount’ of thermal conductive filler (grey) in a non-thermal conductive matrix (white). Case A is characterized by a ‘perfect’ dispersion, case B shows some dispersion characteristics but with a tendency to form agglomerates, while case C has a low dispersion quality with big clusters of filler and large gaps in between. In these examples, case B will most likely show the best TC in all directions. The semi-agglomeration creates a path for phonons to travel far distances in an unhindered manner. While the perfectly dispersed case might have a path with less distance to

cover in the non-conductive matrix, it has far more interfaces to cross. This high number of interfaces might be a bigger obstacle for thermal transport than the little extra distance the phonons have to travel in an insulating matrix, making case B a better thermal conductor than A, despites being less dispersed. In case C, the gaps of non-conductive matrix between the filler agglomerations are too large to obtain a good TC. It should be kept in mind that this is a simplified explanation, since the intensity of the above trend can also depend on the thermal interfacial resistance, the contact resistance between fillers, the TC of the matrix itself and other factors. This reasoning is comparable with the reasoning why larger particles perform better than small particles at the same filler amount.

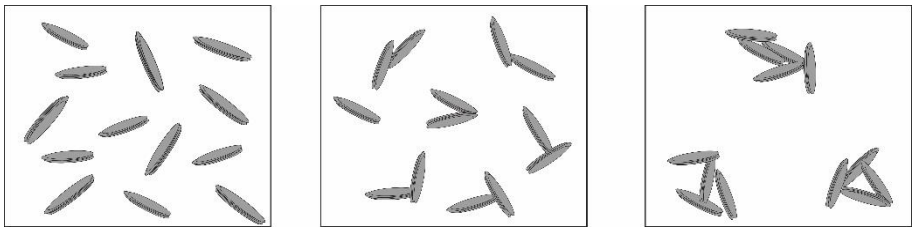

Figure 2: A composite with high-AR fillers. Case A shows well dispersed fillers, case B is less well dispersed and case C has the worst dispersion and most agglomeration; case B has the highest potential to achieve a high TC.

The orientation of fillers is more straightforward to explain. Flow in a molten polymer or polymer solution causes the filler to orientate. Figure 3 shows the filler distribution before and after such orientation. The TC will increase in the direction of the filler orientation, while the TC in the other directions will drop. It is clear that the thermal conductive path in the filler orientation direction has improved while the paths in the other directions have worsened, since it has more interfaces to cross and longer travel distances in the non-conductive matrix.

It is important to realize that compatibilizers or coupling agents can improve the interaction between the filler and the matrix and can increase the dispersion quality of the filler. Since thermal interfacial resistance is a main cause for low TC, the use of compatibilizers and coupling agents seem to be a solution to improve the TC. The main advantage of coupling agents and compatibilizers is that the TC of the composite can be increased without increasing the filler volume. Several publications have confirmed that compatibilizers in combination with an epoxy [38] or a thermoplastic [33], [39]–[41] matrix increase the composite TC values. On the other hand, severe chemical reactions of filler materials, such as oxidation of CNTs, can damage the surface causing a lower TC of the filler [42]. This can result in a lower composite TC despite a better matrix-filler interaction.

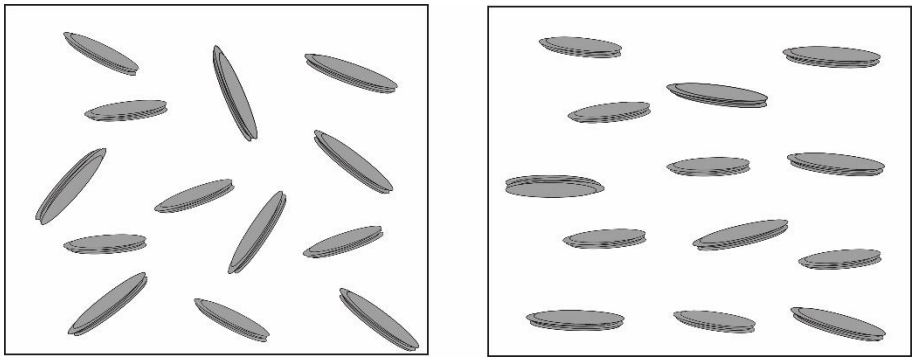

Figure 3: Composite with high-AR filler. Case A shows the composite before processing (or processing that cause little polymer flow), case B is after processing in which polymer flow has occurred. Fillers align in the flow direction, resulting in an anisotropic material and show improved TC in this flow direction. The sample before processing will have isotropic properties.

Zhang et al. [40] tested the effect of compatibilizers on the TC of injection moulded high density polyethylene (HDPE) with Al_2O_3 fibres as filler. The in-plane TC of the composites with compatibilizer was higher than the in-plane TC of the composite without compatibilizer. In contrast, the through-plane values of composites with

compatibilizer were lower than the through-plane conductivity of the composite without compatibilizers. All the in-plane TC values were higher than the through-plane TC values. The general trend of higher in-plane values can be explained by the filler being orientated in the flow-direction, resulting in a higher in-plane conductivity. Scanning electron microscopy (SEM) showed a better adhesion between matrix and filler upon using compatibilizers, which should normally improve TC. However, due to the strong matrix-filler adhesion with compatibilizers, the fillers showed even more orientation in the injection direction. The composite without coupling agent also showed alignment in the injection direction, but less explicit than the composite with compatibilizers. These phenomena can explain the increase in in-plane conductivity and decrease in through-plane conductivity with compatibilizers. Due to the orientation phenomena of the filler, the effect of better interfacial contact between filler and matrix on TC cannot be exploited.

Ha et al. [41] pointed out that an improved dispersion quality can have a negative effect on TC in case additional interaction processes are active. These authors combined Graphene Nano Platelets (GNPs) with regular and carboxyl-CNT. The composite TC with surface-treated CNTs was lower than that of the composite with the regular CNTs. Regular CNTs form thermal conductive bridges between the different GNPs, increasing the TC of the composite. However, the functionalized CNTs show more attraction to the matrix and will be better dispersed, thus not forming a bridge between the other fillers. The damage to the nanotubes because of the functionalization process might also play part in the TC lowering. This bridge-formation effect is seen in many combinations of CNTs with a second filler [43]–[47] and shows great promise for improving the TC of polymer composites. The CNTs also seem to be severely less effected by polymer flow, thus show less orientation in the flow direction after processing [46].

1. 5. 2. Mixing

In order to obtain a uniformly dispersed composite compound, the matrix and filler material need to be well-mixed. The most commonly used mixing techniques in research laboratories are explained in this subsection. A differentiation can be made between melt, solution, and a powder mixing.

In a melt mixing process, the polymer is heated above its melting temperature and mixed with the filler material due to shear in the mixing equipment [48]. Melt mixing is the preferred mixing method in industry because of its cost efficiency and low environmental impact [49]. Commonly used machines for melt mixing in industry are extruders and compounders, which are available in different shapes and sizes. The material can be extruded in filaments and granulated to use for further processing [50], [51]. Alternatively, the molten material can directly be extruded in tubes or plates [52]. Many researchers combine the use of 'batch' melt mixers (instead of extrusion) followed by granulation for further processing [23], [50], [51]. This allows a longer mixing time, thus an increase of the dispersion quality of the filler. Melt mixing has some drawbacks, despites being the most commonly used industrial mixing method. Because of the increase in dynamic viscosity, the amount of filler that can be blended in is limited. Fillers with high AR and irregular shapes cause more shear than sphere-shaped fillers, making it harder to blend in higher amounts of fillers with a high AR. Compared with other mixing techniques, melt mixing performs rather poor on the dispersion quality of filler; especially with nano-fillers. After melt mixing, these nano-scaled fillers show strong agglomerated bundles rather than being well dispersed (*cf.* case C in Figure 2). Large fillers will likely be damaged and shortened after the extrusion process due to the shear forces [53].

In contrast, in solution mixing a solvent is added to the polymer to lower the dynamic viscosity and is stirred until the polymer is completely dissolved. The filler material can be directly added in the polymer solution or dispersed separately in the solvent before being added to the polymer solution. Ultrasound treatment can be used to improve the dispersion quality by breaking agglomeration of small filler particles [48], [54]. The solution is then cast out on a surface and the solvent is evaporated mostly by increased temperature or reduced pressure, leaving behind a composite film. Alternatively, the composite can be precipitated by adding a non-solvent to the polymer solution [46], [55]. As with melt mixing, the precipitated composite can be used in further processing steps. Composite films can be left intact, stacked for compression moulding or granulated for extrusion, injection moulding or compression moulding. Compared with melt mixing, solution compounding shows excellent dispersion quality and leaves the fillers undamaged since there are no excessive shear forces. Despite that this technique can drastically reduce agglomeration of fillers, it is overall less favourable in industry because of the environmental impact, higher costs and health risks [23], [49].

Finally, powder mixing or dry mixing [22], [56] is the mixing of filler and polymer at temperatures lower than the melting point of the polymer. This results in extremely weak dispersions. Equipment like a ball mill can improve contact between filler and polymer. Despite this inherent poor dispersion, creative use of these techniques can provide quite good results by changing the shape of the filler, which as explained above allows to alter the TC [30]. Too long mixing times result however in too small particles and a lower TC [30].

1. 5. 3. Shaping

After the mixing step, the composite compound requires a finishing step to give it the desired shape. The processing technique used in this step will mainly determine the final filler alignment, thus anisotropy of the material. Processing methods involving a high shear intensity, such as injection moulding and extrusion, can although possibly damage (shorten) the filler [57], [58]. In what follows, the key characteristics of shaping via compression moulding, solution casting, injection moulding, pultrusion, extrusion, and 3D-printing are discussed.

In compression moulding, a mould is filled with polymer-based materials, combined with other materials if desired. This model has commonly a disc or plate-shaped shape for property test samples. The mould is heated up above the melting point of the polymer matrix and closed under increased pressure for a few minutes to several hours. The mould can be filled with granules of a pre-mixed composite [2], [59], solution-cast films [60], [61] or even ‘sandwich’ structures of alternately polymer layers and fibres or other materials [62], [63]. Fibres can be aligned in a controlled manner to improve the materials properties in the desired directions. Though compression moulding is widely used by researchers, it is less seen on an industrial scale due to long processing times, non-consistent quality, limited freedom in part design, and in some cases requirement of manual labour [64]. If a powder mixture is compression moulded, the resulting product will remain heterogeneous, showing filler-rich and filler-poor regions. This can be useful for creating controlled thermal conductive pathways in the composite [56]. Large polymeric particles can be covered with a thin layer of thermal conductive filler, resulting in good conductive pathways after compression moulding. This process is sketched in Figure 4. However, the resulting material will likely show very low strength and will break easily around the

filler-rich zones. When pellets of a pre-mixed composite are used in compression moulding, it will likely result in a sample with isotropic properties. This is because that during the compression moulding process, there is little to no flow of the molten matrix, thus no significant orientation of fillers, resulting in an isotropic material.

Cast films obtained from solution mixing after solvent evaporation can be used to test material characteristics [36], [43]. Besides that the cast film will hardly have any practical applications without further processing. As explained above, the film casting process is too polluting and hard to scale-up for profitable industrial mass production. Film blowing or film extrusion are preferred for industrial scale film production. Note also that characteristics of the same composite can be significantly different when processed via another method. Fibre size, for instance, can be significantly reduced by processing via extrusion or injection [50], [65] while film casting leaves the fibres/filler untouched.

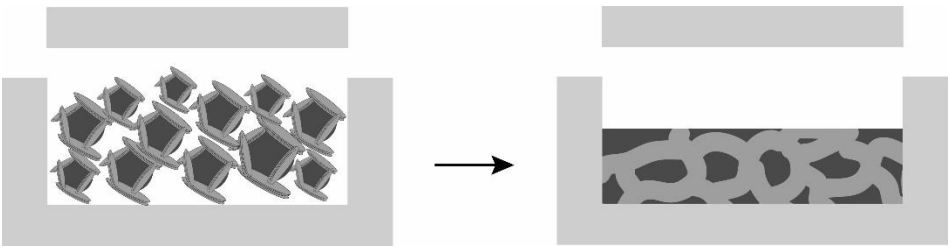

Figure 4: By 'coating' the surface or by using powder mixtures instead of well dispersed fillers, thick thermal conductive paths can remain after compression molding.

Injection moulding is a widely used and popular method for shaping polymers and thus also for the production of composite materials. At a first approximation it follows that the fillers align with the flow direction during the injection. Because of this, samples produced by injection moulding will generally show a much higher through-plane TC than in-plane conductivity [27], [40], [46]. Changing parameters of the

injection moulding process can however influence the filler orientation [66], likely also changing the TC of the composite. Note that because of the increased TC cycle times can be reduced since the parts will cool faster. On the other hand, this might have a negative impact on other factors such as crystallinity [67]. Injection moulding of a composite can 'break' an existing thermal conductive network achieved by blending filler and matrix, as shown in Figure 5 (still assuming the alignment hypothesis). The random orientated fillers before injection moulding (A) form a percolation network throughout the whole sample. After processing, fillers align in the flow direction and break the through-plane percolation network (B), though the in-plane network might end up better. This mostly results in a better in-plane TC and a worse through-plane TC. The reality, however, is more complicated. Depending on the type of polymer used, design of the part, amount of fillers and processing parameters, filler alignment cannot be complete. The 'skin-core model', *i.e.* a model developed for specific fibre-reinforced polymers, shows that fibres close to the wall will have orientation in the flow direction, while the core has fibres orientated perpendicular with the flow direction (transverse direction) or a more random orientation [66], [68], [69]. Manipulating the orientation of these fibres will likely change the TC as well, though it is yet to be investigated how significant the impact will be.

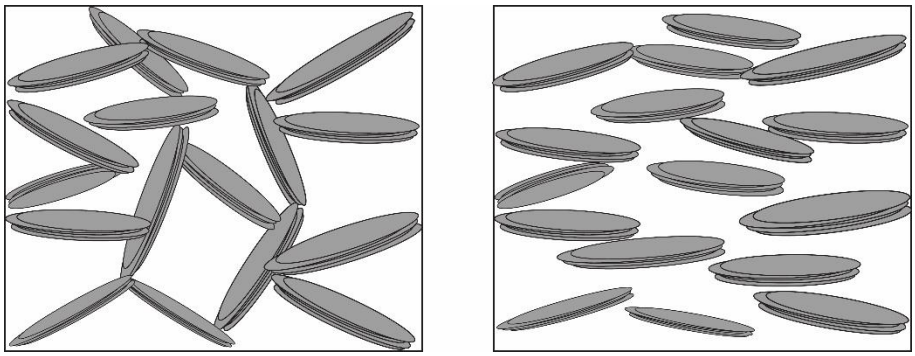

Figure 5: Simplified version of filler orientation before and after injection moulding. The through-plane conductivity will drop as the percolation network is broken.

To further highlight the difference between the above discussed processing methods specific focus is put on the work of Takahashi et al. [70] who clearly demonstrated that the mixing and processing methods have a severe impact on the through-plane TC. These authors made composites of BN (plate-like shape) and PP. One sample was prepared by melt mixing followed by injection moulding, the second sample was prepared by solution mixing followed by compression moulding. As seen in Figure 6, the sample prepared by melt mixing and compression moulding showed overall a higher TC. This is mainly because of the filler orientation caused by the injection moulding process.

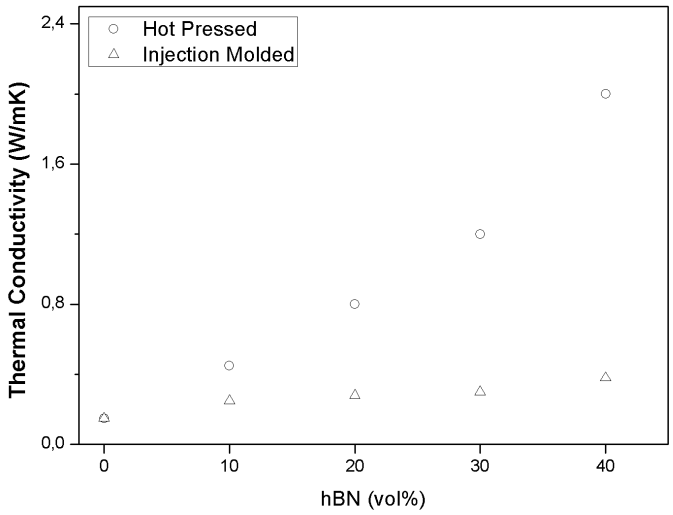

Figure 6: TC of BN-filled PP by melt mixing/compression moulding and by solution/mixing injection moulding [70]

Furthermore, extrusion is widely used in industry for the production of polymer sheets, pipes, films, and other continuous profiles. Because of the flow and shear, fillers will align in the direction of the extrusion, resulting in a high in-plane TC and lower through-plane conductivity [24]. Due to shear in the melting step, large fillers particles could however break. Much like extrusion, pultrusion also allows the production of continuous profiles, but reinforced with continuous fibres. Although as almost no experiments have been performed with this technique for thermal conductive composites it can be expected that using thermal conductive continue reinforced fibres, such as carbon fibres, will result in a profile with excellent in-plane thermal performances but a rather low through-plane TC. Note that the combination of thermal conductive fibres with thermal conductive composite matrices could be interesting to investigate.

Related to conventional extrusion is also extrusion-based 3D-printing. Despite that there has been few to no research activities on the improved thermal conductivity of

3D printed parts, this recent emerged technique could be of value for producing subcomponents for *e.g.* heat exchangers. A thermal conductive polymeric composite with a (continuous) carbon fibre reinforcement could be printed in order to achieve a good TC. Besides the possibility of making complex shapes without requiring an expensive mould, printing patterns could be adjusted to improve the conductivity in a certain direction. Figure 7 shows two different theoretical printing patterns. The light line is a continuous fibre reinforcement and shows the path of the print head. It is clear that, on the condition that the fibre is a thermal conductive material such as a carbon fibre, the printing pattern can adjust the direction of high TC. The first figure will have an improved TC in the vertical direction while the second figure will show a higher TC in the horizontal direction. It is worthwhile in the future to investigate the actual TC improvement, the strength and other properties of 3D printed materials and whether this production method could be industrial applicable.

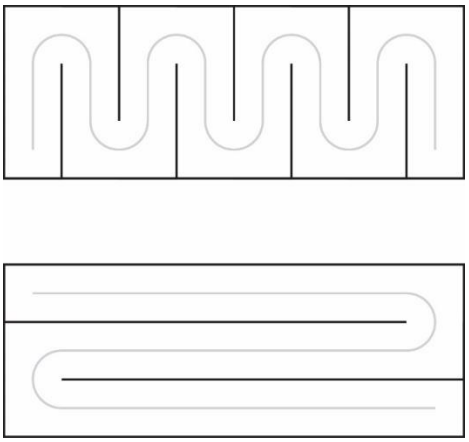

Figure 7: How the printing pattern of 3D printed parts can influence the direction of high thermal conductivity.

It should be further reminded that industry prefers the use of melt-mixing equipment and injection-moulding or extrusion for processing polymeric materials. Researchers

focusing on lab-scale production typically prefer solution mixing and/or compression moulding with long residence times, generally resulting in higher TC values. These long processing times are not economically feasible, thus results should be interpreted with care when planning on upscaling or applying on industrial processes.

1. 5. 4. Disrupting alignment

Some applications require a high through-plane TC rather than a high in-plane TC. As fillers are mostly oriented in the in-plane direction after injection moulding or extrusion, disrupting this alignment can increase the through-plane TC at a cost of the in-plane TC. For example, Tian et al. [71] suggest the combination of sphere-like aluminium (Al) fillers to disrupt the in-plane alignment of the graphite nanoplatelets for the use in thin thermal interface materials. Combining 4.5 m% graphite nanoplatelets with 44.5 m% Al resulted in a TC of 2.5 W m^{-1} K^{-1}, while only 4.5 m% graphite nanoplatelets or 44.5 m% Al resulted in a TC of respectively 0.6 and 0.5 W m^{-1} K^{-1}. Furthermore, Yuan et al. [72] and Lin et al. [73] tried to change the alignment of hBN in an epoxy matrix by coating the BN with ferromagnetic nanoparticles and applying a magnetic field. Despite the increase of the through-plane TC of this technique, it is doubtful whether this would work for thermoplastic matrices. The high dynamic viscosity of the matrix would likely prevent the fillers from aligning with the magnetic field, considering the dynamic viscosity of the uncured epoxy system with 20 m% BN filler was already too high to align the platelets [73].

In addition, Xu et al. [74] successfully increased the through-plane TC of injection moulded flake-graphite filled polyamide 6 (PA6) in combination with PP. Since PP and PA6 are immiscible, the PP formed droplets in the PA6 matrix. These droplets slightly changed the orientation of the flake-shaped filler in the matrix. Too large

droplets will separate the flakes, preventing a dense thermal conductive network. Too small droplets on the other hand will have no effect on the filler orientation. The size of the droplets could be controlled by the compatibilizer concentration. The optimal result was gained by adding 1 m% compatibilizer to a 50 mt% PA6 matrix with 20 m% PP and 30 m% flake graphite composite, resulting in a through-plane TC of 2.703 W/mK. The TC of only PA6 with 30 m% flake graphite was 2.03 W m^{-1} K^{-1} and the TC of PA6, PP, and flake graphite without compatibilizer was 2.23 W m^{-1} K^{-1}. However, it should be noted that these through plane values, compared with other literature using the same amount of fillers, is exceptionally high, indicating that some sort of error might have occurred.

It can be concluded that any further advancement in filler orientation techniques could mean a big step forward in producing high through-plane thermal conductive composites [72]. A few techniques have been tested on experimental scale, such as magnetic alignment in thermosets and the use of foaming agents, but their industrial applicability for thermoplastics remains questionable [53], [72] or is yet to be tested on TC [75].

1. 6. Conclusions

This section thoroughly reviews the current state-of-the-art in the field of thermal conductivity of thermoplastic composites. Particular emphasis was put on the material design (*e.g.* filler type and shape), the material anisotropy and its relation to conventional processing (*e.g.* dispersion quality, mixing and shaping).

Related to measuring the thermal conductivity of composites, it should be stressed that not all techniques are recommended for anisotropic materials. Besides that, it is important to notice that the bulk thermal conductivity of an anisotropic material has

no relevance. In-plane and through-plane values should rather be measured and it should be clearly indicated whether the value given is an in-plane or through-plane value.

Since spherical fillers show little to no promise in significantly increasing the TC of thermoplastics, sufficiently large fillers with a high aspect ratio (AR) are recommended. Besides that fillers with a high AR require a lower loading level to achieve at least the percolation threshold.

The mixing during the processing step can also have a significant influence on the composite TC, as it determines the dispersion quality and the (an)isotropic behaviour. A perfect dispersion is not always desirable because of the increased number of matrix-filler interfaces which can cause a drop in TC. Close and dense packs of fillers are also not recommended because of the large distance in the non-conductive matrix that has to be crossed. Ideally, a relatively unhindered network of thermal conductive filler should thus be formed throughout the matrix. Further processing or shaping can cause anisotropy, where the composite will show a higher TC in the direction of the flow because of the filler orientation with in the limit even a destruction of the percolation network.

In many cases, heat sinks for electronics and others can be designed in such a manner that the heat flow has the same direction as the orientation of the fibres, thus leading to a high in-plane TC. On the other hand, subcomponents for tube or plate-based heat exchangers require a high through-plane TC. Higher through-plane conductivity with extrusion or injection moulding can be achieved by disrupting the alignment of fillers. Adding spherical fillers or adding an immiscible second polymer aides this process. Other techniques have been being tested but currently show little potential for being adapted on an industrial scale. It is clear that more research activities are required in

order to achieve high through-plane TC values for injection moulding and extrusion applications. On the other hand, the combination of the regular thermal conductive fillers like graphite or BN with CNTs seems already promising as CNTs are less affected by the flow orientation. Furthermore, compression moulding shows a high through-plane TC since fillers do not display orientation but this technique is unfortunately less industrially attractive.

Coupling agents and compatibilizers can increase the TC by reducing the thermal interfacial resistance and by increasing the dispersion quality of the filler. On the other hand, very pronounced dispersions can decrease the overall TC by breaking thermal conductive bridges and the chemical bonding process of the coupling agent can reduce the TC of the filler itself. For injection and extrusion applications, the in-plane TC can increase due to a better filler orientation, while the through-plane TC is expected to decrease.

Overall it can be concluded that there are still uncertainties when it comes to unambiguously quantifying the TC of composites. This is because of the numerous factors influencing the TC, often depending on one another. This makes it very tedious to study one aspect without unintentionally changing another parameter. While high in-plane values are already achievable, the improvement of through-plane TC after injection moulding or extrusion needs more attention in future research.

1. 7. Scope

In this doctoral research, the goals are to understand the relation between polymer material/processing parameters and TC and specifically to increase the TC of thermoplastic composites for use in heat management applications by optimizing these parameters. A literature survey has been first conducted (see Section 1.1), covering subjects less debated in other recent review papers, such as the effect of processing conditions for the production of and the anisotropy in thermal conductive composites. The effect of filler types, shapes and the dispersion of fillers correlated with the dispersion techniques has been discussed, as well as possible methods to counter the effect of filler orientation. This literature review has been published in 'Polymer Engineering and Science' upon invitation.

As significant research had already been performed concerning the effect of fillers on TC of composites, it has been chosen to first dive deeper into the effect of (commercial) polymer matrices using a certain filler. This can be useful for future applications, as heat exchangers and heatsinks subjected to different conditions might require better suitable matrix materials. As heat exchangers and/or electronics heat sinks can be heavily subjected to moisture, the effect of moisture has been analysed. The effect of other properties of commercially available polymers such as average molar mass and crystallinity on the TC has been investigated as well. These findings can be found in Chapter 2: entitled "Effect of Matrix and Graphite Filler on Thermal Conductivity of Industrially Feasible Injection Moulded Thermoplastic Composites", as published in the journal 'Polymers' also upon invitation.

As explained in Section 1.1, a noticeable increase in through-plane TC requires significant amounts of thermal conductive fillers. Besides potentially increasing the cost of the composite material, high amounts of fillers typically decrease the ease of

processing. Therefore, Chapter 3 focuses on increasing the through-plane TC of composites with low filler loading. Two methods have been tested: (i) the use of a matrix consisting of two phases, and (ii) the use of a foaming agent in the last step of the processing. Both methods are shown to increase the through-plane TC, while the in-plane TC decreases. The content of Chapter 3 is currently under revision for publication as a Special Issue contribution in the journal 'Plastics, Rubber and Composites' and is entitled 'Increased through-plane thermal conductivity of injection moulded thermoplastic composites by manipulation of filler orientation'.

In the next chapter (Chapter 4) focus is on a more special filler type, namely carbon nanotubes. These materials are often praised for their high thermal TC and other outstanding macroscopic properties. Though often used in composites with the intention of increasing thermal properties, performances are not exceptionally good and often problems arise related to processing. Hence, it has been attempted in this chapter to synthesise a "polymer" consisting of repeating carbon nanotubes as "monomer". Through doubtful whether the thermal performance would come close to that of a single nanotube, the potential of this material in other applications and the possibility to fine-tune properties made this worth investigating none the less. Out of the literature survey, several pathways for chemical synthesis have been proposed and explored. The synthesis methods and current preliminary results are included in Chapter 4.

As measuring TC brings along quite some complications relating to anisotropy and sample preparation, the appendix of this doctoral research (Appendix A) covers issues related to that. The measurement technique used during this doctoral research, 'transient plane source (TPS)', is discussed both theoretically and practically.

Figure 8 shows the overview of the researches conducted on the subject of TC of thermoplastics in this doctoral research alongside the discussion above. Currently, a potential patent application is also being prepared on the subject of TC, more precisely the control of composite material properties and processing methods in view of enhanced TC. Due to confidentially the research results associated with the patent are not included in the PhD work.

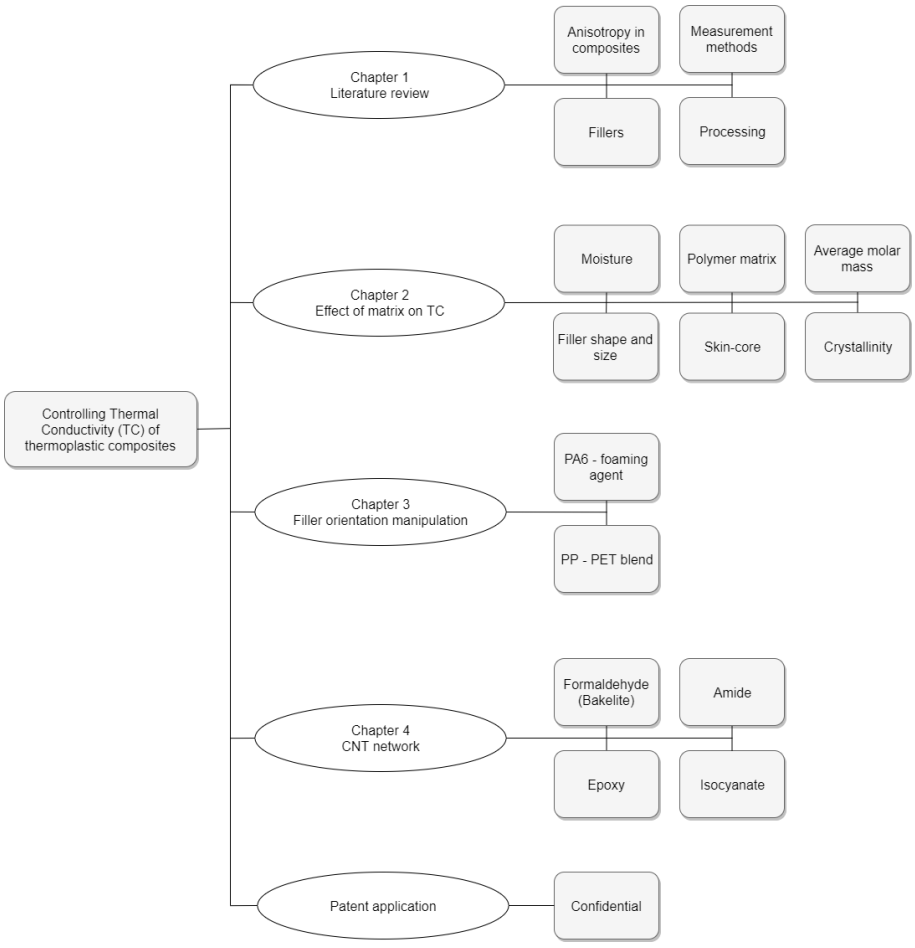

Figure 8: Overview of the research performed in this doctoral research concerning the thermal conductivity (TC) of thermoplastic composites. Appendix A covers the details on the measurement technique and Chapter 5 the conclusions and future outlook.

It should be further put forward that the present doctoral dissertation must be seen in the context of a more technical PhD thesis in line with the targeted PhD degree. Multidisciplinary research is conducted including the engineering research domains of polymer processing and technology and mechanical engineering but also the science fields of polymer and organic chemistry.

REFERENCES

[1] M. A. Vadivelu, C. R. Kumar, and G. M. Joshi, “Polymer composites for thermal management: a review,” *Compos. Interfaces*, vol. 6440, no. August, pp. 1–26, 2016.

[2] S. Ghaffari Mosanenzadeh and H. E. Naguib, “Effect of filler arrangement and networking of hexagonal boron nitride on the conductivity of new thermal management polymeric composites,” *Compos. Part B Eng.*, vol. 85, pp. 24–30, 2016.

[3] H. Y. Ng, X. Lu, and S. K. Lau, “Thermal conductivity of boron nitride-filled thermoplastics: Effect of filler characteristics and composite processing conditions,” *Polym. Compos.*, vol. 26, no. 6, pp. 778–790, 2005.

[4] A. R. J. Hussain, A. A. Alahyari, S. A. Eastman, C. Thibaud-Erkey, S. Johnston, and M. J. Sobkowicz, “Review of polymers for heat exchanger applications: Factors concerning thermal conductivity,” *Appl. Therm. Eng.*, vol. 113, pp. 1118–1127, 2017.

[5] J. R. Couper, W. R. Penney, J. R. Fair, and S. M. Walas, “Heat Transfer and Heat Exchangers,” *Chem. Process Equip. (Second Ed.*, no. c, pp. 159–218, 2010.

[6] P. Rodriguez, P. Rodriguez, and I. Gandhi, “Selection of Materials for Heat Exchangers,” *Heb*, vol. 97, 1997.

[7] X. Huang, P. Jiang, and T. Tanaka, “A review of dielectric polymer composites with high thermal conductivity,” *IEEE Electr. Insul. Mag.*, vol. 27, no. 4, pp. 8–16, 2011.

[8] H. Chen *et al.*, “Thermal conductivity of polymer-based composites: Fundamentals and applications,” *Prog. Polym. Sci.*, vol. 59, pp. 41–85, 2015.

[9] C. T. Joen, Y. Park, Q. Wang, A. Sommers, X. Han, and A. Jacobi, “A review on polymer heat exchangers for HVAC & R applications ` re pour les applications Echangeurs de chaleur en polyme dans le chauffage , la ventilation , le conditionnement d ’ air et le ´ tat de l ’ art froid : e,” *Int. J. Refrig.*, vol. 32, no. 5, pp. 763–779, 2009.

[10] X. Chen, Y. Su, D. Reay, and S. Riffat, “Recent research developments in polymer heat exchangers - A review,” *Renew. Sustain. Energy Rev.*, vol. 60, pp. 1367–1386, 2016.

[11] N. Burger, A. Laachachi, M. Ferriol, M. Lutz, V. Toniazzo, and D. Ruch, “Review of thermal conductivity in composites: Mechanisms, parameters and theory,” *Prog. Polym. Sci.*, vol. 61, pp. 1–28, 2016.

[12] ASTM, “Standard Test Method for Steady-State Thermal Transmission Properties by Means of the Heat Flow Meter Apparatus Title,” *ASTM C518-15*, 2015. [Online]. Available: https://www.astm.org/Standards/C518.htm.

[13] ASTM, “Standard Test Method for Thermal Conductivity of Refractories by Hot Wire (Platinum Resistance Thermometer Technique),” *ASTM C1113/C1113M*, 2013. [Online]. Available: https://www.astm.org/Standards/C1113.htm.

[14] ASTM, “Standard Test Method for Thermal Diffusivity by the Flash Method,” *ASTM E1461-16*, 2013. [Online]. Available: https://www.astm.org/Standards/E1461.htm.

[15] ASTM, “Standard Test Method for Evaluating the Resistance to Thermal

Transmission of Materials by the Guarded Heat Flow Meter Technique," *ASTM E1530-11*, 2016. [Online]. Available: https://www.astm.org/Standards/E1530.htm.

[16] S. E. Gustafsson, "Transient plane source techniques for thermal conductivity and thermal diffusivity measurements of solid materials," *Rev. Sci. Instrum.*, vol. 62, no. 3, pp. 797–804, 1991.

[17] International Organization for Standardization, "Plastics — Determination of thermal conductivity and thermal diffusivity — Part 2: Transient plane heat source (hot disc) method," *ISO 22007-2*, 2015. [Online]. Available: http://www.iso.org/iso/catalogue_detail.htm?csnumber=61190.

[18] D. M. BIGG, "thermal conductivity of heterophase polymer compositions," in *Thermal and electrical conductivity of polymer materials*, vol. 119, Heidelberger Platz 3, W-1000 Berlin 33: Springer-Verlagen Berlin, 1995, pp. 1–30.

[19] P. R. Hornsby, "Rheology, compounding and processing of filled thermoplastics," in *MINERAL FILLERS IN THERMOPLASTICS I*, vol. 139, Heidelberger Platz 3, D-14197 Berlin: Springer-Verlag Berlin, 1999, pp. 155–217.

[20] N. S. Enikolopyan and I. O. Stalnova, "Filled Polymers : Mechanical Properties and Processability," *Adv. Polym. Sci.*, vol. 96, pp. 1–67, 1990.

[21] K. Uetani, S. Ata, S. Tomonoh, T. Yamada, M. Yumura, and K. Hata, "Elastomeric thermal interface materials with high through-plane thermal conductivity from carbon fiber fillers vertically aligned by electrostatic flocking," *Adv. Mater.*, vol. 26, no. 33, pp. 5857–5862, 2014.

[22] W. Zhou, C. Wang, T. Ai, K. Wu, F. Zhao, and H. Gu, "A novel fiber-reinforced polyethylene composite with added silicon nitride particles for enhanced thermal conductivity," *Compos. Part A Appl. Sci. Manuf.*, vol. 40, no. 6–7, pp. 830–836, 2009.

[23] H. Wu, C. Lu, W. Zhang, and X. Zhang, "Preparation of low-density polyethylene/low-temperature expandable graphite composites with high thermal conductivity by an in situ expansion melt blending process," *Mater. Des.*, vol. 52, pp. 621–629, 2013.

[24] S. Ghose, K. A. Watson, D. C. Working, J. W. Connell, J. G. Smith, and Y. P. Sun, "Thermal conductivity of ethylene vinyl acetate copolymer/nanofiller blends," *Compos. Sci. Technol.*, vol. 68, no. 7–8, pp. 1843–1853, 2008.

[25] W. Yu, Y. Qi, Y. Zhou, L. Chen, H. Du, and H. Xie, "Synergistic improvement of thermal transport properties for thermoplastic composites containing mixed alumina and graphene fillers," *J. Appl. Polym. Sci.*, vol. 43242, pp. 1–5, 2015.

[26] D. L. Gaxiola, J. M. Keith, J. A. King, and B. A. Johnson, "Nielsen Thermal Conductivity Model for Single Filler Carbon/Polypropylene Composites," *J. Appl. Polym. Sci.*, vol. 114, no. 5, pp. 3261–3267, Dec. 2009.

[27] M. G. Miller, J. M. Keith, J. A. King, B. J. Edwards, N. Klinkenberg, and D. A. Schiraldi, "Measuring thermal conductivities of anisotropic synthetic graphite-liquid crystal polymer composites," *Polym. Compos.*, vol. 27, no. 4, pp. 388–394, Aug. 2006.

[28] B. Weidenfeller, M. Höfer, and F. R. Schilling, "Thermal conductivity, thermal diffusivity, and specific heat capacity of particle filled polypropylene," *Compos. Part A Appl. Sci. Manuf.*, vol. 35, no. 4, pp. 423–429, 2004.

[29] N. Balachander *et al.*, "Nanowire-filled polymer composites with ultrahigh thermal conductivity," *Appl. Phys. Lett.*, vol. 102, no. 9, 2013.

[30] H. J. Park, A. Badakhsh, I. T. Im, M.-S. Kim, and C. W. Park, "Experimental study on the thermal and mechanical properties of MWCNT/polymer and Cu/polymer composites," *Appl. Therm. Eng.*, vol. 107, pp. 907–917, 2016.

[31] D. M. BIGG, "thermally conductive polymer compositions," *Polym. Compos.*, vol. 7, no. 3, pp. 125–140, Jun. 1986.

[32] J.-Z. Liang, "Thermal conductivity of PP/Al(OH)3/Mg(OH)2 composites," *Compos. Part B Eng.*, vol. 44, no. 1, pp. 248–252, 2013.

[33] G. W. Lee, M. Park, J. Kim, J. I. Lee, and H. G. Yoon, "Enhanced thermal conductivity of polymer composites filled with hybrid filler," *Compos. Part A Appl. Sci. Manuf.*, vol. 37, no. 5, pp. 727–734, 2006.

[34] H. Wu and L. T. Drzal, "High Thermally Conductive Graphite Nanoplatelet/Polyetherimide Composite by Precoating: Effect of Percolation and Particle Size," *Polym. Compos.*, vol. 34, no. 12, pp. 2148–2153, 2013.

[35] T.-L. Li and S. L.-C. Hsu, "Enhanced thermal conductivity of polyimide films via a hybrid of micro-and nano-sized boron nitride," *J. Phys. Chem. B*, vol. 114, no. 20, pp. 6825–6829, 2010.

[36] M. O. Khan, "Thermally Conductive Polymer Composites for Electronic Packaging Applications Applications," *J. Appl. Polym. Sci.*, vol. 65, pp. 2733–2738, 2012.

[37] R. F. Hill and P. H. Supancic, "Thermal Conductivity of Platelet-Filled Polymer Composites," *J. Am. Ceram. Soc.*, vol. 85, no. 4, pp. 851–857, 2002.

[38] Y. Xu, D. D. L. Chung, and C. Mroz, "Thermally conducting aluminum nitride polymer-matrix composites," *Compos. - Part A Appl. Sci. Manuf.*, vol. 32, no. 12, pp. 1749–1757, 2001.

[39] J. Gu, Q. Zhang, J. Dang, J. Zhang, and Z. Yang, "Thermal conductivity and mechanical properties of aluminum nitride filled linear low-density polyethylene composites," *Polym. Eng. Sci.*, vol. 49, no. 5, pp. 1030–1034, 2009.

[40] S. Zhang, Y. Ke, X. Cao, Y. Ma, and F. Wang, "Effect of Al2O3 fibers on the thermal conductivity and mechanical properties of high density polyethylene with the absence and presence of compatibilizer," *J. Appl. Polym. Sci.*, vol. 124, no. 6, pp. 4874–4881, Jun. 2012.

[41] S. M. Ha *et al.*, "Thermally conductive polyamide 6/carbon filler composites based on a hybrid filler system," *Sci. Technol. Adv. Mater.*, vol. 16, no. 6, p. 065001, 2015.

[42] J. G. Park *et al.*, "Thermal conductivity of MWCNT/epoxy composites: The effects of length, alignment and functionalization," *Carbon N. Y.*, vol. 50, no. 6, pp. 2083–2090, 2012.

[43] S. Kumar *et al.*, "Dynamic synergy of graphitic nanoplatelets and multi-walled carbon nanotubes in polyetherimide nanocomposites.," *Nanotechnology*, vol. 21, no. 10, p. 105702, 2010.

[44] K. T. S. Kong, M. Mariatti, A. A. Rashid, and J. J. C. Busfield, "Enhanced conductivity behavior of polydimethylsiloxane (PDMS) hybrid composites containing exfoliated graphite nanoplatelets and carbon nanotubes," *Compos. Part B Eng.*, vol. 58, pp. 457–462, 2014.

[45] A. Yu, P. Ramesh, X. Sun, E. Bekyarova, M. E. Itkis, and R. C. Haddon, "Enhanced thermal conductivity in a hybrid graphite nanoplatelet - Carbon nanotube filler for epoxy composites," *Adv. Mater.*, vol. 20, no. 24, pp. 4740–

4744, 2008.

[46] I. Mazov, I. Burmistrov, I. Il'Inykh, A. Stepashkin, D. Kuznetsov, and J. P. Issi, "Anisotropic thermal conductivity of polypropylene composites filled with carbon fibers and multiwall carbon nanotubes," *Polym. Compos.*, vol. 36, no. 11, pp. 1951–1957, 2015.

[47] S. Kumar *et al.*, "Study on mechanical, morphological and electrical properties of carbon nanofiber/polyetherimide composites," *Mater. Sci. Eng. B Solid-State Mater. Adv. Technol.*, vol. 141, no. 1–2, pp. 61–70, 2007.

[48] Z. Han and A. Fina, "Thermal conductivity of carbon nanotubes and their polymer nanocomposites: A review," *Prog. Polym. Sci.*, vol. 36, no. 7, pp. 914–944, 2011.

[49] R. Sengupta, M. Bhattacharya, S. Bandyopadhyay, and A. K. Bhowmick, "A review on the mechanical and electrical properties of graphite and modified graphite reinforced polymer composites," *Prog. Polym. Sci.*, vol. 36, no. 5, pp. 638–670, 2011.

[50] S. M. Lebedev and O. S. Gefle, "Evaluation of electric, morphological and thermal properties of thermally conductive polymer composites," *Appl. Therm. Eng.*, vol. 91, pp. 875–882, 2015.

[51] Z. Antar, J. F. Feller, H. Noël, P. Glouannec, and K. Elleuch, "Thermoelectric behaviour of melt processed carbon nanotube/graphite/ poly(lactic acid) conductive biopolymer nanocomposites (CPC)," *Mater. Lett.*, vol. 67, no. 1, pp. 210–214, 2012.

[52] G. Droval, J.-F. Feller, P. Salagnac, and P. Glouannec, "Thermal conductivity enhancement of electrically insulating syndiotactic poly(styrene) matrix for diphasic conductive polymer composites," *Polym. Adv. Technol.*, vol. 17, no. 9–10, pp. 732–745, 2006.

[53] K. Kim and J. Kim, "Vertical filler alignment of boron nitride/epoxy composite for thermal conductivity enhancement via external magnetic field," *Int. J. Therm. Sci.*, vol. 100, pp. 29–36, 2016.

[54] A. M. Díez-Pascual, M. Naffakh, C. Marco, G. Ellis, and M. A. Gómez-Fatou, "High-performance nanocomposites based on polyetherketones," *Prog. Mater. Sci.*, vol. 57, no. 7, pp. 1106–1190, 2012.

[55] C. Guthy, F. Du, S. Brand, K. I. Winey, and J. E. Fischer, "Thermal Conductivity of Single-Walled Carbon Nanotube/PMMA Nanocomposites," *J. Heat Transfer*, vol. 129, no. 8, p. 1096, 2007.

[56] Y. P. Mamunya, V. V. Davydenko, P. Pissis, and E. V. Lebedev, "Electrical and thermal conductivity of polymers filled with metal powders," *Eur. Polym. J.*, vol. 38, no. 9, pp. 1887–1897, 2002.

[57] S. Y. Fu, B. Lauke, E. Mäder, C. Y. Yue, and X. Hu, "Tensile properties of short-glass-fiber- and short-carbon-fiber-reinforced polypropylene composites," *Compos. Part A Appl. Sci. Manuf.*, vol. 31, no. 10, pp. 1117–1125, 2000.

[58] J. H. Phelps, A. I. Abd El-Rahman, V. Kunc, and C. L. Tucker, "A model for fiber length attrition in injection-molded long-fiber composites," *Compos. Part A Appl. Sci. Manuf.*, vol. 51, pp. 11–21, 2013.

[59] W. Bin Zhang *et al.*, "Largely enhanced thermal conductivity of poly(vinylidene fluoride)/carbon nanotube composites achieved by adding graphene oxide," *Carbon N. Y.*, vol. 90, pp. 242–254, 2015.

[60] X. Huang, P. Jiang, and L. Xie, "Ferroelectric polymer/silver nanocomposites with high dielectric constant and high thermal conductivity," *Appl. Phys.*

Lett., vol. 95, no. 24, pp. 1–4, 2009.

[61] T. Terao, C. Zhi, Y. Bando, M. Mitome, C. Tang, and D. Golberg, "Alignment of Boron Nitride Nanotubes in Polymeric Composite Films for Thermal Conductivity Improvement," *J. Phys. Chem. C*, vol. 114, pp. 4340–4344, 2010.

[62] A. M. Díez-Pascual *et al.*, "Influence of carbon nanotubes on the thermal, electrical and mechanical properties of poly(ether ether ketone)/glass fiber laminates," *Carbon N. Y.*, vol. 49, no. 8, pp. 2817–2833, 2011.

[63] G. Yuan *et al.*, "Mesophase pitch-based graphite fiber-reinforced acrylonitrile butadiene styrene resin composites with high thermal conductivity," *Carbon N. Y.*, vol. 95, pp. 1007–1019, 2015.

[64] U. Martin's Rubber Company, "Advantages and Disadvantages of Compression Moulding," 2016. [Online]. Available: http://www.processindustryforum.com/article/advantages-and-disadvantages-of-compression-moulding.

[65] J. A. Heiser and J. A. King, "Thermally conductive carbon filled nylon 6,6," *Polym. Compos.*, vol. 25, no. 2, pp. 186–193, 2004.

[66] P. Shokri and N. Bhatnagar, "Effect of packing pressure on fiber orientation in injection molding of fiber-reinforced thermoplastics," *Polym. Compos.*, vol. 28, no. 2, pp. 214–223, 2007.

[67] A. Suplicz, F. Szabo, and J. G. Kovacs, "Injection molding of ceramic filled polypropylene: The effect of thermal conductivity and cooling rate on crystallinity," *Thermochim. Acta*, vol. 574, pp. 145–150, 2013.

[68] S. W. Lee, J. R. Youn, and J. C. Hyun, "Prediction of fiber orientation structure for injection molded short fiber composites," *Mater. Res. Innov.*, vol. 6, no. 4, pp. 189–197, 2002.

[69] M. Gupta and K. K. Wang, "Fiber orientation and mechanical properties of short-fiber-reinforced injection-molded composites: Simulated and experimental results," *Polym. Compos.*, vol. 14, no. 5, pp. 367–382, 1993.

[70] S. Takahashi, Y. Imai, A. Kan, Y. Hotta, and H. Ogawa, "Dielectric and thermal properties of isotactic polypropylene / hexagonal boron nitride composites for high-frequency applications," vol. 615, pp. 141–145, 2014.

[71] X. Tian, M. E. Itkis, and R. C. Haddon, "Application of Hybrid Fillers for Improving the Through-Plane Heat Transport in Graphite Nanoplatelet-Based Thermal Interface Layers," *Nat. Publ. Gr.*, no. August, pp. 1–7, 2015.

[72] C. Yuan, B. Xie, M. Huang, R. Wu, and X. Luo, "Thermal conductivity enhancement of platelets aligned composites with volume fraction from 10% to 20%," *Int. J. Heat Mass Transf.*, vol. 94, pp. 20–28, 2016.

[73] Z. Lin, Y. Liu, S. Raghavan, K. Moon, and S. K. Sitaraman, "Magnetic Alignment of Hexagonal Boron Nitride Platelets in Polymer Matrix : Toward High Performance Anisotropic Polymer Composites for Electronic Encapsulation," *ASC Appl. Mater. Interfaces*, vol. 5, pp. 7633–7640, 2013.

[74] H. Xu, H. Zhou, X. Chen, and Y. Liu, "High thermal conductive composites based on flake graphite filled in a partial compatible polyamide 6/polypropylene," *Polym. Sci. Ser. A*, vol. 57, no. 5, pp. 644–655, Sep. 2015.

[75] G. H. Motlagh, A. N. Hrymak, and M. R. Thompson, "Improved through-plane electrical conductivity in a carbon-filled thermoplastic via foaming," *Polym. Eng. Sci.*, vol. 48, no. 4, pp. 687–696, 2008.

Chapter 2

Effect of matrix and filler on the thermal conductivity of industrially feasible injection moulded thermoplastics

2. 1. Abstract

To understand how the thermal conductivity (TC) of virgin commercial polymers and their composites with low graphite filler amounts can be improved, the effect of material choice, annealing and moisture content is investigated, all with feasible industrial applicability in mind focusing on injection moulding. Comparison of commercial HDPE, PP, PLA, ABS, PS, and PA6 based composites under conditions minimizing the effect of the skin-core layer (measurement at half the sample thickness) allows to deduce that at 20 m% of filler, both the (overall) in- and through-plane TC can be significantly improved. The most promising results are for HDPE and PA6 (through/in-plane TC near 0.7/4.3 $Wm^{-1}K^{-1}$ for HDPE and 0.47/4.3 W $m^{-1}K^{-1}$ for PA6 or an increase of 50/825% and 45/1200% respectively, compared to the virgin polymer). Testing with annealed and nucleated PA6 and PLA samples shows that further increasing the crystallinity has a limited effect. A variation of the average molar mass and moisture content is also almost without impact. Intriguingly, the variation of the measuring depth allows to control the relative importance of the TC of the core and skin layer. An increased measurement depth, hence, a higher core-to-skin ratio measurement specifically indicates a clear increase in the through-plane

TC (e.g., factor 2). Therefore, for basic shapes, the removal of the skin layer is recommendable to increase the through-plane TC.

2. 2. Introduction

Thermally conductive polymers are of great interest for a vast amount of applications, including heat sinks for light-emitting diodes, batteries and other electronic devices. They are also promising for heat transfer processes that can profit from reduced weight and improved corrosion resistance compared to conventional metal-based heat exchangers [1]. Significant lab-scale research has already been conducted on the improvement of the thermal conductivity (TC) of polymer composites. Focus has been on the use of fillers such as carbon fibres [2], [3], graphite and carbon nano particles [2], [4]–[6], metals [7]–[9], and more recently carbon nanotubes [10], [11] and graphene [12], [13] for applications that allow electrical conductivity and fillers such as boron nitride, aluminium nitride [14], ceramics [15], and metal oxides [16] for non-electrical conductive applications. Typical conductivity values are between 0.15 and 0.50 $W \cdot m^{-1}K^{-1}$, which are lower than the conventional metal counterparts with values around $10–5 \times 10^2$ $W\ m^{-1}K^{-1}$ [1]. A high filler content, often more than 35% in volume [17], [18], is required in order to improve the TC of lab-scale polymer composites. Only at high filler amounts, a continuous thermal conductive path of fillers can be formed. This critical loading level is called the thermal percolation threshold to differentiate e.g., from an electric percolation threshold [19]. Fillers with a high aspect ratio require lower loading levels to reach this threshold, and carbon nanotubes can help to form conductive connections between the fillers [20], [21].

The TC of a composite is in general determined by the TC of the matrix and strongly influenced by the number of interfaces, making, for a given amount, fillers with a high

aspect ratio more favourable. It is postulated that polymers with a higher crystallinity possess a better TC, though there are plenty of exceptions as other factors such as side groups, (average) molar mass, bond strength, and processing conditions also play a role [1], [10], [17], [22]. The relevance of processing conditions in view of TC design is less studied but essential, as it can contribute to anisotropy and result in brittle materials with reduced mechanical properties [17]. The most commonly used processing methods for thermoplastic polymers, i.e., injection and extrusion, are known to cause the fillers to orientate with the main flow direction. This results in a high in-plane TC and a low through-plane TC [23], [24].

Although the effect of crystallinity has been studied theoretically [25] and at a lab scale [26], almost no data is available on the effect of crystallinity on the TC on an industrial applicable scale. The mismatch in TC during processing can also be expected to be enhanced under industrial scale conditions, which aim at high throughputs, with the same being true for other polymer composite characteristics. In particular, stronger morphological changes are likely. For example, in injection moulding, the skin-core effect causes fillers close to the mould wall to show strong orientation with the flow direction, while the fillers in the core are more randomly orientated [27]–[29], though a specific core pattern has been claimed as well [30]. As manipulation of or control over orientation can strongly influence the in-plane and through-plane TC [31], further investigation of the skin-core effect seems appropriate. Furthermore, to the best of the authors' knowledge, a very limited number of studies with both in-plane and through-plane TC measurements have been devoted on a scale transcending the lab scale [23], [24], [32]. These lab scale studies typically focus on the effect of aspect ratio [33], the combination of different fillers [34] and a comparison with theoretical models [18] rather than the explicit evaluation of the effect of the skin-core formation and matrix related variations on the TC.

In this work, the effect of average molar mass, crystallinity and filler size is therefore studied at a (semi)-industrial manufacturing scale, considering commercial polymers. Since a manifold of thermal management applications are subjected to moisture, the effect of moisture on TC is investigated as well. The focus is on samples prepared with injection moulding, as it is one of the most common methods and more scalable techniques for polymer processing, and graphite fillers to obtain a simple and relatively inexpensive, thus industrially relevant manufacturing procedure. Specific focus is on the identification of the most optimal polymer matrix and the effect of skin and core layers on the TC. It is shown that these layers have a significant effect on the TC and the effective reduction of the thickness or modification of the filler spatial arrangement can strongly improve the through-plane TC, at least for basic shapes.

2. 3. Materials and Methods

2. 3. 1. Materials

Flake graphite (Asbury, 3806) with an average size of 19 micrometer was compounded with different matrices: polypropylene (PP; Sabic, 575P), high density polyethylene (HDPE, Dow, 25055E), acrylonitrile-butadiene-styrene (ABS, LG, HI-121), polyamide-6 (PA6; Solvay, Technyl C 230 Natural), polystyrene (PS; Ineos, Styrolution 165N and 124N), and poly(lactic acide) (PLA; Natureworks, 3100HP). Nucleating agent (Bruggolen P252), kindly supplied by Bruggemann Chemical, Heilbronn, Germany, was used to investigate the effect of crystallinity.

2. 3. 2. Manufacturing Approach

The overall manufacturing procedure is highlighted in Figure 1. For each polymer matrix, compounds with 0, 10 and 20 m% of the flake graphite filler were produced.

Additionally, PLA and PA6 filaments with 0.2, 0.5 and 1.0 m% nucleating agent (N.A.) were produced without fillers. Prior to this, the PLA was dried overnight at 60 °C, while PA6, ABS and PS were dried at 80 °C. The carbon fillers were compounded with thermoplastics using a co-rotating twin screw extruder (APV MP19TC-40 Baker, Peterborough, England) with variable temperature profiles for different matrices (e.g., for PA6 from 220 °C at the inlet to 250 °C at the die). The extruded filaments were directly cooled in a water bath at room temperature and chopped in pellets. Prior to injection moulding, the pellets were dried overnight. The composites were moulded into tensile bars according to ISO 527-2 specimen type A, using an injection molding machine (Engel e-victory, Schwertberg, Austria). The dosing speed was maintained as low as possible to avoid damage to the graphite filler.

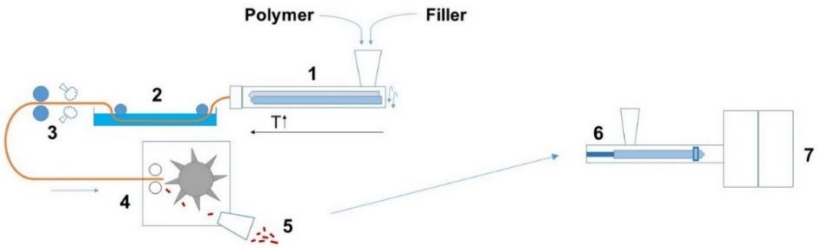

Figure 1: Semi-industrial scale processing of thermally conductive composites includes compounding (left) and injection moulding (right) with (1) twin screw extruder; (2) water bath; (3) drying and pulling; (4) pelletizer; (5) pellets; (6) injection moulding machine; and (7) mould.

Prior to characterization, all samples were conditioned in a climate controlled room at 23 °C and relative humidity of 50% for at least 48 h. In order to measure the TC, the wide parts of the dogbones were cut off and a cube with a flank size of 10 mm was cut out of the middle of the dogbone of the grip end, as shown in Figure 2 (closest to

the gate). The samples were grinded on sandpaper (grit 300) on one side till the surface was smooth to assure good contact between sensor and sample.

In order to further investigate the effect of crystallinity, PLA samples were tested as prepared and after annealing (–a in sample notation). The annealing treatment consisted of treating the samples, after injection moulding, for 2 h in a furnace at 80 °C and slowly letting them cool down to room temperature. Before testing the TC, these samples were sanded and conditioned as all previous samples. PA6 samples were annealed for 5 h at 175 °C and slowly cooled to room temperature. The effect of moisture on TC was performed by confronting PA6, known as a hygroscopic material, under different humidity conditions before measuring. PA6-samples were installed in a drier at 80 °C for 24 h. Afterwards, they were put in moisture resistant bags and cooled down to 23 °C before measuring. Other samples were placed for a week in distilled water at 23 °C before measurement. The reference samples were measured under regular conditions as mentioned before (23 °C and 50% relative humidity).

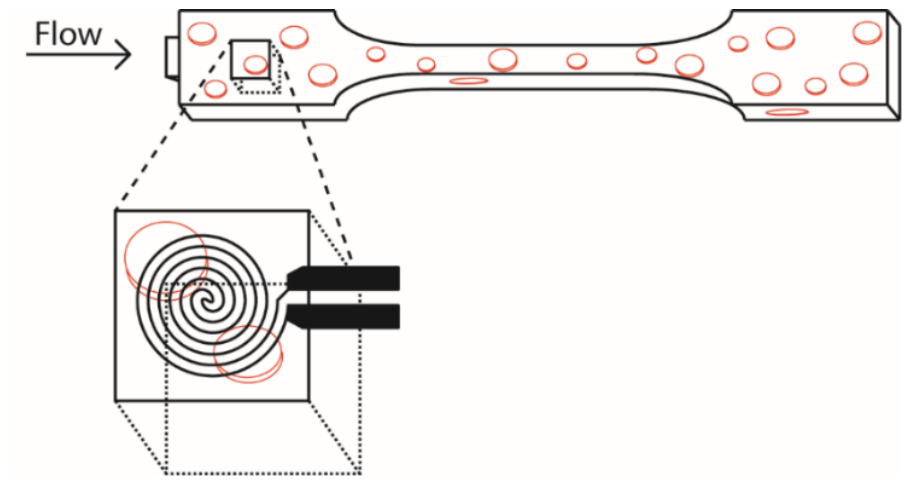

Figure 2: Thermal conductivity (TC) measurement is performed on the injection moulded part of the dogbone closest to the gate; cf. Figure 1 (right).

2. 3. 3. Characterization

The density of the samples was measured by buoyancy in air and ethanol, using a Precisa XR 205SM-DR balance (Precisa, Dietikon, Switzerland). Heat capacity was measured using the Hot Disk TPS 2500S (Hot Disk, Göteborg, Sweden) heat capacity module with the gold cell reference. All TC numbers are an average of three measurements with acceptable standard deviations (below 5%), unless mentioned otherwise. TC in the in- and through-plane direction were measured using the anisotropic module according to the ISO 22007-2 standard. To compensate for the skin-core effect, the probing depth for the measurements aiming at overall TC values (most measurements) was as close as possible to half the sample thickness (B = 2 mm in Figure 3). Isotropic bulk samples were measured using the isotropic module.

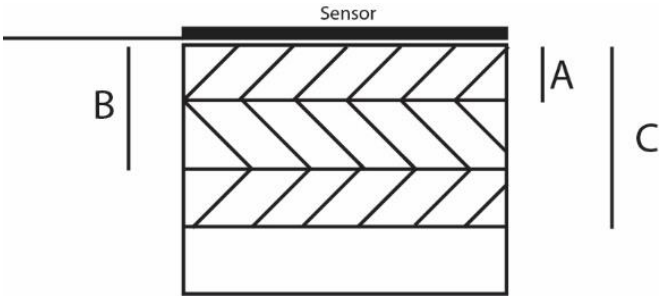

Figure 3: Different measurement times result in the average TC over increasing volumes. Short measurement times result in low probing depth (A) and will thus give an average TC over that measured volume. Longer measurement times (B and C) will give an average TC over larger volumes.

The probing depth can be varied by adjusting measurement times so that the skin-layer effect can be explicitly studied alongside the determination of overall TC values. Longer measurements allow the heat wave to travel further, thus allowing to measure TC over a larger volume, as can be seen in Figure 3. Measuring for a short time results in a low measuring depth (A), and will measure the TC of what is mostly the skin layer. At half of the sample thickness (B), the overall value results assume that the morphology is identical for both sides of the sample. Longer measurements (C) give values of the TC of a larger sample volume and will relatively contain more core layers.

The crystallinity of the semi-crystalline polymers (x_c) was measured using differential scanning calorimetry (DSC; Netzsch Polyma, Selb, Germany). Different maximum temperatures were chosen for different polymers, but heating rate and starting temperature were maintained constant at 10 °C min^{-1} and 30 °C. Peak surface and temperatures were determined using the Protheus software. Data from the first heating run was used. Crystallinity was calculated using [35], [36]:

$$x_{\mathrm{c}}\,(\%) = \frac{\Delta H_{\mathrm{melt}} - \Delta H_{\mathrm{cc}}}{\Delta H_{\mathrm{m}}^{0}} 100$$

in which ΔH_{m} stands for melt enthalpy, ΔH_{cc} for cold crystallization or post-crystallization enthalpy, and $\Delta H_{\mathrm{m}}^{0}$ for the theoretical melt enthalpy of 100% crystalline material. The values for $\Delta H_{\mathrm{m}}^{0}$ are displayed in Table 1.

Table 1: Melt enthalpy of 100% crystalline material [37], [38].

Polymer matrix	HDPE	PP	PLA	PA6
Enthalpy of fusion (J g^{-1})	293	207	94	230

Scanning electron microscopy (SEM) images were taken using a Phenom desktop SEM gen 1 (Phenom-world, Eindhoven, the Netherlands). No gold sputtering was required since a sample holder with charge reduction (low vacuum) was used. Samples were frozen in liquid nitrogen before being fractured.

2. 4. Results and Discussion

In this section, the effect of process variables such as average molar mass, crystallinity, the presence of moisture, and filler size/amount is investigated, considering the semi-industrial scale manufacturing approach in Figure 1 and focusing both on overall TC values and TC values validating skin-core layer formation. It is reminded that all TC values are averages obtained after statistical analysis.

2. 4. 1. Effect of Average Molar Mass

One could argue that a higher average molar mass should improve the TC of a polymer matrix, since the TC along chains is higher than that between chains. To test this theory, the TC of two commercial grades of polystyrene (Ineos styrolution 124N (lower average molar mass) and Ineos styrolution 165N (higher average molar mass) were measured. These grades of polystyrene were chosen as they are amorphous, meaning that crystallization effects can be eliminated.

Table 2 shows the recorded (overall) TC values. Focus is on isotropic measurements, as no fillers are present. There seems to be no clear difference in the TC of both polymers but this could be within the error range of the measurement equipment. Hence, based on the data in the present work, it seems that the average molar mass plays at most a very minor role in the TC. This is likely because, besides molar mass, the orientation of the chains and chain entanglement could counter this effect, or perhaps the difference in molar mass for the selected commercial polystyrenes is insufficient.

Table 2: Thermal conductivity (TC) of PS with different average molar mass; isotropic (bulk) values; no fillers; no significant differences are recorded; TC at half the sample thickness.

Grade	TC ($W\ m^{-1}K^{-1}$)
PS 124N	0.1768
PS 165N	0.1761

2. 4. 2. Effect of Crystallinity

Table 3 shows the relation between TC and crystallinity for several commercial polymers with no nucleation agent (N.A.) added. The amorphous polymers clearly show a lower TC than the semi-crystalline polymers. However, the effect of crystallinity should not be overestimated. While PP has a crystallinity of 44%, the TC is well below that of PA6, with only a crystalline fraction of 16%. This could be caused by the relatively low crystal density and the methyl groups on the polypropylene causing phonon scattering [17]. Other factors such as crystal size, polymer backbone composition and molar mass could also influence the TC of the virgin polymers.

In order to further investigate the effect of crystallinity, samples of PLA and PA6 were produced with N.A. and measured before and after annealing treatments. The N.A. works well for both PA6 and PLA, as can be seen in Table 4. An increase in crystallinity for both PA6 as PLA is visible upon its introduction, already at a mass concentrations as low as 0.2 m%. Higher amounts of N.A. show little additional improvement. Annealing treatments further improve the crystallinity of both PLA and PA6. For PA6, a new DSC peak around 195 °C appears after annealing. This peak can be ascribed to the γ crystalline state of PA6 [39], while the peak around 224 °C can be ascribed to the α crystals. The DSC run of PLA shows no cold crystallization after the annealing treatment (see Figure 4 and 5). For PLA with N.A., however, only a (very) small increase in TC can be noticed with increasing crystallinity.

Table 3: Crystallinity (x_c) and thermal conductivity (TC) of several commercial polymers without nucleation agent and filler; polymers ranked according to increasing TC; annealing for second PLA; TC at half the sample thickness.

Polymer	x_c **(%)**	**TC (W m^{-1}K^{-1})**
PS 165N	0	0.1768
ABS	0	0.1891
PLA (amorphous)	0	0.2082
PLA (semi-crystalline)	48	0.2202
PP	44	0.2456
PA6	16	0.3271
HDPE	62	0.4657

It should be mentioned though that this small increase in TC will barely have an effect on the cooling time within the injection process or result in an improved efficiency for heat exchange applications. The crystallinity of such products should thus be tailored for mechanical properties rather than TC. A small decrease in TC can be noticed for PA6, even though crystallinity increases with added N.A. This could possibly be explained by the increased amount of crystals, hence, reduced size of the crystals increasing the number of interfaces between amorphous and crystalline phase or two crystal phases, which has a negative impact on the TC. Annealed PA6 shows slightly increased TC compared with their non-annealed counterpart, since annealing allows crystals to grow in size, reducing the amount of the aforementioned interfaces.

Table 4: Crystallinity (x_c; %) and thermal conductivity (TC; $W \cdot m^{-1}K^{-1}$) of PA6, annealed PA6 (PA6-a), PLA and annealed PLA (PLA-a) with different amounts of nucleating agents (N.A.); 0.2% N.A. is sufficient; to increase x_c; x_c increases are mainly useful for controlling mechanical properties as similar TC values are obtained; no filler; TC at half the sample thickness.

		0% N.A.	**0.2% N.A.**	**0.5% N.A.**	**1.0% N.A.**
PA6	TC	0.3271	0.3154	0.3183	0.3210
	x_c	16	24	25	27
PA6-a	TC	0.3352	0.3273	0.3239	0.3355
	x_c	31	31	29	31
PLA	TC	0.2082	0.2092	0.2124	0.2138
	x_c	0	18	17	19
PLA-a	TC	0.2202	0.2246	0.2246	0.2240
	x_c	48	50	49	49

2. 4. 3. Effect of Moisture

After injection moulding and sanding, the PA6 samples were conditioned at 23 °C with 50% relative humidity, while the other samples were maintained in distilled water at 23 °C, hence, wet, and some samples were dried at 80 °C; all for at least 24 h. Before measuring the dried samples, they were cooled down to 23 °C in moisture-tight plastic bags.

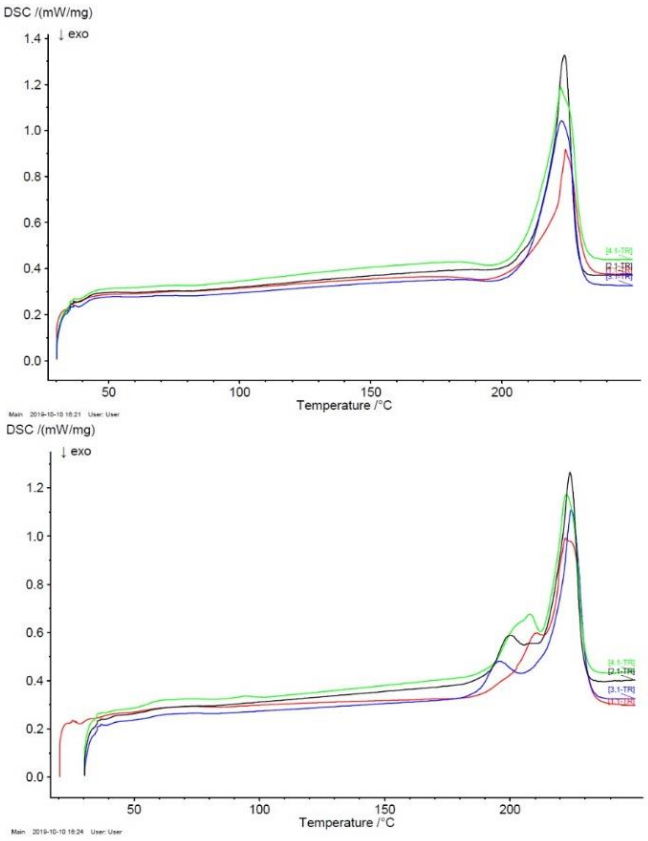

Figure 4: DSC curves of PA6 (top) and PA6 annealed (bottom). The red line represents PA6 without nucleating agent. The green, blue and black lines represent 0.2, 0.5 and 1.0 wt% nucleating agent respectively.

The results are given in Table 5. There seems to be only a very little difference in TC between the different conditions. This difference will not have severe implications on the performance of thermal management systems, which is a positive finding.

Table 5: Thermal conductivity (TC) of wet, dry and conditioned PA6 samples (no filler). Very small changes are observed, which is interesting for thermal management systems; TC at half the sample thickness.

PA6	Conditioned	Dry	Wet
TC ($W \cdot m^{-1}K^{-1}$)	0.3273	0.3196	0.3142

2. 4. 4. Effect of Filler Amount and Matrix Type

The in-plane and through-plane (top/bottom part) TCs for several virgin polymers and their composites are shown in Table 6, with filler amounts up to 20 m%. These results, which include absolute data and relative data with respect to the virgin polymer, clearly show that the in-plane TC increases more rapidly than the through-plane TC with increasing filler content. This phenomenon can be explained by the manufacturing method. Injection moulding is a process that causes the polymer chains to flow, therefore causing the flake fillers to orientate with the flow. The heat flow in the in-plane direction has to cross less filler-matrix interfaces, which is beneficial for TC. Moreover, the TC of graphite as such is anisotropic, with a higher "in-plane" than "through-plane" TC.

There seems to be no clear connection between the in-plane composite TC and the TC of the matrix (top part of Table 6). This is likely because the flow behaviour and the related processing parameters, which are different for each polymer, will determine how well the graphite platelets are aligned and therefore how high the TC shall be. Compatibility seems to also play little role in TC of the composites for in-plane measurements. For example, PE shows low compatibility with most fillers [40], while HDPE composites show amongst the highest TCs both in the in- and through-plane

direction in Table 6. A simple conclusion for through-plane TC (bottom part of Table 6) is also difficult to make. Most promising are HDPE and PA6 with a through-plane TC near 0.5 $W \cdot m^{-1}K^{-1}$ and higher at 20 m% filler. This might be partially due to the already relative high TC of the virgin matrix, as PS shows a similar relative increase but has a lower initial TC. On the other hand, the increase in through-plane TC of ABS and PS is about relatively the same. In some cases (e.g., PP), a decrease in through-plane TC can be noticed with an increasing amount of filler as well. This could be explained by the increasing number of interfaces, causing more phonon scattering and thus reduced TC. The relative low TC of the through-plane direction of graphite, the short distance, and the high number of interfaces are dominant factors under such conditions, causing the TC to drop instead of increase.

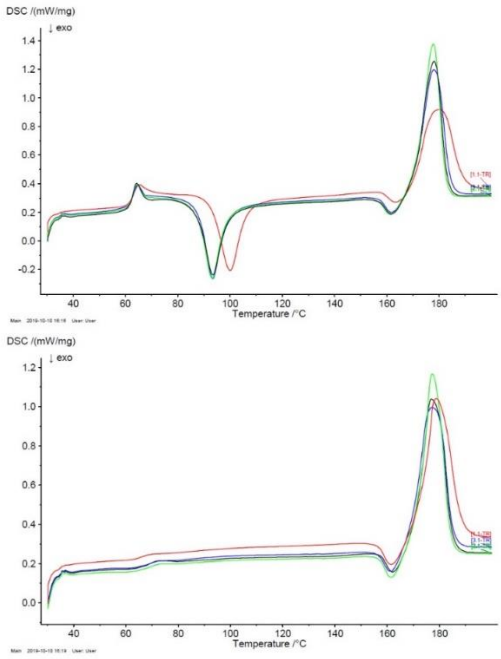

Figure 5: DSC curves of PLA (top) and PLA annealed (bottom). The red line represents PLA without nucleating agent. The green, blue and black lines represent 0.2, 0.5 and 1.0 wt% nucleating agent respectively.

Most promising for small electronics heat sinks are modified HDPE, PA6 and PLA, with large in-plane TCs and acceptable through plane TCs, if process design is done properly. Compared to other state of the art options, the modified HDPE outperforms a PP-carbon fibre-carbon nanotube composite [41] in both in-plane and through-plane TC with less filler at a likely lower production price. Through-plane TC of PA6 with 20 m% of filler approaches the through-plane TC of the previously mentioned composite, while heavily outperforming it in in-plane TC. As the previously mentioned PP-based composite was suitable for cooling LEDs, composites presented in this work will likely perform likewise. For heat exchanger applications, performance would strongly depend on thickness of the used components.

2. 4. 5. Relevance of Morphology: Skin-Core Effect

As seen above (Tables 2–6), probing depth was regulated (ca. half the sample thickness) to minimize the impact of the skin-core effect and thus obtain an overall in/through-plane TC. However, an important research task is the identification of the TC gradient along the thickness, which is covered in the present subsection. By adjusting the measurement time on the Hot Disk TPS 2500s, the average TC over different depths can be measured. The TCs at different probing depths for PLA and ABS with 20 m% of graphite filler (optimal amount from Table 6) are given in Table 7. The influence of the skin-core effect on the TC of composites becomes very clear here. Upon measuring at a small probing depth, the skin layer is mainly measured. This layer is known for its strong orientation with the flow, where TC in the through-plane will be at a minimum and in-plane TC will be higher. As the probing depth increases, the fraction of the core layer compared to the skin layer will increase, displaying an increased through-plane TC traded off for a decrease in in-plane TC. By

increasing the probing depth of ABS, a through-plane TC value twice as high as the value at half the thickness of the sample is found.

Table 6: Thermal conductivity (TC) of virgin polymers and their composites materials, with different amounts of fillers alongside relative increases (with respect to virgin polymer); no nucleation agent or annealing; virgin materials were measured as isotropic, hence, the same in-plane and through-plane values: TC at half the sample thickness.

	In-Plane TC ($W \cdot m^{-1}K^{-1}$)			**In-Plane TC (relative in %)**		
m% of filler	0	10	20	0	10	20
HDPE	0.4657	1.5996	4.3084	0	243	825
ABS	0.1891	0.9485	3.0778	0	401	1527
PP	0.2456	1.0998	2.1126	0	347	760
PA6	0.3271	1.4975	4.3415	0	35	1227
PS (165N)	0.1761	0.9342	2.9346	0	43	1566
PLA	0.2082	1.2724	4.3328	0	51	981
	Through-Plane TC ($W \cdot m^{-1}K^{-1}$)			**Through-Plane TC (relative in %)**		
m% of filler	0	10	20	0	10	20
HDPE	0.4657	0.5499	0.6957	0	18	49
ABS	0.1891	0.2129	0.2526	0	12	33
PP	0.2456	0.176	0.1902	0	-28	-22
PA6	0.3271	0.4444	0.4711	0	35	44
PS (165N)	0.177	0.1676	0.2576	0	-5	45
PLA	0.2082	0.2007	0.2464	0	-3	18

Figure 6 shows the corresponding SEM images (20 m%), where the injection direction is from right to left. Images A to C display composites with well-dispersed fillers. No clear coagulations of graphite are visible, as these could cause strong changes in the local thermal conductivity. Figure 6A was taken for ABS near the edge of the sample, hence, in the skin layer. Fillers show strong alignment with the flow direction, improving in-plane and decreasing through-plane TC. This image also shows the 2D (platelet) character of the filler. Figure 6B was taken at the centre of the ABS sample or thus the core layer. The graphite fillers show no clear alignment or preferred direction and seem to be orientated randomly. This orientation could be able to form a 3D interconnected network at the core, improving in-plane as through-plane TC.

Table 7: Thermal conductivities (TCs) as a function of probing depth to identify the relevance of gradients (cf. Figure 3); in Tables 2–6, focus was on values with a minimization of the skin-core layer by a regulated probing depth at half the sample thickness; at lower probing depths, the influence of the skin layer becomes clear.

	Probing Depth (mm)	**Through-Plane TC**	**In-Plane TC**
PLA 20 m%	1.21	0.2081	4.5699
	1.94	0.2385	4.4190
	2.99	0.4251	3.1111
ABS 20 m%	1.10	0.1626	3.9392
	2.04	0.2487	3.0215
	3.51	0.5131	1.7326

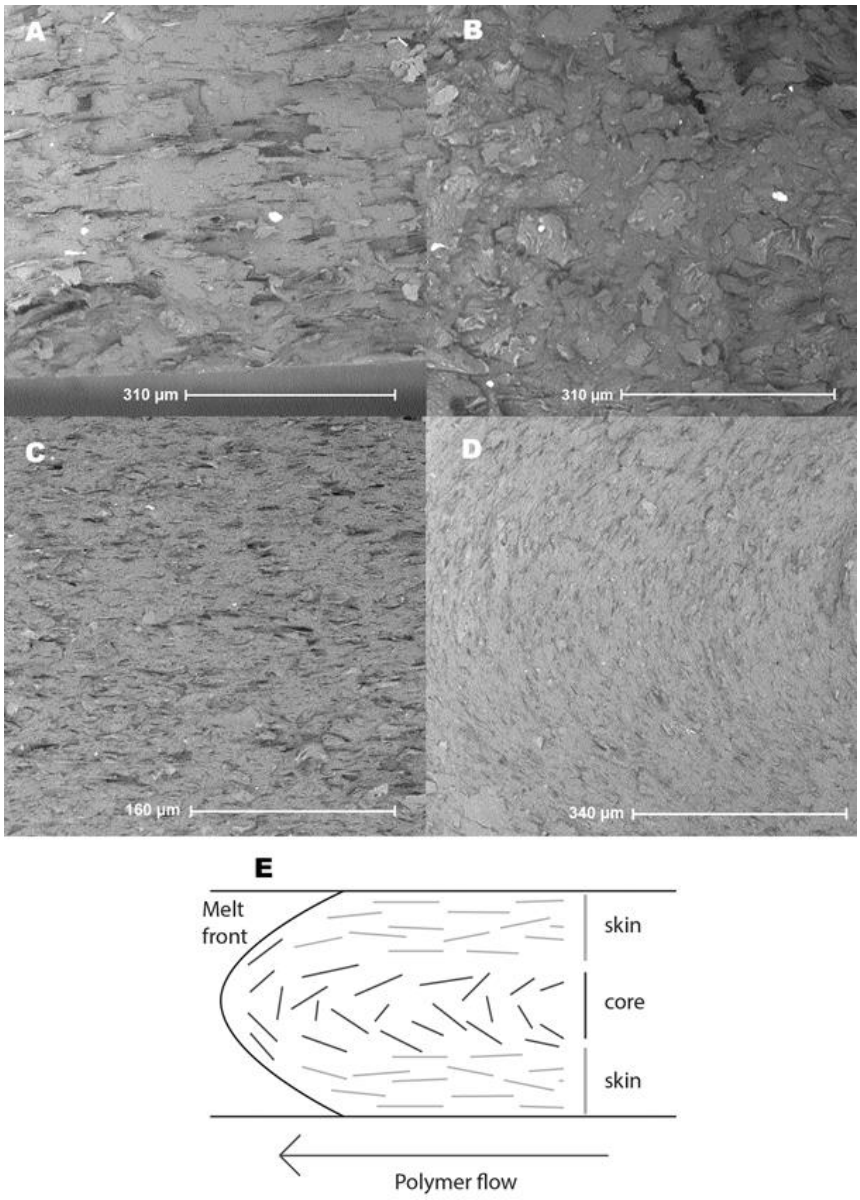

Figure 6: SEM image of ABS with 20 m% of graphite; (A) near the edge, where the skin effect is clearly visible and (B) at the centre of the sample, where more random orientation is visible; SEM image of PA6 with 20 m% of graphite (C) near the edge of the sample, where the same orientation as the ABS sample is visible and (D) at the centre of the sample, where the fillers show a clearer orientation following the melt front; (E) global SEM interpretation: orientation of fillers due to the skin-core effect (exaggerated); the 2D graphite platelets are represented as 2D lines for simplification.

Closer examinations of multiple SEM images, however, showed a distinguished pattern where the fillers in the core still oriented with the flow front but much less outspoken than the skin-layer orientation. Figure 6C,D shows the skin and core layer with PA6, with specifically the core layer of PA6 clearly showing the orientation with the melt front (Figure 6D). Much like Figure 6A, the skin effect is well visible in Figure 6C. An exaggerated representation of filler orientation after injection moulding is shown in Figure 6E. It can be concluded that the effect of skin-core layer formation should not be underestimated for TC. For improved through-plane TC, the skin layer should be as small as possible.

Alternatively, removal of the skin layers of less complex shapes could make it possible to achieve high through-plane TC, even at low filler amounts. To further support this claim, the top 1.5 mm was grinded off the samples. However, the through-plane TC or thickness of the sample were respectively too high or too low in order to be measured, as the probing depth exceeded the sample thickness

2. 4. 6. Relevance of Morphology: Filler Size and Shape

Morphology can also be influenced by filler size. In order to eliminate the aforementioned (small) effect of crystallinity and other factors, amorphous PS 165N was chosen as matrix material and combined with graphite filler of two different sizes, henceforth called “macro-graphite” (used before; Tables 3–7) and “nano-graphite”. The different compositions and the TC of these compounds are given in Table 8, again selecting the optimal amount of 20 m% but also including additional data for 10 m% of filler.

Table 8: Thermal conductivities (TCs; $W \cdot m^{-1} K^{-1}$) of PS 165N composites with different amounts of macro- and nano-graphite; the use of macro-graphite (Tables 3–7) is preferred (20 m%); TC at half the sample thickness.

nano/macro (m%/m%)	0/20	0/20	5/15	10/10	15/5	10/0	20/0
In-plane TC	2.9345	0.9341	1.4434	1.2000	0.9236	0.4409	0.4526
Through-plane TC	0.2576	0.1676	0.1809	0.1984	0.2120	0.1905	0.2280

Upon comparing the macro-graphite at 20 m% with the nano-graphite at 20 m%, it can be noticed that the former performs better both in- and through-plane. This is more than likely due to the increased number of interfaces in the nano-composite compared with the macro-composite. Only the macromaterial can likely form more conductive paths. Upon combining nano with macro-graphite (overall still 20 m%), a decrease in both in-plane and through-plane TC can be noticed in Table 8. Increasing the amount of nano-graphite while decreasing the amount of macro-graphite causes the in-plane TC to fall further, since the existing percolation network in this direction becomes broken by removing macro-fillers, further highlighting the preference of macro-graphite.

It should be put forward that also the shape of the fillers plays a role. Figure 7A,B shows SEM-images of both fillers. While it is clear that the nano-fillers (A) are easily a factor 10 smaller (besides some clusters) than the macro-fillers (B), the nano-fillers appear as more or less spherical lumps, while the macro-fillers appear as 2D-platelets. The lumps will show less preferred orientation upon injection, besides having a more

uniform TC individually. This can explain the smaller gap between in-plane and through-plane TC of the nano-composites compared with the macro-composites in Table 8. This could also explain why the nano-filler at 10 m% has a higher through-plane TC than the macro-filler at the lower amount of 10 m%. Figure 7 (C) and (D) show SEM images for nano-fillers (20 m%) and a combination of nano and macro-fillers (10/10 m%) in a PS matrix. The nano-fillers in (C) still appear as more or less spherical clusters, some indicated with arrows, whereas the macro-fillers in (D) appear as two-dimensional platelets. The nano-fillers are not noticeable in the rough sample fracture where macro-fillers are present as well. Hence, the shape of the macro-fillers is more suited for a TC increase, provided that the correct filler amount (20 m%) is selected.

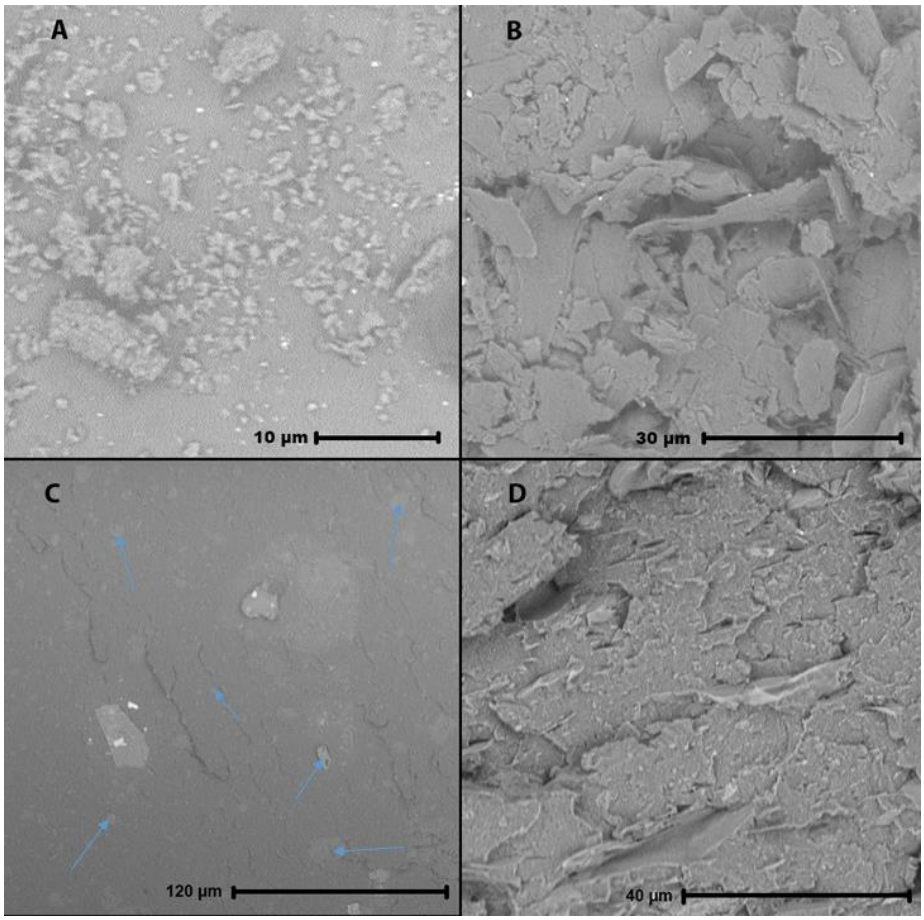

Figure 7: SEM images of (A) the nano-and (B) the macro-graphite, with spherical lumps vs. 2D-platelets; (C) shows 20 m% of nanofiller in PS 165N: particles are visible as slightly lighter spots, some indicated with arrows. Nanofillers are harder to detect in (D) 10 m% of each filler in PS 165N.

2. 5. Conclusions

The effect of average molar mass, crystallinity, moisture, matrix type, and filler amount and type on the (overall) TC was studied based on commercial polymers and their composites that were produced on a semi-industrial scale, using twin-screw compounding and injection rather than lab-scale techniques such as solvent mixing

and compression moulding. The effect of average molar mass was found to be insignificant, whereas a higher crystallinity does imply a higher TC although it is not the only contributor. Further increase of the crystallinity for instance by annealing is more relevant in view of the increase of mechanical properties. Notably, moisture has no significant effect on the thermal conductivity.

A general trend of higher in-plane and lower through-plane TC was noticed in all polymers, caused by the flow during the processing. The consideration of graphite fillers (20 m%) can increase both the in- and through plane TC. Although HDPE and PA6 composites generally showed a higher TC than other polymers with a better overall performance than for instance previously developed PP-carbon fiber-carbon nanotube composites, it is non-trivial to notice emerging trends in the TC of all the composites. This is likely because of the complexity of the whole system, where the skin-core effect also plays an important role. This skin-core effect has a substantial influence on the overall TC of the composite. An increase up to 100% in through-plane TC is noticed upon measuring deeper, hence, in the core-layer. For thermal applications requiring a high through-plane TC, the skin layer should therefore be as thin as possible. Removing the skin layer after injection could thus be considered for improved performance, at least if a basic shape is considered.

Macro-fillers generally perform the best, showing a higher in-plane and through-plane TC at 20 m%. Adding nano-fillers decreases both TCs, likely because they have more interfaces to cross, resulting in more phonon scattering. SEM images revealed that, besides the size, macro- and nano-fillers show a different shape. The spherical shape of the nano-filler causes a lower increase in the in-plane TC, since spheres are less affected by flow and thus orientation. The low aspect-ratio also makes it more difficult to form thermal conductive networks in contrast to the preferred macro-fillers.

REFERENCES

[1] T. Wieme, D. Tang, L. Delva, D. R. D'hooge, and L. Cardon, "The relevance of material and processing parameters on the thermal conductivity of thermoplastic composites," *Polym. Eng. Sci.*, vol. 58, no. 4, pp. 466–474, Apr. 2018.

[2] J. A. Heiser and J. A. King, "Thermally conductive carbon filled nylon 6,6," *Polym. Compos.*, vol. 25, no. 2, pp. 186–193, 2004.

[3] X. Lu and G. Xu, "Thermally conductive polymer composites for electronic packaging," *J. Appl. Polym. Sci.*, vol. 65, no. 13, pp. 2733–2738, Sep. 1997.

[4] I. Krupa, I. Novák, and I. Chodák, "Electrically and thermally conductive polyethylene/graphite composites and their mechanical properties," *Synth. Met.*, vol. 145, no. 2–3, pp. 245–252, 2004.

[5] H. Xu, H. Zhou, X. Chen, and Y. Liu, "High thermal conductive composites based on flake graphite filled in a partial compatible polyamide 6/polypropylene," *Polym. Sci. Ser. A*, vol. 57, no. 5, pp. 644–655, Sep. 2015.

[6] H. Y. Nezhad and V. K. Thakur, "Effect of Morphological Changes due to Increasing Carbon Nanoparticles Content on the Quasi-Static Mechanical Response of Epoxy Resin," *Polymers (Basel).*, vol. 10, no. 10, 2018.

[7] I. H. Tavman, "Thermal and Mechanical Properties of Aluminum Powder-Filled High-Density Polyethylene Composites," *J. Appl. Polym. Sci.*, pp. 2161–2167, 99AD.

[8] A. Boudenne, L. Ibos, M. Fois, J. C. Majesté, and E. Géhin, "Electrical and thermal behavior of polypropylene filled with copper particles," *Compos. Part A Appl. Sci. Manuf.*, vol. 36, no. 11, pp. 1545–1554, 2005.

[9] Y. P. Mamunya, V. V. Davydenko, P. Pissis, and E. V. Lebedev, "Electrical and thermal conductivity of polymers filled with metal powders," *Eur. Polym. J.*, vol. 38, no. 9, pp. 1887–1897, 2002.

[10] Z. Han and A. Fina, "Thermal conductivity of carbon nanotubes and their polymer nanocomposites: A review," *Prog. Polym. Sci.*, vol. 36, no. 7, pp. 914–944, 2011.

[11] A. Muhulet, F. Miculescu, S. I. Voicu, F. Schuett, V. K. Thakur, and Y. K. Mishra, "Fundamentals and scopes of doped carbon nanotubes towards energy and biosensing applications," *Mater. TODAY ENERGY*, vol. 9, pp. 154–186, Sep. 2018.

[12] A. Li, C. Zhang, and Y.-F. Zhang, "Thermal Conductivity of Graphene-Polymer Composites: Mechanisms, Properties, and Applications," *Polymers (Basel).*, vol. 9, no. 9, Sep. 2017.

[13] R. Atif, I. Shyha, and F. Inam, "Mechanical, Thermal, and Electrical Properties of Graphene-Epoxy Nanocomposites-A Review," *Polymers (Basel).*, vol. 8, no. 8, Aug. 2016.

[14] Y. Xu, D. D. L. Chung, and C. Mroz, "Thermally conducting aluminum nitride polymer-matrix composites," *Compos. - Part A Appl. Sci. Manuf.*, vol. 32, no. 12, pp. 1749–1757, 2001.

[15] H. Hong, J. U. Kim, and T.-I. Kim, "Effective Assembly of Nano-Ceramic Materials for High and Anisotropic Thermal Conductivity in a Polymer Composite," *Polymers (Basel).*, vol. 9, no. 9, Sep. 2017.

[16] S. Zhang, Y. Ke, X. Cao, Y. Ma, and F. Wang, "Effect of Al2O3 fibers on the thermal conductivity and mechanical properties of high density polyethylene with the absence and presence of compatibilizer," *J. Appl. Polym. Sci.*, vol. 124, no. 6, pp. 4874–4881, Jun. 2012.

[17] H. Chen *et al.*, "Thermal conductivity of polymer-based composites: Fundamentals and applications," *Prog. Polym. Sci.*, vol. 59, pp. 41–85, 2015.
[18] D. L. Gaxiola, J. M. Keith, J. A. King, and B. A. Johnson, "Nielsen Thermal Conductivity Model for Single Filler Carbon/Polypropylene Composites," *J. Appl. Polym. Sci.*, vol. 114, no. 5, pp. 3261–3267, Dec. 2009.
[19] L. Duan, D. R. D'hooge, M. Spoerk, P. Cornillie, and L. Cardon, "Facile and Low-Cost Route for Sensitive Stretchable Sensors by Controlling Kinetic and Thermodynamic Conductive Network Regulating Strategies," *ACS Appl. Mater. Interfaces*, vol. 10, no. 26, pp. 22678–22691, 2018.
[20] F. Zhang, Q. Li, Y. Liu, S. Zhang, C. Wu, and W. Guo, "Improved thermal conductivity of polycarbonate composites filled with hybrid exfoliated graphite/multi-walled carbon nanotube fillers," *J. Therm. Anal. Calorim.*, vol. 123, no. 1, pp. 431–437, 2016.
[21] S. Y. Pak, H. M. Kim, S. Y. Kim, and J. R. Youn, "Synergistic improvement of thermal conductivity of thermoplastic composites with mixed boron nitride and multi-walled carbon nanotube fillers," *Carbon N. Y.*, vol. 50, no. 13, pp. 4830–4838, 2012.
[22] N. Burger, A. Laachachi, M. Ferriol, M. Lutz, V. Toniazzo, and D. Ruch, "Review of thermal conductivity in composites: Mechanisms, parameters and theory," *Prog. Polym. Sci.*, vol. 61, pp. 1–28, 2016.
[23] J. a. King, K. W. Tucker, B. D. Vogt, E. H. Weber, and C. Quan, "Electrically and thermally conductive nylon 6,6," *Polym. Compos.*, vol. 20, no. 5, pp. 643–654, 1999.
[24] E. H. Weber, M. L. Clingerman, and J. A. King, "Thermally conductive nylon 6,6 and polycarbonate based resins. I. Synergistic effects of carbon fillers," *J. Appl. Polym. Sci.*, vol. 88, no. 1, pp. 112–122, Apr. 2003.
[25] C. L. Choy, "Thermal conductivity of polymers," *Polymer (Guildf).*, vol. 18, no. 10, pp. 984–1004, 1977.
[26] D. B. MERGENTHALER, M. PIETRALLA, S. ROY, and H. G. KILIAN, "THERMAL-CONDUCTIVITY IN ULTRAORIENTED POLYETHYLENE," *Macromolecules*, vol. 25, no. 13, pp. 3500–3502, Jun. 1992.
[27] J. Brezinová and A. Guzanová, "Friction conditions during the wear of injection mold functional parts in contact with polymer Composites," *J. Reinf. Plast. Compos.*, vol. 29, no. 11, pp. 1712–1726, 2010.
[28] S. Liparoti, V. Speranza, A. Sorrentino, and G. Titomanlio, "Mechanical properties distribution within polypropylene injection molded samples: Effect of mold temperature under uneven thermal conditions," *Polymers (Basel).*, vol. 9, no. 11, 2017.
[29] N. Billon, J. Giraudeau, J. L. Bouvard, and G. Robert, "Mechanical Behavior-Microstructure Relationships in Injection-Molded Polyamide 66," *Polymers (Basel).*, vol. 10, no. 10, 2018.
[30] P. Shokri and N. Bhatnagar, "Effect of packing pressure on fiber orientation in injection molding of fiber-reinforced thermoplastics," *Polym. Compos.*, vol. 28, no. 2, pp. 214–223, 2007.
[31] M. Spoerk *et al.*, "Anisotropic properties of oriented short carbon fibre filled polypropylene parts fabricated by extrusion-based additive manufacturing," *Compos. PART A-APPLIED Sci. Manuf.*, vol. 113, pp. 95–104, 2018.
[32] M. G. Miller, J. M. Keith, J. A. King, B. J. Edwards, N. Klinkenberg, and D. A. Schiraldi, "Measuring thermal conductivities of anisotropic synthetic graphite-liquid crystal polymer composites," *Polym. Compos.*, vol. 27, no. 4, pp. 388–394, Aug. 2006.

[33] T. Evgin *et al.*, "Effect of aspect ratio on thermal conductivity of high density polyethylene/multi-walled carbon nanotubes nanocomposites," *Compos. PART A-APPLIED Sci. Manuf.*, vol. 82, pp. 208–213, 2016.

[34] S. M. Ha *et al.*, "Thermally conductive polyamide 6/carbon filler composites based on a hybrid filler system," *Sci. Technol. Adv. Mater.*, vol. 16, no. 6, p. 065001, 2015.

[35] J. D. Menczel and R. B. Prime, *Thermal analysis of polymers: Fundemental and applications*. JOHN WILEY & SONS INC, 2009.

[36] G. Kaiser, S. Schmölzer, C. Strasser, S. Pohland, and S. Turan, *Handbook DSC*. Netzsch, 2015.

[37] R. L. Blaine, "Polymer Heats of Fusion," *Therm. Appl. Note*, pp. 1–2.

[38] D. Garlotta, "A Literature Review of Poly (Lactic Acid)," *J. Polym. Environ.*, vol. 9, no. 2, pp. 63–84, 2002.

[39] X. Y. Zhao and B. Z. Zhang, "The effects of annealing (solid and melt) on the time evolution of the polymorphic structure of polyamide 6," *J. Appl. Polym. Sci.*, vol. 115, no. 3, pp. 1688–1694, Feb. 2010.

[40] H. Wu, C. Lu, W. Zhang, and X. Zhang, "Preparation of low-density polyethylene/low-temperature expandable graphite composites with high thermal conductivity by an in situ expansion melt blending process," *Mater. Des.*, vol. 52, pp. 621–629, 2013.

[41] I. Mazov, I. Burmistrov, I. Il'Inykh, A. Stepashkin, D. Kuznetsov, and J. P. Issi, "Anisotropic thermal conductivity of polypropylene composites filled with carbon fibers and multiwall carbon nanotubes," *Polym. Compos.*, vol. 36, no. 11, pp. 1951–1957, 2015.

Chapter 3

Increased through-plane thermal conductivity of injection molded thermoplastics by manipulation of filler orientation

3. 1. Abstract

This chapter aims to increase the through-plane thermal conductivity of polymer composites by adjusting the filler orientation. Two methods are tested: a combination of immiscible polymers, polypropylene (PP) and polyethylene terephthalate (PET) and adding a foaming agent (FA) to a polyamide 6 (PA6) based composite. In both , flake graphite was used as thermal conductive filler. Compounds with 10, 20 and 30 m% graphite were made for both methods. The through-plane thermal conductivity increased for all PA6-FA composites, while the in-plane TC decreased compared to PA6 without FA. PP-PET combinations generally outperformed the PP in through-plane performances as well.

Tensile strength decreased with increasing amounts of graphite. As expected, adding foaming agents and a second phase decreased strength as well compared with virgin materials. With further optimization, a combination of fillers and foaming agents in thermoplastics or two-phase systems could prove to be valuable in thermal management applications.

3. 2. Introduction

Increased thermal conductivity of intrinsically thermally insulating polymer resins could open a variety of new markets in the polymer industry. The heat exchanger market, strongly dominated by heavy, expensive and corrosion vulnerable metals, could make valuable use of these new kinds of polymers. Electronics packing, like LED housing, could vastly improve the operation lifetime by dispersing waste heat.

Research has shown that increased thermal conductivity can be achieved by adding thermal conductive fillers to the polymer matrix[1]–[3]. Here, it is of utter importance to take into account the anisotropy after processing. The thermal conductivity in the direction of the polymer flow (in-plane thermal conductivity) will reveal a far higher thermal conductivity compared with the direction perpendicular to the flow (through-plane thermal conductivity) [4]–[6]. While certain designs of heat sinks could benefit more from a high in-plane thermal conductivity[7], the majority of applications require an increased through-plane thermal conductivity for improved efficiency (e.g. shell-tube heat exchangers).

Despite the significant amount of research that has already been conducted on this topic, the best results can only be achieved by either adding stupendous amounts of fillers to the matrix or by compression moulding the composites[8]. Heavy filler loading can cause a severe decline in mechanical properties and hinder processing because of increased shear[9]. Compression moulding, on the other hand, is a less favourable technique when it comes to production efficiency, notably for more complex shapes or continuous profiles, where respectively injection moulding and extrusion are more common. Because of the lack of/low flow during compression moulding (compared with injection or extrusion), fillers won’t orientate much and

thus won't show such anisotropic properties. In order to achieve an enhanced thermal conductivity in the through-plane direction with low filler content and injection moulding or extrusion, the filler orientation must be manipulated. Filler orientation by magnetic fields or electrostatic charges have proven to improve thermal conductivity of thermosetting composites[10], [11]. However, the high viscosity of thermoplastics prevents these techniques from being used.

This research focuses on increasing the through-plane thermal conductivity of two different injection moulded systems: polyamide 6 (PA6)-graphite composites and polypropylene (PP)-graphite composites. In both systems, it is attempted to increase the through-plane TC by adjusting the final filler orientation. The PA6-system used foaming agents (FA) to achieve this goal, polyethylenterephthalat (PET) particles present to PP could cause a shift in orientation as well. Besides an increased through-plane thermal conductivity, the weight reduction caused by the foaming agents can be beneficial for several applications like automotive, further highlighting the relevance of the conducted research. Similar thermal performances with lower filler content could ease processing of the materials.

3. 3. Materials and methods

Injection-grade Polyamide 6 (Technyl C 230 Natural, Solvay) was employed as matrix material for the PA6-based composites. Polypropylene (575P, Sabic) and polyethylene terephthalate (PET;Lighter C93, Equipolymers) were used as matrix in the PP-PET composites. Grafted PP with maleic anhydride (PPgMA;Scona TPPP 2003, BYK) was employed as a compatibilizer.

Clusters of graphite filler (Timrex KS500, Imerys) with and average size of 250 micrometer, was used as thermal conductive filler in both cases. Endothermic carbon dioxide foaming agent (Cell Span CFA 897) was kindly provide by AxiPolymer.

PA6, PET and graphite were dried at 80°C overnight prior to compounding. Compounds of 10, 20 and 30 weight percentage (m%) graphite-PA6 were prepared by compounding in a twin-screw compounder (APV MP19TC-40, England). The filament from the compounder was cooled in a water bath, chopped in pellets and dried overnight at 80°C. The dried pellets were dry mixed with 3 m% foaming agents before injection moulding. An Engel e-victory 28T injection moulding system (Engel Austria) was used to produce tensile bars. No holding pressure was applied for the samples containing FA's. PP and PET (with and without PPgMA) were pre-compounded at a 7 to 3 ratio of PP to PET, pelletized and dried before compounding with graphite. The compounding with graphite employed temperatures below the melting point of PET, to avoid the graphite migrating to the PET-phase. A PP-PET blend with 1% of compatibilizer was created as well. PP, PP-PET and PP-PET-PPgMA were compounded with 10, 20 and 30 m% graphite. It could be argued that, since the graphite can't migrate to the PET phase, the artificial increase of graphite content in the PP phase could cause the increase in TC, rather than the adjusted orientation. Therefore, PP was compounded with graphite at 14, 26 and 38 m% graphite (correlated with the actual concentration of graphite in PP in the PP-PET-graphite composite) in order to compensate the artificial increase, further named 'PP adjusted'. This process is sketched in image 1. Holding pressure was applied to compensate for shrink. The compositions of all different samples made are shown in Table 1.

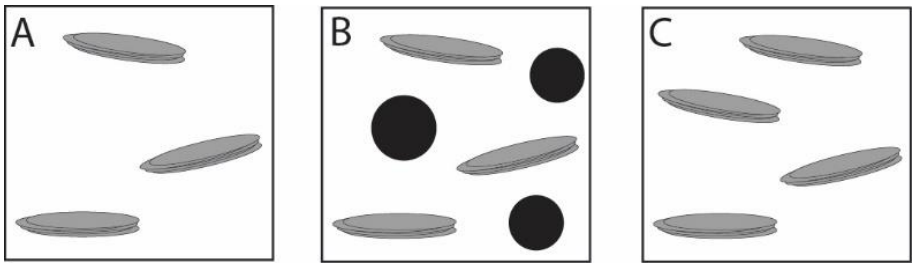

Figure 1: PP compensated samples. Assume system A where graphite (grey flakes) are dispersed in the PP matrix (white) at a concentration of, as example, 10 m%. System B represents the PP-PET-graphite composite (PET spheres in black). The system as a whole contains 10% graphite as well. Since the graphite cannot migrate to the PET, the actual concentration of graphite in the PP phase is higher than 10% (14% in a 7-3 PP-PET matrix). In order to wrongly conclude that the TC increased because of the orientation rather than this artificial increase of fillers in the PP-phase, a 'compensation' composite, system C, was made where the concentration of graphite in PP is equal to the concentration of graphite in PP in the PP-PET composite (14%, as seen in system B). Size, orientation and volume in this figures are not to scale nor representative for the actual orientation in the sample.

For thermal conductivity measurements, the wide part of the tensile bars closest to the injection gate was cut off and sanded (grit 500) to assure good contact between the sensor and sample. Prior to measuring material properties, all the samples were conditioned at 50% relative humidity at 23°C for at least one week.

The thermal conductivity of the samples were determined using the Transient Plain Source method with a Hot Disk TPS 2500S (Hot Disk Sweden) using the anisotropic module. This allowed the measurement of in-plane and through-plane thermal conductivity of the samples. Measurement time and power output of the sensor varied from sample to sample, so that probing depth remained around 2 mm (half sample thickness) in order to take the skin-core effect into account[12].

Table 1: composition of different samples in m%

	PA6	FA	PP	PET	PPgMA	graphite
PA6-0	100	-	-	-	-	-
PA6-10	90	-	-	-	-	10
PA6-20	80	-	-	-	-	20
PA6-30	70	-	-	-	-	30
PA6-FA-0	97	3	-	-	-	0
PA6-FA-10	87,3	3	-	-	-	9,7
PA6-FA-20	77,6	3	-	-	-	19,4
PA6-FA-30	67,9	3	-	-	-	29,1
PP-0	-	-	100	-	-	-
PP-10	-	-	90	-	-	10
PP-20	-	-	80	-	-	20
PP-30	-	-	70	-	-	30
PP-adj-10	-	-	86	-	-	14
PP-adj-20	-	-	74	-	-	26
PP-adj-30	-	-	62	-	-	38
PP-PET-0	-	-	70	30	-	0
PP-PET-10	-	-	63	27	-	10
PP-PET-20	-	-	56	24	-	20
PP-PET-30	-	-	49	21	-	30
PP-PET-PPgMA-0	-	-	69,3	29,7	1	0
PP-PET-PPgMA-10	-	-	62,37	26,73	0,9	10
PP-PET-PPgMA-20	-	-	55,44	23,76	0,8	20
PP-PET-PPgMA-30	-	-	48,51	20,79	0,7	30

Scanning Electron Microscopy images were taken on a Phenom G1 SEM (PhenomWorld, The Netherlands) using a ‘porous’ sample holder.

Tensile tests were performed on an Instron 5565 tensile bench (Instron USA). An extension meter was employed to determine the Young modulus at a tensile speed of 1 mm/min. The extension meter was removed after an extension of 0.3% and the test continued at a speed of 50 mm/min. The modulus was calculated as the slope between 0.05 and 0.25% strain within the Bluehill 2 software (Instron USA).

3. 4. Results and discussion

3. 4. 1. Thermal conductivity

The through-plane and in-plane thermal conductivity for the different compounds are displayed in Figure 2. As expected, both PA and PP shows an increasing thermal conductivity with increasing amount of graphite. The in-plane thermal conductivity increases more rapidly than the through-plane thermal conductivity. This phenomenon has two major causes, all related to alignment of the fillers due to the flow during processing. First of all, the graphite filler itself is anisotropic, with a higher thermal conductivity in the layer direction (in-plane) compared to the interlayer direction (though-plane). Secondly, the in-layer free path is far longer than the through-layer path, meaning less matrix-filler interfaces and shorter distances through the non-conductive polymer, thus a better thermal conductivity in that direction. These effects are visualized in Figure 3. The most efficient thermal paths for in-plane and through-plane conduction are drawn as a straight line and dotted line respectively. Each transition from interface is drawn encircled. This alignment due to flow is more outspoken in the skin layer of the samples, as shown in other research (skin-core effect)[12].

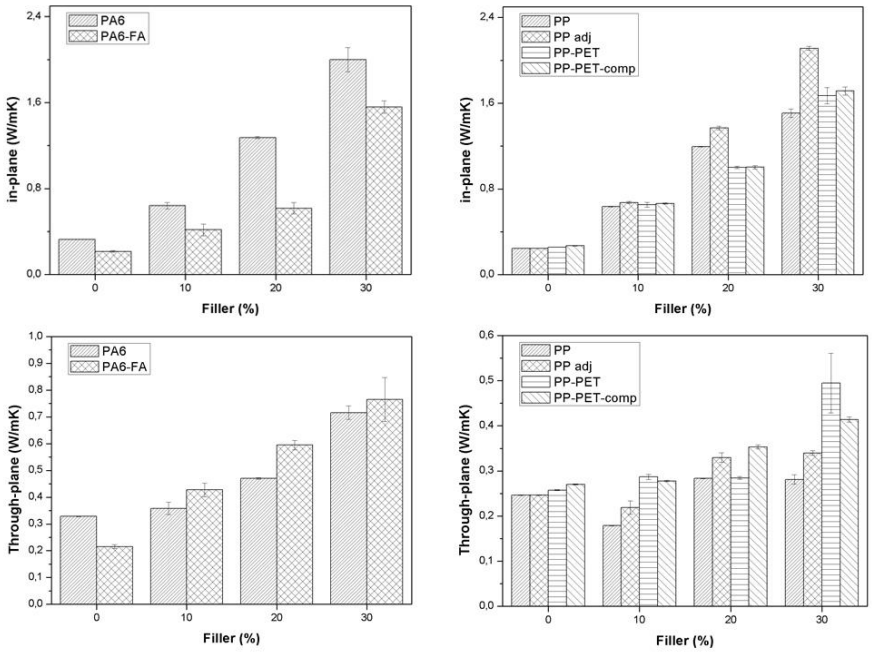

Figure 2: In-plane and through-plane thermal conductivity of the composites

Adding foaming agents to the PA6 composites causes a general decrease in thermal conductivity because of the insulating effect of (trapped) gas, which can clearly be seen in the virgin material with foaming agents. The through-plane thermal conductivity of 10 and 20 m% of fillers increases for the composite with added foaming agent. This effect becomes less outspoken at 30 m% of fillers. The in-plane thermal conductivity of the foaming compounds remains lower due to the insulating effect and the reduction of graphite platelets aligned in this direction. The increase in through-plane TC and decrease in in-plane TC for the PA6-foaming agent can be explained as following: the gas formed by the foaming agents starts to expand as the pressure in the system decreases. This expansion of gas causes the fillers to rotate, effectively declining the orientation in the in-plane direction and increasing the randomness of the filler orientation. This process is illustrated in Figure 4.

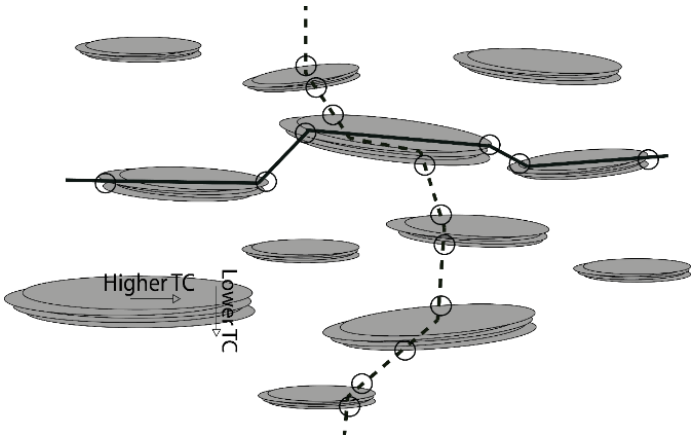

Figure 3: The orientation of the fillers after injection molding can explain the high in-plane and low through-plane thermal conductivity. The polymer flow during injection is from left to right (in-plane).

Strong anisotropy due to the air bubbles and graphite clusters can create local spots with strongly increased or decreased thermal conductivity, explaining the rather big deviation in the results. It is possible that the less outspoken effect of the through-plane TC with 30 m% filler is because the composite without foaming agent also starts to create a thermal conductive network through the thickness, meaning that the insulating effect of the foam starts to play a bigger role again.

Polypropylene shows a rather low TC for a semi-crystalline polymer. Adding PET increases the TC, and it even increases further with the addition of compatibilizers. These compatibilizers create a smoother transition from one phase to the other, decreasing the interfacial resistance. Though there seems to be no clear pattern in the thermal conductivity of the PP-PET and PP-PET-PPgMA composites with increasing graphite loading, there is a clear and large increase in through-plane thermal conductivity of PP-PET with 30 m% of graphite. It should be noted, though, that the deviation of these measurements were fairly large compared with other samples. Still, the PP-PET with 30 m% graphite showed a through-plane thermal conductivity higher

than the PP with 30 m% graphite and is also way above the adjusted PP. PP-PET-PPgMA with 30 m% graphite performed better that the (adjusted) PP 30 m% graphite, but its performance were inferior to those of PET-PP.

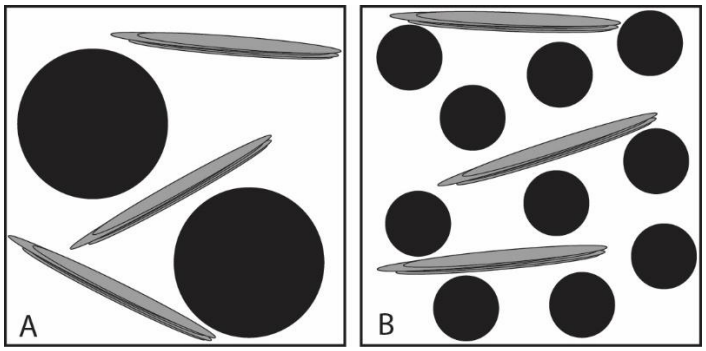

Figure 4: graphite filler orientation caused by PET particles. This 2D drawing shows in both cases A and B a same cross-section surface of 'PP matrix' (white, 70% minus graphite) and PET particles (black spheres, 30%). The larger PET particles physically hinder the graphite from orienting with the flow (left to right). This in contrast with the smaller particles as seen in B, whom are too little to physically hinder the graphite from orienting with the flow. This simplified drawing is not to scale with the actual PET particles and/or graphite platelets.

Three different theories can possibly explain this phenomena: PET forms large clusters in the PP phase. These large clusters, much like the foaming agent, hinder the alignment of the fillers with the flow. This causes in-plane TC to decrease and the through-plane TC to increase. PPgMA decreases the average size of PET particles. Once these particles are a couple of factors smaller than the average graphite flake, these will have little effect on the orientation of said flakes, as shown in Figure 5. SEM images of PP-PET without filler show that PET particles in the PP-PET system are not that much larger compared with the PP-PET-PPgMA system; though particles in the PP-PET system cluster together to form larger conglomerates, while the PET particles in the PP-PET-PPgMA system are more evenly distributed. Once these PET

particles/clusters are a couple of factors smaller than the average graphite flake, these will have little effect on the orientation of said flakes, as shown in Figure 5.

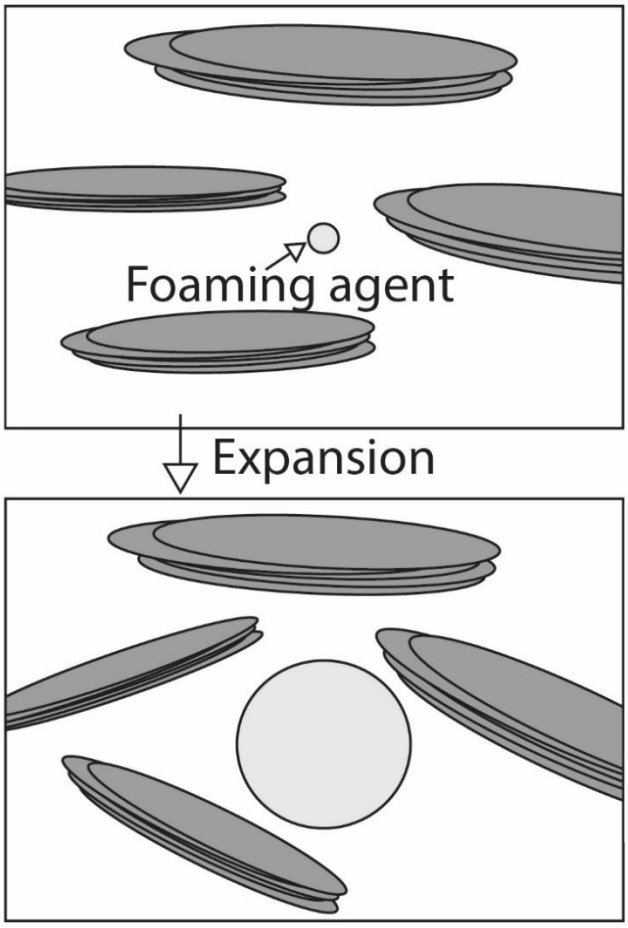

Figure 5: Expanding gas causes the fillers to re-orientate

Figure 5 also gives insight on the fact that, besides the relation between PET particle size and graphite platelet size, the ratio of PP-PET also play a significant role. For example, in case A, if the concentration (surface) of PET fraction were to be halved (i.e. only one sphere), the graphite could orient way easier with the flow, thus resulting in a lower through-plane TC.

A second theory is that (smaller) flakes of graphite prefer to be as close as possible to the more hydrophilic PET phase rather than the hydrophobic PP. This thermally conductive 'coating' around the spherical PET particles/clusters improves the through-plane thermal conductivity compared with PP, since spheres/clusters exhibit isotropic properties.

Last but not least, it might be possible that irregular PET particles disturb the linear flow behaviour of the polymer-composite. This more geometrically disturbed flow causes less orientation with the flow direction, resulting in an improved through-plane thermal conductivity

3. 4. 2. Tensile strength

The modulus, tensile stress at yield and strain at break are shown in Figure 6. The results are within the line of expectation for PA6: the modulus decreases with addition of foaming agents, but increases with increasing amount of graphite. The tensile stress at yield decreases with increasing amount of filler, which could be explained by the low tensile strength of graphite, presence of poorly dispersed graphite clusters and relative weak interaction between the matrix and fillers. This poor interaction between filler and matrix also explain the significant decrease in strain at break. From SEM analysis (Figure 7) it follows that the dispersion of graphite in the composite wasn't optimal, as some graphite plates were still forming clusters in the composite. Gas pockets introduced by the foaming agents further decrease the mechanical properties.

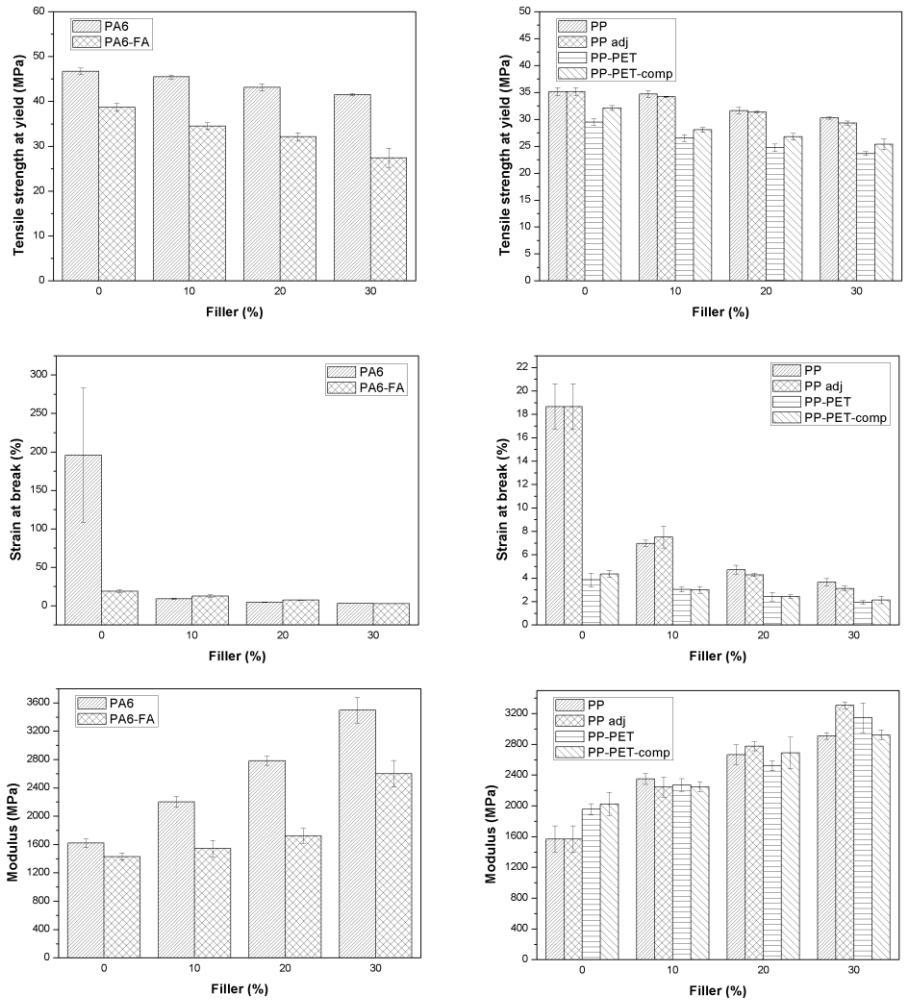

Figure 6: Modulus, tensile stress at yield and elongation at break of the different compounds. In general, FA's and graphite have a negative impact on the properties

The results of the PP, PP-PET and PP-PET-PPgMA composites are in line with expectations as well: adding a second phase (PET) decreased the tensile strength and strain because of poor compatibility of both phases. The modulus of PP-PET increases compared with PP because of the higher modulus of PET. Adding graphite further decreases the strength and strain while increasing the modulus, as seen with the PA6 composites. Adding compatibilizer slightly increases the interaction between the PP

matrix and PET particles. This can be seen in the tensile strength, where the PP-PET-PPgMA and its composites perform slightly better than the PP-PET and their composites.

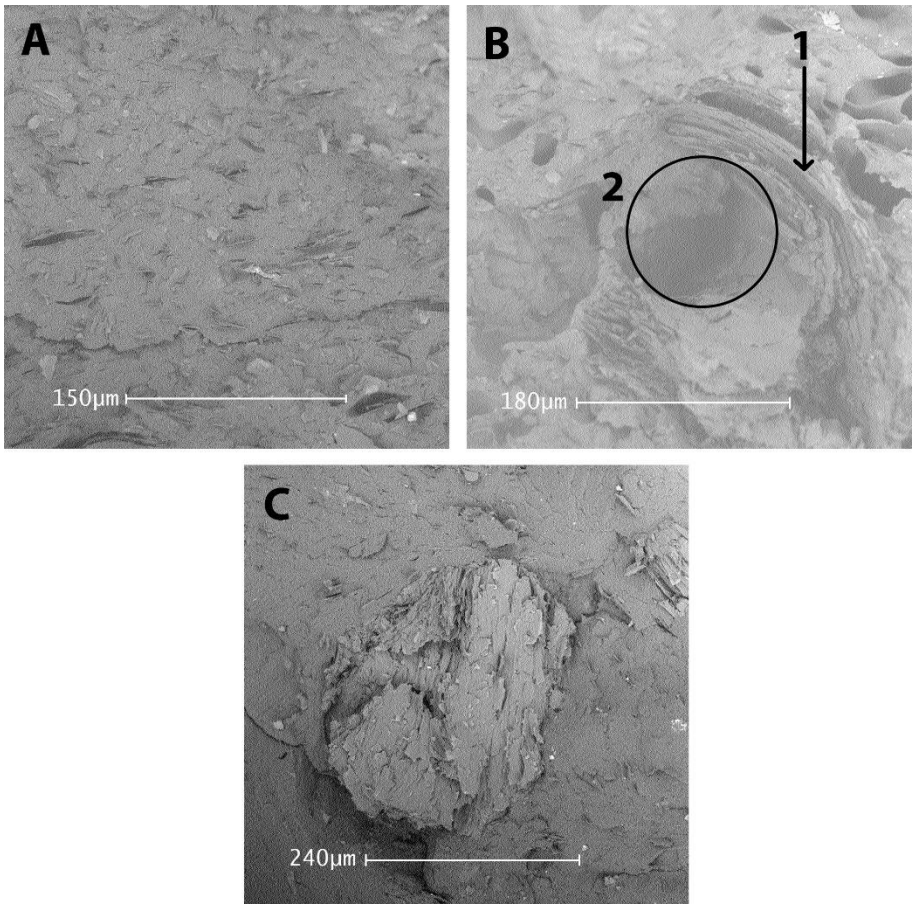

Figure 7. SEM images of (A) PA6 with 10 m% of graphite (B) PA6 with 30 m% graphite and FA and (C) PA6 with 10 m% graphite. Indicated in image B is (1) the graphite platelet and (2) a bubble caused by expanding air.

3. 4. 3. Scanning Electron Microscopy

Figure 7A and B shows the composite of 30 m% graphite without and with FA, respectively. The pictures are taken from side view, the desired through-plane

direction is from the top to the bottom of the image. Image A clearly shows the graphite plates have a preferred orientation, that being the direction of flow during the injection process. This readily explains the high in-plane and lower through-plane thermal conductivity. Image B shows the graphite (1) being bend in a more through-plane direction by a bubble (2), most likely caused by the expansion of the FA (cf. Figure 3). This shows how the through-plane TC increases whilst decreasing the in-plane TC.

For completeness, Image C (PA6 with 10 m%) shows a large cluster of poorly dispersed graphite. While this will likely improve both in- and though-plane TC (since a sphere won't orientate with the flow and a cluster reduces the amount of matrix-filler interfaces), it will most certainly decrease the mechanical properties of the material.

SEM images of PP-PET and PP-PET-PPgMA show that average particle size differs little, though the spread is larger for the PET particles without compatibilizer. PET particle shapes other than spheres also appear in the PP-PET system without compatibilizer, while these are absent in the PP-PET-PPgMA system. PET particles in PP-PET form larger clusters and poor adhesion with PP, while PET particles in the PP-PET-PPgMA form smaller clusters and are better dispersed overall.

Images of PP-PET combined with graphite showed very poor contrast between filler and matrix, making it difficult to distinguish one from another. The theory of increased thermal conductivity caused by adjusted filler orientation could thus not be confirmed visually for PP-PET blends.

3. 5. Conclusions

Despites the well-known insulating effect of foaming, the combination of FA's and thermal conductive fillers can improve directional TC by changing the filler orientation caused by processing. As an inevitable side effect, the thermal conductivity in the opposite direction decreases. This effect is mostly visible at lower filler loadings, as the difference between through-plane TC with and without FA decreases with increasing graphite content. On the other hand, the TC of the PP-based composites show the highest differences at 30 m% of filler. The through-plane TC of PP-PET outperformed PP and PP adjusted for 30% filler. Different theories were discussed for this phenomena, but none could be confirmed by SEM. PET particles in combination with compatibilizer were likely too small to cause noticeable orientation adjustment in the samples, thus only slight improvement was noticeable.

The yield strength of the samples decrease with increasing amount of fillers, due to the inferior tensile properties of graphite in general and poor interaction between filler and matrix. Lumps of badly wetted and distributed graphite reduce the yield strength even more. Gas bubbles caused by the foaming agent reduce the strength further for PA6 while poor compatibility between PET and PP decreased the mechanical properties for the PP-based materials. Adding compatibilizers to the system does improve the properties, but strength remained below that of PP or PP adjusted.

Because of the high Young modulus of the filler, the Young modulus of the composites increased as well with increased graphite content.

Further optimization concerning the yield strength and fine-tuning the TC by controlling the size and amount of gas bubbles/PET spheres could prove these materials to be useful for thermal applications that require through-plane TC rather

than in-plane TC. Better dispersion of the graphite could improve the mechanical properties and reduce local differences in TC or properties. Addition of short fibre reinforcements or swapping graphite for carbon fibre in general could be considered for both improved strength with increased thermal conductivity, though there is a significant price difference between graphite and carbon fibre.

REFERENCES

[1] N. Burger, A. Laachachi, M. Ferriol, M. Lutz, V. Toniazzo, and D. Ruch, “Review of thermal conductivity in composites: Mechanisms, parameters and theory,” *Prog. Polym. Sci.*, vol. 61, pp. 1–28, 2016.

[2] H. Chen *et al.*, “Thermal conductivity of polymer-based composites: Fundamentals and applications,” *Prog. Polym. Sci.*, vol. 59, pp. 41–85, 2015.

[3] Z. Han and A. Fina, “Thermal conductivity of carbon nanotubes and their polymer nanocomposites: A review,” *Prog. Polym. Sci.*, vol. 36, no. 7, pp. 914–944, 2011.

[4] M. G. Miller, J. M. Keith, J. A. King, B. J. Edwards, N. Klinkenberg, and D. A. Schiraldi, “Measuring thermal conductivities of anisotropic synthetic graphite-liquid crystal polymer composites,” *Polym. Compos.*, vol. 27, no. 4, pp. 388–394, Aug. 2006.

[5] A. R. J. Hussain, A. A. Alahyari, S. A. Eastman, C. Thibaud-Erkey, S. Johnston, and M. J. Sobkowicz, “Review of polymers for heat exchanger applications: Factors concerning thermal conductivity,” *Appl. Therm. Eng.*, vol. 113, pp. 1118–1127, 2017.

[6] T. Wieme, D. Tang, L. Delva, D. R. D’hooge, and L. Cardon, “The relevance of material and processing parameters on the thermal conductivity of thermoplastic composites,” *Polym. Eng. Sci.*, vol. 58, no. 4, pp. 466–474, Apr. 2018.

[7] I. Mazov, I. Burmistrov, I. Il’Inykh, A. Stepashkin, D. Kuznetsov, and J. P. Issi, “Anisotropic thermal conductivity of polypropylene composites filled with carbon fibers and multiwall carbon nanotubes,” *Polym. Compos.*, vol. 36, no. 11, pp. 1951–1957, 2015.

[8] S. Takahashi, Y. Imai, A. Kan, Y. Hotta, and H. Ogawa, “Dielectric and thermal properties of isotactic polypropylene / hexagonal boron nitride composites for high-frequency applications,” vol. 615, pp. 141–145, 2014.

[9] N. S. Enikolopyan and I. O. Stalnova, “Filled Polymers : Mechanical Properties and Processability,” *Adv. Polym. Sci.*, vol. 96, pp. 1–67, 1990.

[10] Z. Lin, Y. Liu, S. Raghavan, K. Moon, and S. K. Sitaraman, “Magnetic Alignment of Hexagonal Boron Nitride Platelets in Polymer Matrix : Toward High Performance Anisotropic Polymer Composites for Electronic Encapsulation,” *ASC Appl. Mater. Interfaces*, vol. 5, pp. 7633–7640, 2013.

[11] K. Kim and J. Kim, “Vertical filler alignment of boron nitride/epoxy composite for thermal conductivity enhancement via external magnetic field,” *Int. J. Therm. Sci.*, vol. 100, pp. 29–36, 2016.

[12] T. Wieme, L. Duan, N. Mys, L. Cardon, and D. R. D’hooge, “Effect of Matrix and Graphite Filler on Thermal Conductivity of Industrially Feasible Injection Molded Thermoplastic Composites,” *Polymers (Basel).*, vol. 11, no. 1, 2019.

Chapter 4

Chemical modification of carbon nanotubes in view of composite production with better control over macroscopic properties including conductivity

4. 1. Abstract

Carbon nanotubes (CNTs) are chemically modified to obtain multifunctional CNT-monomers aiming at subsequent CNT-based network polymer formation. Four chemical modification routes have been attempted focusing on the relevance of the stoichiometry of the reaction conditions. The targeted 3D structures are a Bakelite, an epoxy, a polyurethane and a polyamide based network. DSC, TGA and FTIR analysis are performed to confirm the success of the CNT-functionalization and network formation, though strong contamination prevented interpretation so far. For the Bakelite synthesis route, a solid mass is obtained after doping the reactant with phenol, though it is likely that the obtained composites are rather CNTs dispersed in Bakelite matrices than a nanotube-based polymer. The polyamide-based modification results in a fiber-like structure that is not dissolvable nor dispersible in water or ethanol, indicating that a polymerization has taking place. Nevertheless, further analysis is still needed to support this claim.

4. 2. Introduction

Ever since the discovery of carbon nanotubes (CNTs) in 1991 [1], their properties have baffled scientists and engineers. Essentially a CNT is based on the rolling up of sheet of graphene, with each sheet in turn a single layer of sp2-hybridized carbon, as can be seen in Figure 1 (middle) resulting in a hexagonal 'honeycomb' configuration. In general, CNTs can appear as 'zigzag', 'armchair' or 'chiral' depending on how the graphene is rolled up. The ends of these nanotubes are capped with half buckyballs (fullerene; Figure 1; left). CNTs can be divided in different classes by how many layers of tubes encapsulate one another. Single-walled carbon nanotubes (SWCNTs) exist out of a single rolled up sheet of graphene (Figure 1; middle), whereas few-walled carbon nanotubes (FWCNTs) and multi-walled carbon nanotubes (MWCNTs) consist of multiple of these nanotubes nested in one another (Figure 1; right). SWCNTs possess diameters of *ca.* 0.8 to 2 nm, while MWCNTs typically possess diameters in the range from 5 to 20 nm and more. The length of a nanotube can range from a few 100 nanometer to a few centimeters [2].

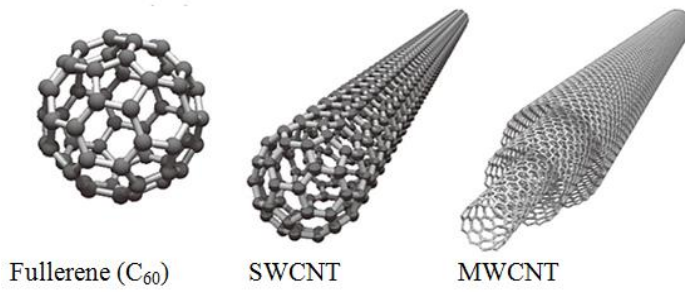

Figure 1: from left to right a buckminsterfullerene (C60) or 'bucky ball', an end-capped single wall carbon nanotube (SWCNT) and a multi-walled carbon nanotube (MWCNT)[3]

With measured tensile strengths up to *ca.* 60 GPa for MWCNTs and an estimate 300 GPa for SWCNTs [4], CNTs exhibit the second highest strength-to-mass ratio of any

material ever measured, only being surpassed by graphene itself. This, combined with a claimed Young modulus of 1.8 TPa [5], offers mechanical properties as never seen before. Furthermore, a MWCNT is an electric conductor capable of carrying heavy currents without heating [6], while a SWCNT can be semi-conducting or conducting [2]. The thermal conductivity of a SWCNT can reach up to 3500 W m^{-1} K^{-1} [2], making it the second most thermal conductive material at room temperature, only to be exceeded by graphene again.

On the downside, however, it seems to be very challenging to extrapolate these properties to macro-scale applications [7], [8] in which the nanotubes are embedded. While great improvement of mechanical properties can be noticed in polymer composites at low CNT loading levels, these barely come close to the properties of a pure nanotube. Besides that, CNTs happen to be incredibly difficult to efficiently incorporate in matrices, as they tend to form clusters. Weaker properties of the CNT-matrix composites can be partially traced back to the poor dispersion, with the composite failing because the CNT-CNT and CTN-matrix interactions fail rather than the CNT itself fails. Conventional polymer processing such as melt mixing can already achieve in certain cases acceptable dispersion [9], though too long mixing times can introduce nanotube breakage and polymer degradation [10]. A strong interaction between the nanotube and the matrix should be present for the stress to be elegantly transferred to the nanotubes [11]. Even though functionalization of the nanotubes can increase the interaction [9], the resulting composite properties are still far from what a single nanotube can achieve.

A single CNT can already achieve lengths up to a few centimeters[2], which is much longer than common polymer chains with for instance 10^5 monomer units and likely a coiled configuration at the nm scale[12]. Research has shown that mats or ropes of

these materials, while being incredibly strong, are still far from what a single nanotube can be[6]. This is because a mat or rope of nanotubes are more or less single nanotubes laid out next to and/or on top one another. To achieve better properties, the nanotubes should be more entangled [7] or interconnected. Breaking and chemically re-bonding these nanotubes could achieve a higher order of connectivity resulting in stronger interactions in between nanotubes, thus improving macroscopic properties. Excessive branching during these chemical modifications could even further improve physical entanglement. A complete 3D network structure, equivalent to thermosetting polymers, would even go a step further, fully chemically bonding all carbon nanotube fragments instead of relying only on physical entanglement or basic chemical interaction, Van der Waals forces and pi-pi-stacking [6], [13]–[15].

In the present work, focus is on the synthesis of a macro-scale CNT-based composite material that can achieve properties close(r) to these of a single nanotube. To achieve this, preliminary results are reported regarding the post-modification or in brief "polymerization" of CNT's toward CNT physical/chemical networks to enable a better interaction and composite integration. Polyamide, Bakelite, polyurethane and epoxy-based systems were chosen to investigate.

A more detailed explanation of the theory and reasoning behind the chosen pathways can be found in Appendix B.

4. 3. Materials and methods

4. 3. 1. Materials

Multi-walled carbon nanotubes (NC7000) were purchased for Nanocyl (Belgium). The tubes were produced by catalytic chemical vapor deposition. Single walled

carbon nanotubes (purity > 60%) were purchased from US Research Nanomaterials Inc. (USA). Potassium bromide (IR spectroscopy grade), sodium hydroxide pellets, anhydrous calcium sulfate, tetrahydrofuran (THF), fomaldehyde 37%, hydrogen peroxide 35%, methanol, and *n*-hexane were purchased from Chem-lab Analytical (Belgium). (3-Amonopropyl)trioxysilane (APTES), sebacoyl chloride, dibutyltin dilaurate (DBTDL), ethylene diamine, hexamethylenetetramine, Hexafluorophosphate Azabenzotriazole Tetramethyl Uronium (HATU), 4,4' methylenebis(phenylisocyanate) (MDI) and (±)-epichlorohydrine were purchased from Sigma-Aldrich (Germany). Iron II sulphate heptahydrate was obtained from Merck (Germany). Phenol was purchased from Arcos Organics (Belgium). A commercial epoxy harder (Epoxy-BK, component B) was purchased from Voss Chemie (Germany). All chemical were used as received if not stated otherwise.

4. 3. 2. Characterization

Differential Scanning Analysis (DSC) was performed on a Netzsch Polyma (Germany) with Pt-Rh or Aluminum concave pans with closed lids, not pierced. Infrared samples were manufactured by intensively mixing 200 mg Potassium Bromide with 0.30 mg sample with mortar and pestle and pressing it to disks. The CNTs were dried for at least 24h at 80°C before being mixed and pressed in tablets. Before measurement, all the samples were dried at 80°C in vacuum. Fourier-transform infrared spectroscopy FTIR analysis was performed on a Bruker Tensor 27 (USA) with a resolution of 4 cm^{-1} and 20 scans per sample, unless mentioned otherwise. Thermal gravimetric analysis (TGA) tests were performed using a Netzsch Jupiter STA 449 F3 (Germany) in Platinum-Rhodium crucibles following a temperature trajectory from 60°C to 800°C increasing by 10°C min^{-1}.

4. 4. Results and discussion

4. 4. 1. Precursors

4. 4. 1. a. Hydroxylation of carbon nanotubes

Two methods for hydroxylation of CNTs were investigated. The first method consists of stirring CNTs in a strong basic environment with hydrogen peroxide, based on the synthesis of Li et al.[16], with some minor adjustments, while the other method makes use of Fenton reagent. The main reactions for both methods are shown in Figure 2.

In the first method, 250 ml of a 10 mol L^{-1} NaOH solution was cooled to room temperature and 2.5 g of MWCNTs were added in a 500 ml Erlenmeyer flask. The solution was put in a ultrasonic bath for 30 minutes. Next, the solution was put on a stirring plate and 10 mL H_2O_2 was added dropwise. After 20h stirring, the solution was put in a separation funnel and allowed to let the nanotube float to the surface. The nanotubes were separated, filtered, washed with distilled water until pH neutral state and dried in a furnace at 80°C for 24h (henceforth called MWCNT-OH).

For the Fenton reagent based method, 1.5 g of MWCNT was added in 450 mL H_2O and put in an ultrasonic bath for 1h. Afterwards, the mixture was put on a stirring plate and 0.75 g $FeSO_4.7H_2O$ was added. While stirring, 150 ml H_2O_2 was added dropwise. The mixture was stirred for 24h and filtered, washed and dried in an oven at 80°C (henceforth called f-MWCNT-OH).

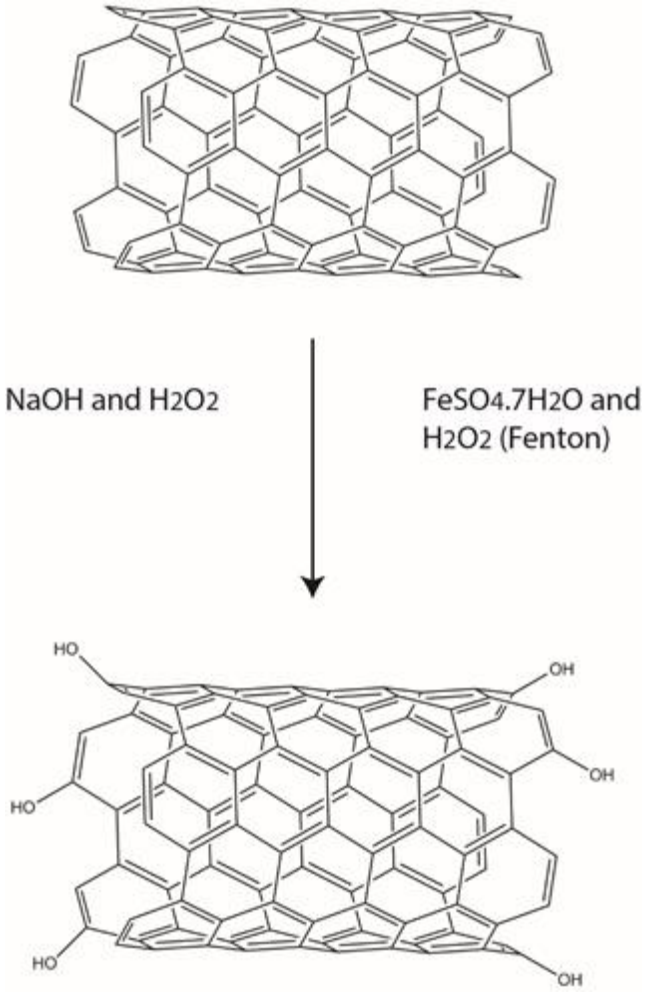

Figure 2: Hydroxylation of carbon nanotubes (precursor synthesis part 1) via method 1 and method 2. The reported results in the present work focus mostly on method 1.

The TGA curves of untreated MWCNTs and hydroxylated CNTs are shown in Figure 3.

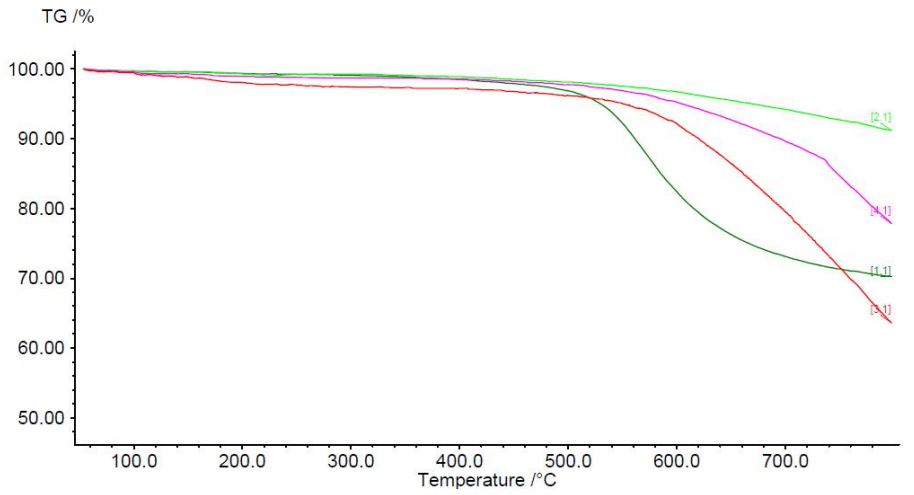

Figure 3: TGA curves of as-received MWCNT's (red and magenta) and MWCNT-OH (light and dark green).

The weight loss found in the MWCNT-OH is caused by the elimination of hydroxyl functional groups and the disordered carbon [17], though it should be noted that in the other cited sources, this is a two-step decay starting around 350°C. The TGA results show great variation, even amongst the same material under the same conditions. It is unclear what caused these large variations, but it shows that great care should be taken with interpretation of these results.

As far as FTIR spectra are concerned, great care should be taken with interpretation of the data, as it seems that contamination of an unknown source has taken place in nearly every sample, including KBr, as seen in Figure 4 (blue). Even though every sample was dried, all the spectra show the classic broad (mostly water-related) hydrogen-oxygen peak (H-bridge) at 3450 cm^{-1}. The recognizable peak between 2800 and 3000 cm^{-1} indicates the stretch of C-H bonds. More specifically, a triple forked peak indicates the presence of a $–CH_3$ bond, which normally is not present in CNT, before nor after any reaction described in this chapter, and certainly not in KBr. Figure

4 also shown the spectrum of MWCNT-OH when using the contaminated KBr as background signal, in red. This spectrum is still somewhat interpretable, likely because the KBr blanc and MWCNT-OH were from the same pressing badge. The first highlighted peak around 3600 cm^{-1} can be linked to free O-H stretch, though in most cases the peak should be smaller. The second peak, located at 3400 cm^{-1} can be linked to O-H bridge formation, potentially due to water or hydrogen bridge formation between different hydroxyl functional groups in the MWCNT-OH. The strange peak at the large section between 3400 and 2500 cm^{-1} (not highlighted) is likely overcompensation for the CH_3 bonds in the contaminated blanks. The last and largest peak located around 1100cm^{-1} can mostly be linked to carbon-oxygen stretch. Thus, the presence of O-H and C-O vibrations indicate that hydroxyl groups are indeed added onto the carbon nanotubes.

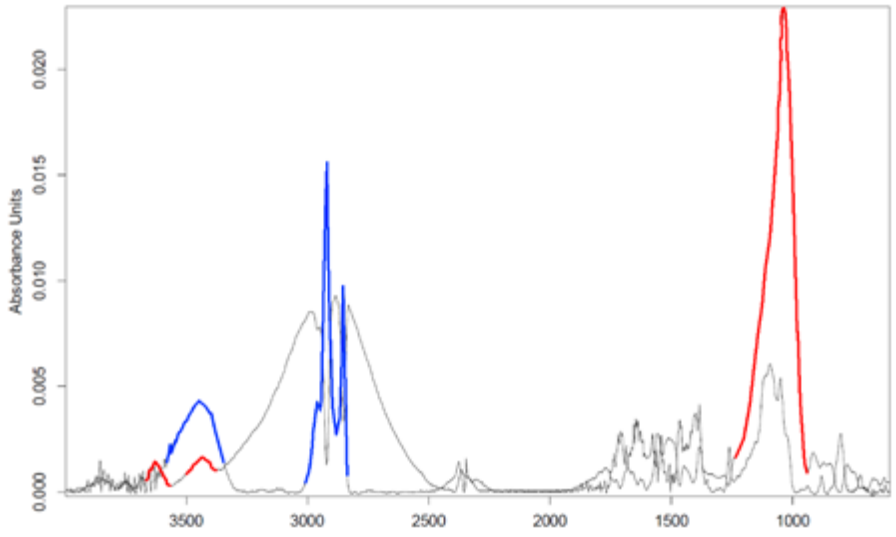

Figure 4: FTIR spectra of contaminated KBr with most important peaks highlighted in blue, and MWCNT-OH, with the most important peaks highlighted in red.

Other FTIR samples were unfortunately to heavily contaminated to extract any useful information. At this point, the source of contamination is still uncertain. New samples containing more CNT's for stronger signals should be measured, once the source of contamination has been confirmed.

4. 4. 1. b. Carboxylation of carbon nanotubes

SWCNT's were carboxylated by adding 0.5 g of the SWCNT's to 200 mL of a H_2SO_4-HNO_3 mixture in a 3-1 volume ratio and put in a ultrasonic bath for 3h at 40°C, as described by Ramanathan et. al. [18]. After that, the slurry was diluted with 250 mL distilled water and filtered over a 0.65 µm polyvinylidene difluoride (PVDF) membrane. The CNTs were washed with distilled water until pH neutral state and dried in an oven for 24h at 80°C (henceforth called SWCNT-COOH). The chemical modification is shown in Figure 5.

Both FTIR and TGA testing of the carboxylated carbon nanotubes were performed, but the results were not open to interpretation due to contamination.

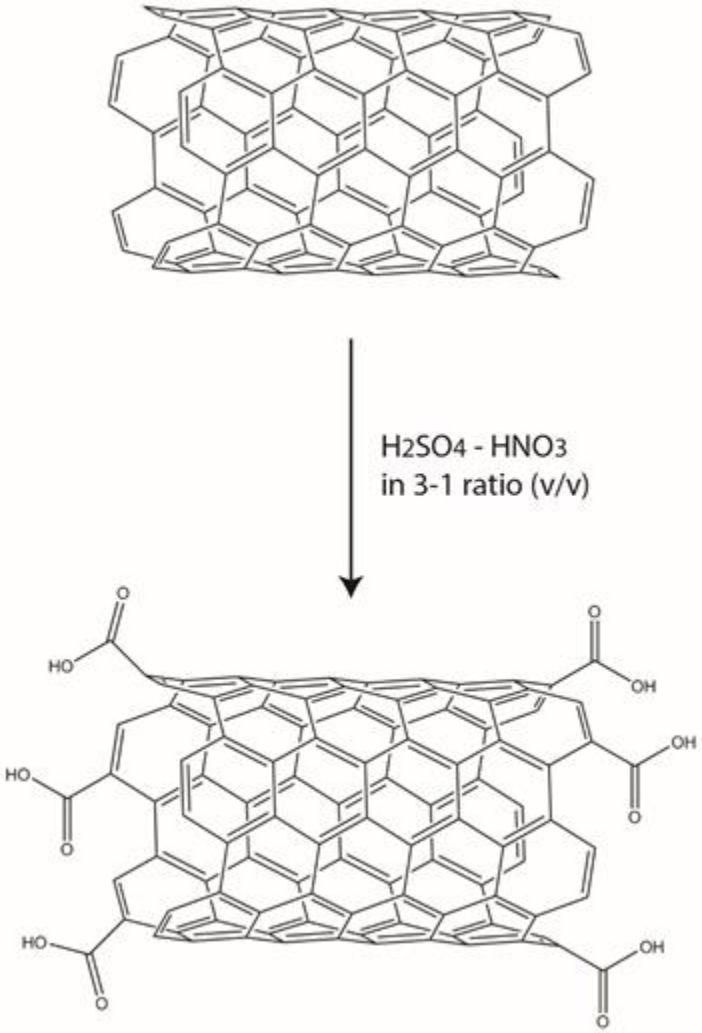

Figure 5: Carboxylation of carbon nanotubes

4. 4. 2. Network formation

4. 4. 2. a. Bakelite modification route

0.770 g MWCNT-OH was crushed with a mortar and pestle, and added in an Erlenmeyer flask with 200 mL distilled water. Subsequently 1 g NaOH and 15 mL formaldehyde were added. The mixture was stirred for 4 hours at 80°C. After that, the temperature was increased to 180°C and all the water was allowed to evaporate. At the end of the reaction, a white-grey powder was left, which was still dissolvable/dispersible in water after ultrasonic treatment. No analysis was performed on these samples.

In another configuration, 1g MWCNT-OH, 1.18 g phenol and 20 mL formaldehyde were added in a beaker. 20 mL of a 5 mol L^{-1} NaOH solution was added. The solution was stirred at 80°C for 1h. The temperature was further increased to 180° for several hours. A solid black ball was formed in the beaker, as seen in Figure 6A, leaving behind a red-ish liquid indicating that all the nanotubes were contained in the ball. After further heating, the red-ish liquid turned into a red-yellow powder (Figure 6B).

The spherical shape of the Bakelite CNT can be explained by the presence of a stirring bar during polymerization, pushing and rolling the growing polymer against the beaker wall, with the resulting ball having the same diameter as the space between the end of the stir bar and the beaker wall. At this point, it remains unclear whether the carbon nanotubes are chemically incorporated in the polymeric structure as intended, or if the nanotubes are just dispersed in the Bakelite. Further analysis is thus needed.

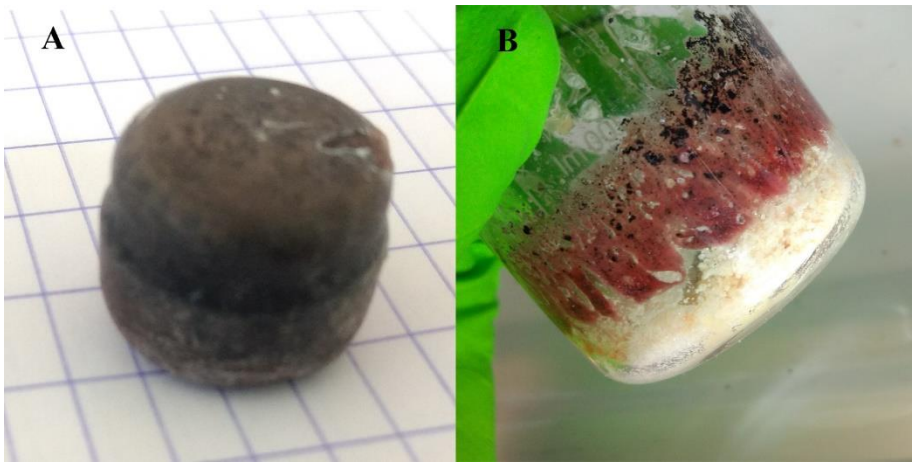

Figure 6: A: the black ball after the Bakelite modification attempt with phenol; B: rest fraction in the beaker with possibly NaOH (white), Bakelite (red) and spatters of CNT (black) left in the beaker

As it was unclear whether any reaction with the nanotubes occurred, a second configuration was prepared as following: 2 g NaOH was dissolved in 20 mL distilled water and 0.1g MWCNT-OH was dispersed in 30 mL water by ultrasonic treatment for 15 min. 1 mL of the NaOH solution and 2 mL formaldehyde were added. After another 15 minutes of ultrasound, the sample was stirred for 3h at room temperature. Samples were taken for DSC and FTIR analysis. The temperature was increased to 85°C and the reaction mixture stirred for another 4 h, after which new samples were taken for FTIR analysis. No further curing was attempted.

DSC analysis of the hydroxylated carbon nanotubes with formaldehyde and NaOH has been performed from room temperature till 90°C. As fear for potential damage to the equipment when using aluminum crucibles (side reaction of NaOH with aluminum), the first tests were performed in Platinum-Rhodium crucibles. The DSC of hydroxylated CNTs with formaldehyde and NaOH; and water with formaldehyde

and NaOH as a ‘reference’ are shown in Figure 7, with temperature increase till 90°C and 200°C at the same rate.

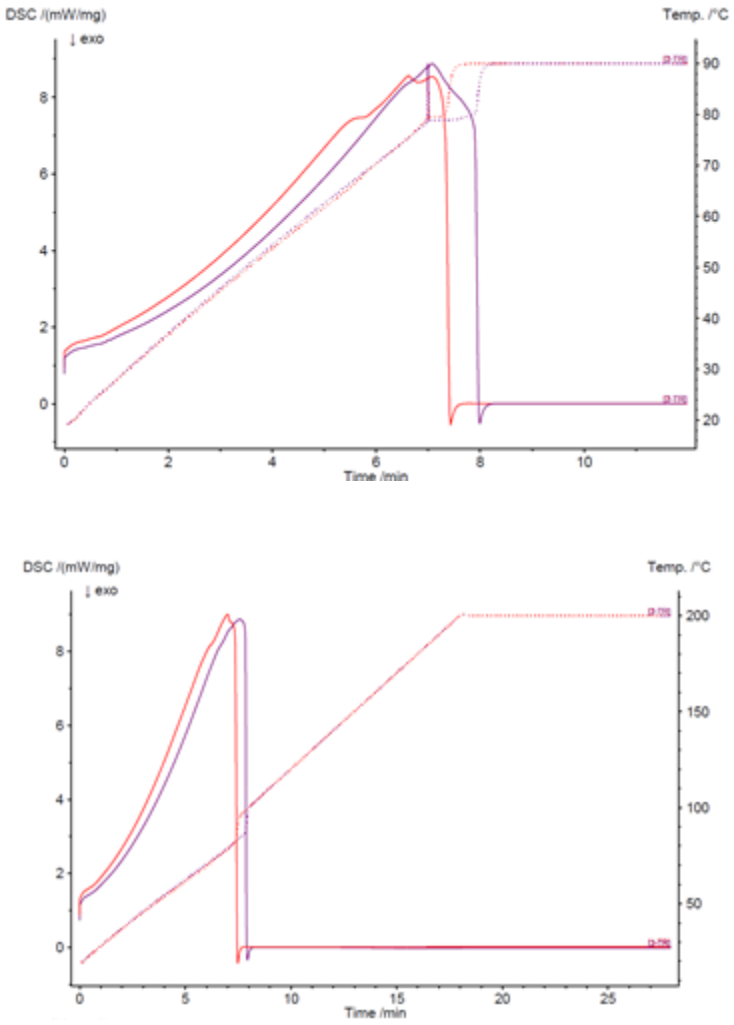

Figure 7: DSC results of hydroxylated carbon nanotubes with formaldehyde and NaOH in red; water with formaldehyde and NaOH in purple; top figure to 90°C; bottom to 200°C.

A sudden temperature spike is noticeable in the top curve, for both the system with and without CNTs, while this spike is absent in the curve to 200°C. The sudden, sharp

increase in temperature and drop in DSC signal at this point is likely coupled to the evaporation of water, as the DSC signal returns to zero. The flat line at 80°C in the top DSC curve with sudden increase to 90°C makes it look like a phase transition is occurring at this temperature. In order to give more meaning to this data, a mixture of phenol, formaldehyde and NaOH and their 'blanks' has been subjected to the same thermal analysis in the DSC, also in open Platinum-Rhodium cups. These DSC results are shown in Figure 8.

In the DSC analysis to 90°C, the same phenomenon as in previous DSC analysis is visible: a sudden spike at 80°C, a flat line around this temperature and a sudden increase to 90°C. The phenol-NaOH and formaldehyde-NaOH show a sharp decrease in DSC signal after 90°C is reached, with a bounce-back in the formaldehyde-NaOH system. The phenol-formaldehyde-NaOH (red) system shows a systematic increase in temperature rather than an isotherm followed by a sharp increase. However, the decrease of DSC signal to 0 eventually, in both the temperature programs, indicate that no material is left after the evaporation. After the analysis though, a red, solid substance is discovered in the phenol-formaldehyde-NaOH crucible. It is possible that the mass of this sample was too small compared with the start mass that no signal could be detected.

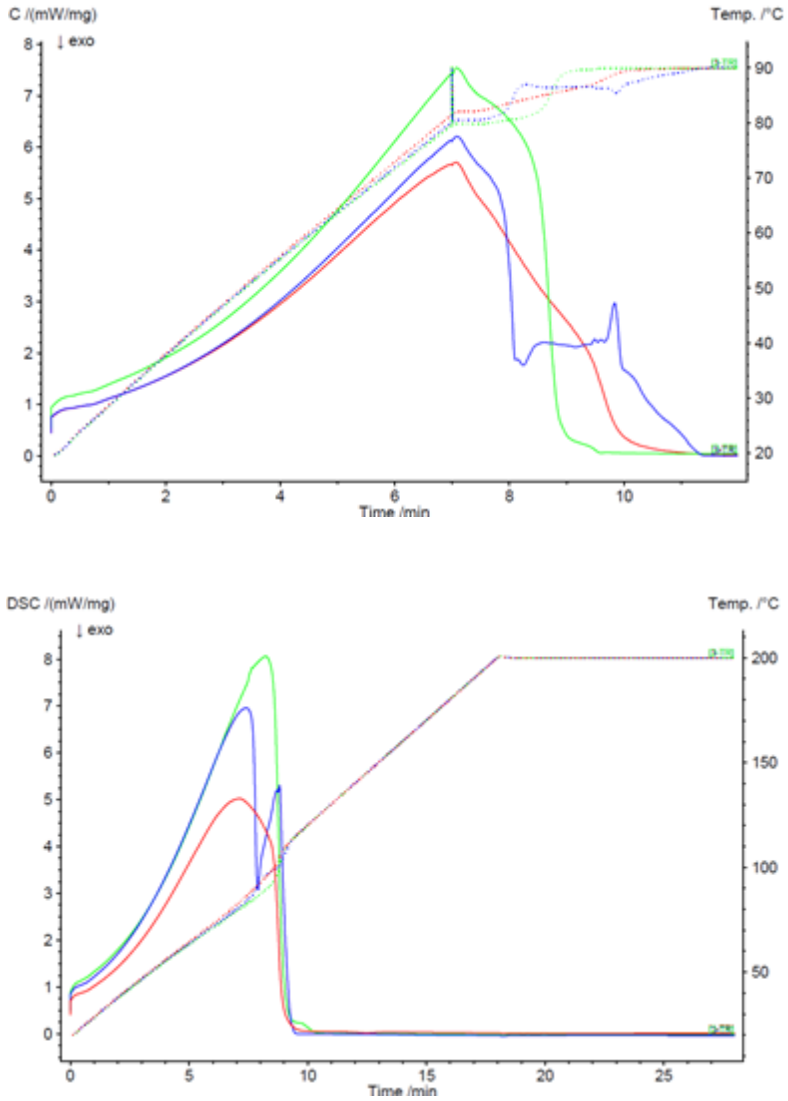

Figure 8: DSC results for phenol, formaldehyde and NaOH (red), phenol and NaOH (green) and formaldehyde and NaOH (blue) to 90°C (top) and 200°C (bottom).

Using the compositions as described in the Experimental section, closed aluminum crucibles were used anyway (cf. Figure 9) after verifying their resistance to the basic environment. This in order to be able to measure any changes without the interference of the solvent evaporating.

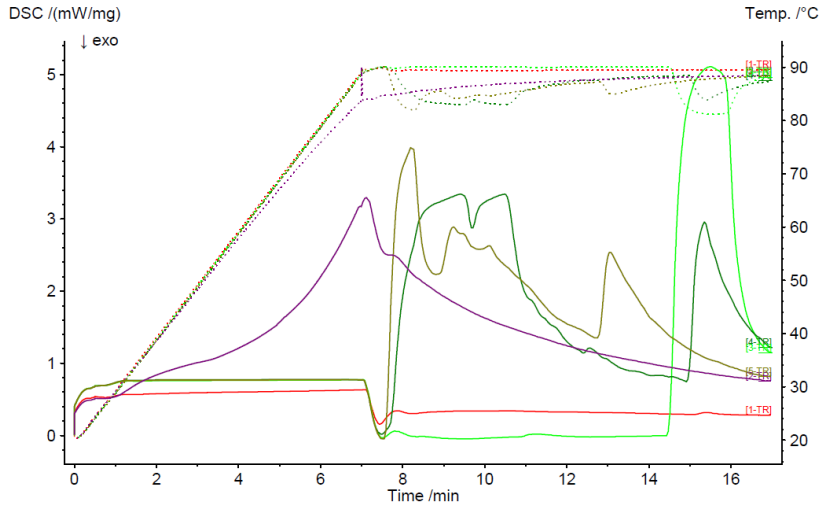

Figure 9: 2 DSC runs of water and formaldehyde in closed, non-pierced aluminum crucibles. The three green-tinted curves show different runs of water, while red and purple are formaldehyde as-received.

For water, the linear temperature increase seems to show no issues here, though it is more than clear that the isothermal region is unstable. On the other hand, as-received formaldehyde shows no predictable pattern, as the red and purple curves look nothing alike. Hence, it is clear that further experiments on DSC with water or formaldehyde containing solvents are not interpretable for analysis. It was thus not possible to monitor the reaction using DSC.

Much like the other FTIR scans, heavy contamination made analysis impossible.

4. 4. 2. b. Epoxy based modification route

As to the best of the author's knowledge, no epoxide functionalization of CNTs has been attempted, this synthesis was partially based on the reaction of 2,6-di(p-hydroxystyril)pyridine as described in NASA-Ames report on 'New polymers for composites' by E. M. Pearce [19].

Here, 0.61 g MWCNT-OH were crushed with a mortar and pestle, and 15 mL epichlorohydrine and 20 mL water were added in an Erlenmeyer with the CNTs. After 30 min ultrasonic treatment, the solution was put on a heating/stirring plate and the solution was heated to 90°C. A solution of 1.03 g NaOH in 80 mL was added dropwise to the solution over a period of 2 h. The mixture was washed multiple times with hot water over a 0.65 µm PVDF membrane filter and dried in an oven at 80°C. A sample was taken for FTIR analysis.

The dried epoxy-functionalized building blocks were mixed with different amounts of commercially available epoxy harder for room temperature hardening (Epoxy BK component B, Voss Chemie, Germany). The commercial harder recommends a 100/60 epoxy-harder mass mix ratio. As it is expected that the epoxy content on the nanotubes is lower than the epoxy content of the commercial epoxy, mixtures of 100 mg - 60 mg down to 100 mg – 10 mg, in decreasing steps of 10 mg, nanotube to harder mixtures were prepared. As the CNTs were poorly wetted by the harder, 1 mL of *n*-heptane was added to each batch as well. After mixing with mortar and pestle, the samples were placed on a high-density polyethylene (HDPE) foil and were dried to the air. During mixing, however, it was already noticeable that the obtained material looked like what could be described as a ‘brittle paste’. After several days, the *n*-heptane was evaporated and what was left was a brittle cluster of nanotubes, with little to no visual indication of further polymerization.

Yet again, FTIR spectra were overshadowed by contamination, thus no useful information could be extracted from the spectra.

4. 4. 2. c. Polyurethane-based modification route

250 mL THF was freshly distilled and caught in a round bottom flask containing 3 g CaSO4 to catch remaining water. 1.5 g of MDI was dissolved in hexane and filtered to remove of the self-polymerized MDI. The remaining hexane was evaporated and the MDI was further dried under vacuum. 0.52 g of said MDI was put in an Erlenmeyer with 0.22 g MWCNT-OH, 150 mL THF and 80 µL DBTDL. The mixture was put in an ultrasound bath for 30 min at 60°C and further stirred at this temperature with a refluxer. After 3h 20 mL THF with 44 µL (0.05g) ethyleneglycol was added. The mixture was stirred for 5 more days at 60°C. As no clear change in viscosity could be noticed, 5 µL water was added. The mixture was stirred further at a lower temperature (50°C) without refluxer. After 10 more days, there was still no clear visual indication of increased viscosity. FTIR data was not open to interpretation due to contamination.

4. 4. 2. d. Polyamide-based modification route

In a first configuration, 2 g pulverized MWCNT-OH was dispersed in ethyl acetate by ultrasound treatment for 15 minutes. The solution was heated to 75°C while stirring. 8 g APTES was added together with 0.1 mL water to activate the APTES. The mixture was stirred for 7 hours, giving the activated APTES time to react with the hydroxylated MWCNT's. The obtained APTES modified-CNTs were filtrated and multiple times washed with ethylene acetate to remove the unreacted APTES. Then the CNTs were dried in an oven at 70°C for 24h. After drying, an increase in mass (2.46 g) was noticed, that could indicate a successful coupling of APTES to the CNT's. The TGA curve of APTES functionalized MWCNT is shown in Figure 10.

0.5 g of the APTES-functionalised MWCNT's were pulverized and dispersed in 500 mL water. 40 mL of this solution was poured in a 100 mL beaker, after which 10 mL 0.25M NaOH solution was added. A solution of 3 mL sebacoylchloride in 30 mL *n*-heptane was gently poured on top of the aqueous CNT-APTES dispersion. The two-phase mixture was placed in an ultrasound bath for 1 h. A grey ball was formed floating atop the liquids, and all the CNTs were pulled from the water phase. The ball was washed with water and dried in an oven at 80°C, where it turned from a more or less solid structure to an ash-like structure.

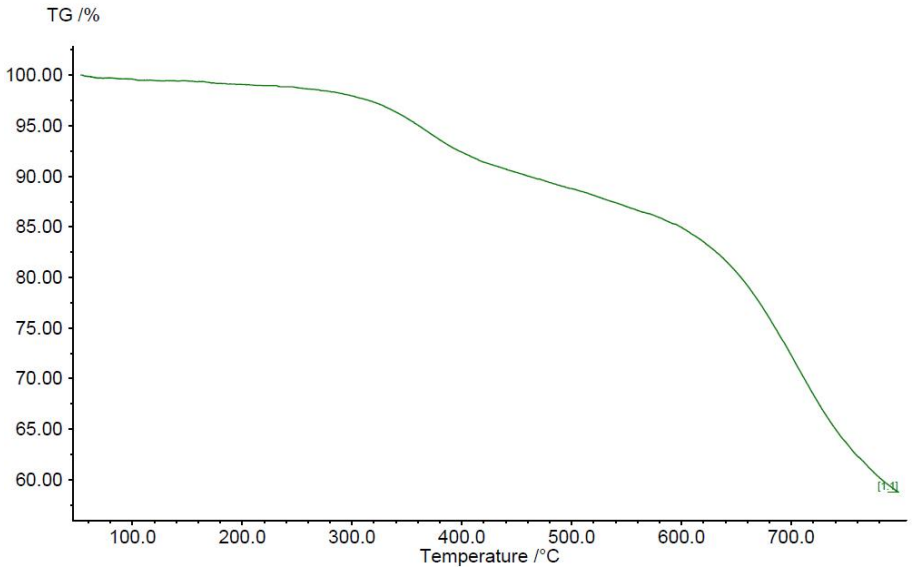

Figure 10: TGA curve of APTES functionalized CNT

The TGA profile for the APTES-MWCNTs shows a two-step decrease, in which the first step can be assigned to the chain scission of aminopropylsilane, while the second step is caused by the decomposition of the carbon-oxygen-silicon bonds, as also seen in the TGA of APTES-MWCNT of Li et al [16]. This indicated that APTES is present in the sample, likely bonded to the nanotubes since they were intensely washed after filtration.

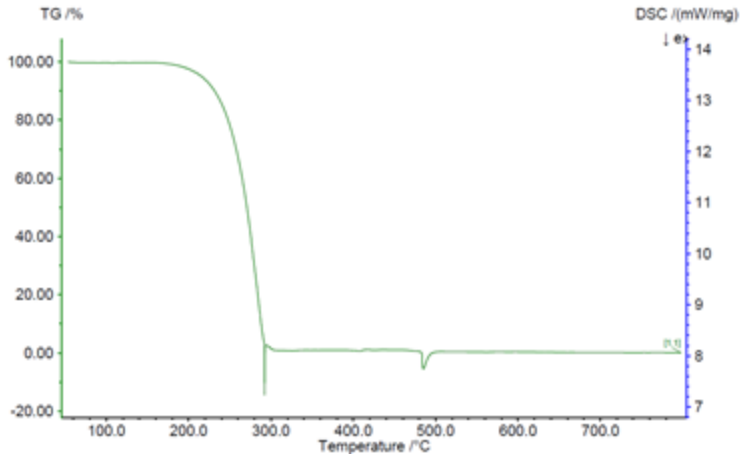

Figure 11: TGA curve of APTES-CNT after 'reaction' with sebacyl chloride

The green line in Figure 11 shows the TGA profile of the APTES functionalized CNTs after reaction (and drying) with sebacoyl chloride. Over 300°C, the sample mass is reduced to zero. As also seen in the FTIR data, the resulting material mostly consisted of the decay product of sebacoyl chloride with water; namely sebacic acid, with a boiling point of 294°C. This shows that the formed solid is most likely sebacic acid with little to no CNT's dispersed in it, as no residual mass is left after 300°C. The ultrasound might have caused this waste product to take an expanded (foam-like) form, which collapses after drying (evaporation of the liquid inside the foam), leaving behind an ash-like substance.

Figure 12 shows the FTIR spectrum of the CNT-APTES after attempted polymerization. The conclusion drawn from TGA analysis can be confirmed, as the spectrum shows a perfect match with the FTIR spectrum of sebacic acid.

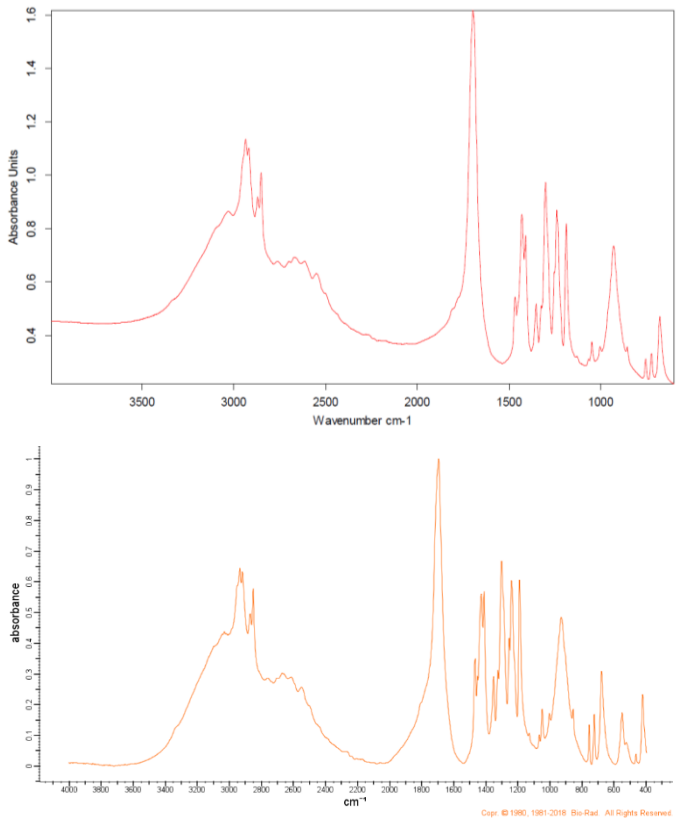

Figure 12: FTIR spectrum of CNT-APTES-polymer, in perfect match with sebacic acid spectrum given below[20].

In a second configuration an adjusted synthesis route for polyamide-based CNT polymer was attempted, in which 220 mg of crushed SWCNT-COOH was added to 100 mL ethylenediamine and 10 mg HATU in a 250 mL Erlenmeyer flask. The mixture was put in an ultrasound bath for 4 h at room temperature in order to form amine functionalized CNTs.

In a next step, 150 mL methanol was added and the mixture was filtrated over a 0.65 µm polyvinylidene difluoride PVDF membrane filter. After washing several times with methanol, the nanotubes were dried in an oven at 80°C for 24 h. 70 mg of these dried CNT's were dispersed in 50 mL water by 15 minutes of ultrasonic treatment.

0.5 mL of a 10% NaOH solution was added to the nanotube dispersion. The nanotubes were poured over in a 100 mL beaker. A solution of 200 µL sebacoyl chloride in 30 mL *n*-heptane was gently poured on top of the nanotube solution in the beaker, forming two clear separate phases. The mixture was set to rest for 1 h, with periodically short (20 sec) ultrasound treatments. After that, a spatula was used to gently stir in the phase separation. A membrane stuck to the spatula and was carefully pulled out, forming a short filament, as seen in Figure 13A.

The filament was washed extensively with water and ethanol. After washing, the sample had a weight of 10 µg. The sample was placed in an oven and was dried for 3h, after which the mass was reduced to 0.5 mg, shown in Figure 13B. The remaining, fiber-like structure was able to support its own weight when being picked up with tweezers.

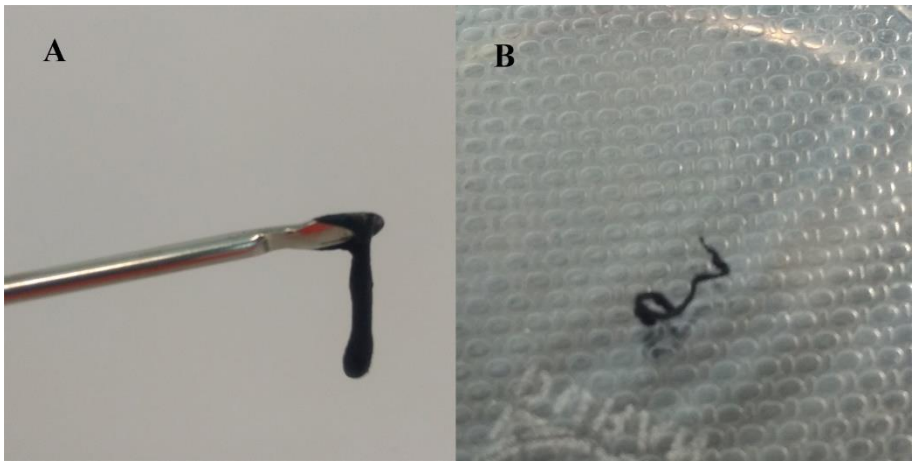

Figure 13: A and B resulting product from the second configuration of the polyamide based modification route before (A) and after (B) drying

Both the shape (fiber) and the location where it was pulled from (phase separation; Figure 7 in appendix B) are in accordance with what the polymer should look like and where it should be formed. The only side product from this reaction, sebacic acid, is

highly dissolvable in ethanol, meaning it should have disappeared after washing. All the other products already present in the reaction mixture are either dissolvable/dispersible in water and/or ethanol. After drying, the structure was rigid enough to support its own weight from any angle, a property that is highly unlikely for different loose carbon nanotubes or any other side product for that matter. The current sample mass is too low (0.5 mg) to perform TGA analysis and FTIR analysis is yet to be performed. On the condition that the sample is not contaminated with unreacted sebacic acid or heptane, the intensity of carbon-hydrogen and amide-related peaks are expected to increase. However, as the currently obtained structure is not dissolvable/dispersible in water or ethanol, it is highly likeable that the intended polymerization reaction has indeed occurred. FTIR analysis of the intermediate steps was again overshadowed by an unknown contaminant.

4. 4. 3. Overview

Table 1 gives an overview of the different attempted reaction, outcomes and other important notes.

Table 1: overview of different reactions

Attempted reaction	Outcome	Notes	Analysis
Hydroxylation of carbon nanotubes	Successful	Better dispersion in polar solvents and successful reaction with APTES proves the success of the reaction	FTIR vaguely interpretable TGA not useful
Carboxylation of carbon nanotubes	Successful	Better dispersion in polar solvents proves the success of the reaction	TGA not useful FTIR contaminated
MWCNT-OH with formaldehyde and NaOH (Bakelite)	Unsuccessful	Reaction product was readily dispersible in water	FTIR contaminated DSC not useful
MWCNT-OH with formaldehyde, phenol and NaOH (Bakelite)	Unsure	Not sure if reaction occurred with phenol and formaldehyde or carbon nanotubes and formaldehyde	No analysis performed
Formaldehyde with phenol and NaOH (Bakelite)	Successful	Reference experiment for DSC	DSC not useful
Epoxy precursor: MWCNT-OH and epichlorohydrin	Unsure	No reference experiments for CNT's available	FTIR contaminated TGA not useful
Epoxy: epoxide-CNT with commercial harder	Unsuccessful	Commercial harder in different amounts, poor wettability of CNT's	FTIR contaminated
Polyurethane: MDI with MWCNT-OH	Unsuccessful	No increase in viscosity, so likely no high yield reaction	FTIR contaminated
Synthesis of APTES-MWCNT	Successful	Increased weight after reaction indicates successful coupling of APTES	TGA confirmed
Polyamide: APTES-MWCNT with sebacylchloride	Unsuccessful	Reaction product turned out to be a side reaction product	FTIR confirmed TGA confirmed

Polyamide: SWCNT-COOH with sebacylchloride	Successful (likely)	Formation on phase separation, fiber-like structure	Non-dissolvable or dispersible in water or ethanol Further analysis required

4. 5. Conclusion

Different modification paths for synthesis of CNT based polymer have been attempted, with focus on Bakelite, epoxy, polyurethane and polyamide based 3D structures. Likely due to the difficulty to disperse the CNTs well in the reaction medium, and thus low reactivity, not all modifications are successful. Moreover, FTIR, DSC and TGA analysis for such complex systems show large variations in measurements, making interpretation of the data difficult. Specifically, DSC analysis shows large variations as the reaction medium evaporated with non-predictable patterns. TGA showed inconsistent results and inexplicable mass losses. It is possible that this is caused by the static charging of CNT during the measurement, as static build-up caused multiple problems during synthesis all around. This theory is yet to be confirmed. FTIR spectra were overall contaminated by an unknown source, making it difficult to use the acquired spectra.

Interestingly two modification routes show potential at this moment. Firstly, the synthesis of the Bakelite-based CNTs doped with phenol turned out to form a solid mass. Analysis is yet to be performed, as it is likely that the nanotubes are embedded in a Bakelite matrix rather than be a part of the polymer structure. Secondly, the synthesis of one of the polyamide-pathways seems even more promising. Though no analysis has been performed yet since the current sample mass was too little, the material is not dissolvable in ethanol or water, which should dissolve all reactants or side-products that can be formed in the reaction. The structure is self-supporting and

formed by phase separation of the two components. A higher functionalization degree of the CNTs should improve the dispersion and reactivity, likely making it possible to make larger samples. Both the epoxy and isocyanate-based pathways could show more potential with shorter and more functionalized, thus better dissolvable, carbon nanotubes. It is clear that FTIR analysis should be re-attempted in order to confirm end results and intermediate steps. For example, it remains unclear whether the coupling epoxychlorohydrine to MWCNT-OH was successful, or if any reaction of MDI with MWCNT-OH has taken place. Better knowledge of the quantity of functionalization could prove to be valuable as well.

REFERENCES

[1] S. Iijima, “Helical microtubules of graphitic carbon,” *Nature*, vol. 354, no. 6348, pp. 56–58, 1991.

[2] M. F. L. De Volder, S. H. Tawfick, R. H. Baughman, and A. J. Hart, “Carbon Nanotubes: Present and Future Commercial Applications,” *Science (80-.).*, vol. 339, no. 6119, pp. 535–539, Feb. 2013.

[3] A. Sahu, A. Jain, and A. Gulbake, “THE ROLE OF CARBON NANOTUBES IN NANOBIOMEDICINES,” *Int. J. Pharm. Pharm. Sci.*, vol. 9, no. 6, pp. 235–251, 2017.

[4] M. F. Yu, O. Lourie, M. J. Dyer, K. Moloni, T. F. Kelly, and R. S. Ruoff, “Strength and breaking mechanism of multiwalled carbon nanotubes under tensile load,” *Science (80-.).*, vol. 287, no. 5453, pp. 637–640, Jan. 2000.

[5] M. M. J. Treacy, T. W. Ebbesen, and J. M. Gibson, “Exceptionally high Young’s modulus observed for individual carbon nanotubes,” *Nature*, vol. 381, pp. 678–680, 1996.

[6] R. H. Baughman, A. A. Zakhidov, and W. a de Heer, “Carbon nanotubes --- the route toward applications,” *Science (80-.).*, vol. 297, no. 5582, pp. 787–92, 2002.

[7] Z. Jiao, D. R. D’hooge, L. Cardon, and J. Qui, “No Title,” *Matter. Chem.*

[8] L. Duan, D. R. D’hooge, and L. Cardon, “No Title,” *Mater. Sci.*

[9] N. G. Sahoo, S. Rana, J. W. Cho, L. Li, and S. H. Chan, “Polymer nanocomposites based on functionalized carbon nanotubes,” *Prog. Polym. Sci.*, vol. 35, no. 7, pp. 837–867, Jul. 2010.

[10] I. Alig *et al.*, “Establishment, morphology and properties of carbon nanotube networks in polymer melts,” *Polymer (Guildf).*, vol. 53, no. 1, pp. 4–28, Jan. 2012.

[11] O. Breuer and U. Sundararaj, “Big returns from small fibers: A review of polymer/carbon nanotube composites,” *Polym. Compos.*, vol. 25, no. 6, pp. 630–645, Dec. 2004.

[12] R. J. Young and P. A. Lovell, *Introduction to Polymers*. 2011.

[13] V. Georgakilas *et al.*, “Multipurpose Organically Modified Carbon Nanotubes: From Functionalization to Nanotube Composites,” *J. Am. Chem. Soc.*, vol. 130, no. 27, pp. 8733–8740, 2008.

[14] V. Georgakilas *et al.*, “Noncovalent Functionalization of Graphene and Graphene Oxide for Energy Materials, Biosensing, Catalytic, and Biomedical Applications,” *Chem. Rev.*, vol. 116, no. 9, SI, pp. 5464–5519, 2016.

[15] I. Chavez-Sumarriva, P. H. M. Van Steenberge, and D. R. D’hooge, “New Insights in the Treatment of Waste Water with Graphene: Dual-Site Adsorption by Sodium Dodecylbenzenesulfonate,” *Ind. Eng. Chem. Res.*, vol. 55, no. 35, pp. 9387–9396, Sep. 2016.

[16] S. Li, Z. Wang, J. Jia, C. Hou, X. Hao, and H. Zhang, “Preparation of hydroxyl and (3-aminopropyl)triethoxysilane functionalized multiwall carbon nanotubes for use as conductive fillers in the polyurethane

composite," *Polym. Compos.*, vol. 39, no. 4, pp. 1212–1222, Apr. 2018.

[17] V. Datsyuk *et al.*, "Chemical oxidation of multiwalled carbon nanotubes," *Carbon N. Y.*, vol. 46, no. 6, pp. 833–840, 2008.

[18] T. Ramanathan, F. T. Fisher, R. S. Ruoff, and L. C. Brinson, "Amino-functionalized carbon nanotubes for binding to polymers and biological systems," *Chem. Mater.*, vol. 17, no. 6, pp. 1290–1295, 2005.

[19] E. M. Pearce, "New polymers for composites: A summary of Research on Polystyrylpyridines," Brooklyn, New York, 1983.

[20] I. Bio-Rad Laboratories, "SpectraBase." [Online]. Available: http://spectrabase.com/spectrum/Lh8GMdSDrXx?a=SPECTRUM_Lh8GMdSDrXx. [Accessed: 07-Jan-2020].

Chapter 5

Conclusions and future outlook

The literature review in Chapter 1 wrapped up the current basics, state of the art and challenges on thermal conductivity of thermoplastic composites. An overview of measurement techniques in this chapter pointed out the importance of selecting the correct technique dependent on the sample; specifically the incorrect technique for an anisotropic sample can lead to wrong conclusions. Large fillers with a high aspect ratio show most promising results. These also reduce the loading level required to achieve the percolation threshold. The mixing step determines the dispersion the fillers; though a perfect dispersion is not always recommended for better thermal conductivity. The final processing step mostly determines whether the sample will show anisotropy or not. As conventional processing such as injection molding does implement anisotropy, product design for applications like heat sinks should take this into account. Heat exchangers do require a high through-plane thermal conductivity, this while the in-plane value is mostly dominant due to the filler orientation. Out of many investigated techniques to improve the through-plane thermal conductivity only a few showed industrial relevance. As indicated in Chapter 1, more research towards the increase of through-plane thermal conductivity could certainly lead to added value in thermal management products. Interfacial thermal resistance between filler and matrix can be lowered by using compatibilizers. However, improved compatibility with the matrix can prevent the formation of a percolation network. This improved compatibility can also cause even stronger orientation of the filler after processing. As numerous factors influence the thermal conductivity of a composite, there are still quite some uncertainties since the study of one parameter can unintentionally change

another. It is clear though, that improved through-plane thermal conductivity, applicable on industrial scale, could use more attention.

As several studies on thermal conductivity of composites focused on lab-scale experiments, some of these established theories were investigated under more industrial conditions in Chapter 2. All the tests made use of commercially available polymers and fillers and used industrially relevant processing methods, namely twin screw compounding and injection molding. Comparison of two polystyrenes with different average molecular mass showed no noticeable change in thermal conductivity. While semi-crystalline polymers generally show a higher thermal conductivity than their amorphous counterparts, increasing the crystallinity by annealing the polymers had no significant contribution to the thermal properties. Moisture, often encountered in thermal management applications, had no effect on the thermal conductivity as well. The thermal conductivity of the studied composites showed strong anisotropy with in-plane thermal conductivities up to a factor 10 higher than through-plane thermal conductivity. Design of the optimal matrix and filler allow increases from 50 to 1000% with respect to the virgin material. The importance of the skin-core effect was also highlighted, with the suggestion of removal of the skin layer for strongly improved through-plane thermal conductivity at least for basic shapes. In Chapter 2, macro-graphite was also compared with nano-graphite in thermal performance, with conclusions in line with the state-of-the art in Chapter 1.. Future work could address the use of fillers with complex shapes and involve theoretical calculations regarding the relation of the composite composition and thermal conductivity profile.

To increase through-plane thermal conductivity of low-filled composites, the use of foaming agents in Chapter 3 showed an increase by disrupting the fiber orientation caused by the processing, although with a decrease in in-plane thermal conductivity.

The use of a two-phase matrix showed increased through-plane and decreased in-plane as well, though the mechanism was less clear. Mechanical properties decrease in both the two-phase and foaming agent composites, due to the weak interface between the two polymers or due to the creation of air pockets in the composite. Besides that, the thermal conductive filler, graphite, shows relative weak mechanical properties. Changing the filler by carbon fibers in future research could mean improved through-plane conductivity and higher strength.

Finally, in Chapter 4, carbon nanotubes were chemically modified and attempted to polymerize in order to achieve a highly thermal conductive polymer with extraordinary mechanical properties. Four chemical modification routes were investigated: epoxy-based, polyurethane-based, Bakelite-based, and polyamide-based. Synthesis of polyurethane seemed unsuccessful, as the viscosity of the solvent remained unchanged (visually) throughout the reaction time. FTIR analysis of the product should give more insight on where the problem occurred: did MDI react with the MWCNT-OH, or can the problem be traced back to the crosslinking process. The same applies to the epoxy-pathway: it remains unclear whether the nanotubes reacted with the epichlorohydrin. The poor wettability of the nanotubes with the commercial harder should be addressed too. An indication to the amount of epoxy functional groups on the CNT's could prove valuable to optimize the amount of added harder. Hydroxyl functionalized carbon nanotubes, combined with phenol and formaldehyde, yielded a black solid material. As detailed analysis was not possible yet, it is likely that the carbon nanotubes are dispersed in the Bakelite matrix rather than part of polymer molecules. The polyamide method yielded a fiber-like structure coming from the interface of the two solvents involved in the process. The final structure was not dissolvable and not dispersible in water or ethanol, while the reactants or unwanted

side products are. This indicates that the formed structure is likely the polymerization product of carbon nanotubes, though further analysis should provide more detail.

In general, increasing the carbon nanotube functionalization in the first step could increase dispersion. With increased dispersion, the reactivity of the carbon nanotubes should improve as well. This could be achieved by making use of strong acids and longer reaction times in the precursor synthesis phase. The carboxyl functional groups could be reduced to hydroxyl with $LiAlH_4$ in a second step. Alternatively, different surfactants could improve carbon nanotube dispersion as well, though these surfactants might interfere in further reaction steps.

Appendix A

Principles of the transient plane source to enable an evaluation of isotropic and anisotropic thermal conductivities in a polymeric composite

A.1 Introduction

The thermal conductivity (TC) of a material often denoted by *k* or λ is defined as the ability of a material to conduct heat, expressed in watts per square meter of surface area for a temperature gradient of 1 Kelvin per unit thickness of 1 meter; or thus W $m^{-1} K^{-1}$. The reciprocal of TC can be compared with resistance in an electrical circuit, as expressed in Ω. A thermal conductive material (e.g. iron surface) at the same temperature as an insulating material (e.g. most unmodified plastics, and wood) will have a colder touch if it is below body temperature, since the metal is more able to conduct heat away from your body. Vice versa, a thermal conductive material at a temperature higher than body temperature will feed hotter compared with an insulating material at the same temperature.

The thermal diffusivity κ, which is defined by the thermal conductivity λ divided by the density and specific heat capacity *c* at a constant pressure (dimension $m^2 s^{-1}$), is a measure for the rate of heat transfer of a material from one end to the other.

Materials can be anisotropic meaning that properties can be different dependent on the direction measured. Unlike most other thermal properties measurement techniques, the transient plane source method (TPS method), as employed in the

present PhD thesis, allows anisotropic samples to be measured in the in-plane and through-plane simultaneously.

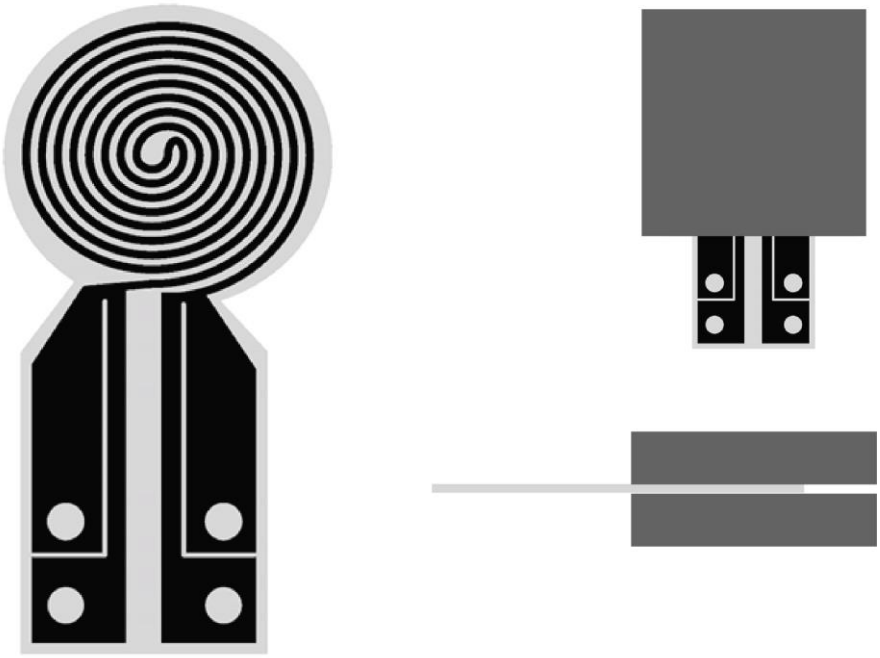

Figure 1: Sketch of a hot disk probe on the left. The black channels represent the nickel or molybdenum path, the light grey represents a film of insulation that covers the front and back of the sensor. On the right a top and side view of how a sample (grey) should be mounted for measurement (double side embedding).

The TPS method is an absolute measurement technique for thermal properties of materials ranging from insulating (λ value less than 0.010 W m^{-1} K^{-1}) to highly conducting (λ up to 500 W m^{-1} K^{-1}) materials. It allows measurements ranging from cryogenic temperatures up to 1000 K. The TPS method is described in an ISO norm as well [1]. The TPS used in this PhD thesis is a TPS 2500s from HotDisk, Sweden, of which the theoretical principles are highlighted in the next section (Section A.2).

Attention is also paid to practical precautions in view of application of the TPS method (Section A.3).

A.2 TPS set-up and theoretical principles

The sensor used for measurements is constructed out of a thin (10 μm) nickel film shaped as a double spiral. The distance between each spiral is the same as the thickness of the spiral and is around 0.20 mm. The spiral is covered by thin insulating films based on polyimide or mica. Figure 1 shows a sketch of such a sensor as such and in combination with a sample.

An electrical current is send through the sensor causing a rise in temperature (ΔT), generating a dynamic thus time dependent temperature variation in the sample. The increase in resistance over the sensor is monitored during the experiment and can be translated to an increase in temperature as focus is on the transient region. Thus, the sensor acts as both a heating element and a temperature sensor at relatively low measuring times. As this technique relies on the precise measurements in temperature increase, it is obvious that the environment temperature has to stay as constant as possible. At the start of every measurement, typically a ‘drift’ is measured showing possible irregularities in background temperature.

There are essentially 3 parameters that can be changed when measuring the TC with this method. This is the measurement time, the power input and the sensor size. The sensor size and measurement time should be chosen as such that the probing depth doesn’t exceed the sample thickness. The power output should be chosen so the total temperature increase during the measurement remains below 5 K and preferably above 3.5 K.

APPENDIX A

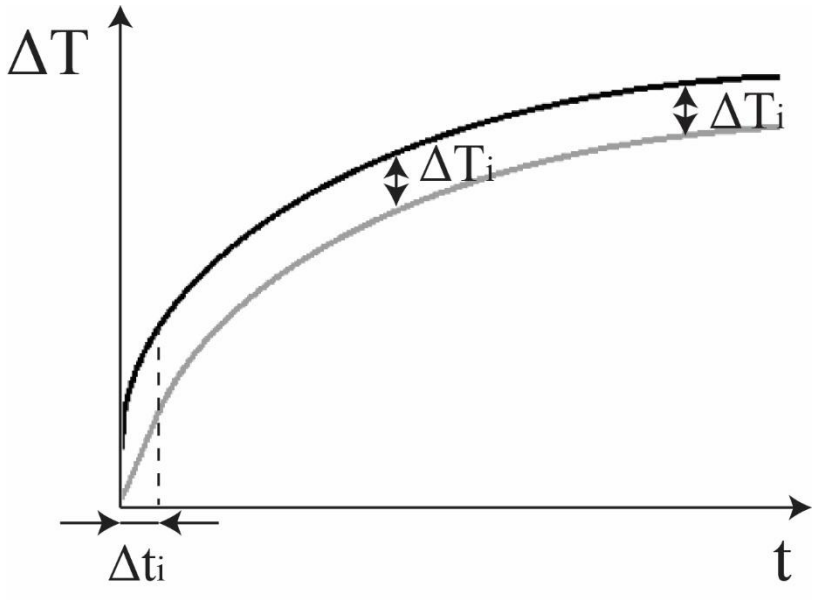

Figure 2: The black curve shows the temperature increase of the sensor itself as a function of time t, while the grey curve shows the temperature increase at the surface of the sample (cf. right part in set-up in Figure 1). Δt_i represents the time from which moment on the difference between the black and the grey curve remains constant (ΔT_i)

As the sensor is heated (thus temperature increases are obtained) the increase in resistance R for the analysed system (dimension: W^{-1} m K) can be described by:

$$R(t) = R_0[1 + \alpha(\Delta T_i(t) + \Delta T_s(t))] \qquad \text{A1}$$

In Equation (A1), R_0 is the resistance before heating starts (t = 0 s), α is the temperature coefficient of resistivity (TCR) of the nickel-based system, ΔT_i is the temperature difference over the insulating layers of the sensor and ΔT_s is the temperature increase of the sample surface in contact with sensor (cf. Figure 1 right). Rewriting of Equation (A1) implies [1]:

$$\Delta T_s(t) = \frac{1}{\alpha}\left(\frac{R(t)}{R_0} - 1\right) - \Delta T_i(t) \quad \text{A2}$$

After a short time the ΔT_i value becomes a constant, as shown in Figure 2. This threshold time can be estimated as follows [1]:

$$\Delta t_i = \frac{\delta^2}{\kappa_i} \quad \text{A3}$$

in which δ represents the thickness of the insulating layer and κ_i the thermal diffusivity of this layer.

For isotropic specimens, the solution for the thermal conduction equation (Equation A2) is given by [1]:

$$\Delta T_s(\tau) = P_0\left(\pi^{3/2} r \lambda\right)^{-1} D(\tau) \quad \text{A4}$$

Here P_0 represents the total power output of the sensor, *r* is the radius of the outer ring of the sensor, λ the thermal conductivity of the sample measured, and *D* is a dimensionless time dependent function [1] with τ given by:

$$\tau = \sqrt{\frac{t}{\Theta}} \quad \text{A5}$$

in which *t* is the time measured from the start of the recording and Θ is the characteristic time, defined by[1]

$$\Theta = \frac{r^2}{\kappa} \quad \text{A6}$$

with κ being the thermal diffusivity of the sample. By plotting the temperature variation ΔT_s as a function of *D*, a straight line is thus expected, with as slope *s* [1]:

$$s = \frac{P_0}{\pi^{3/2} r \lambda} \quad \text{A7}$$

As the total power output and the radius of the sensor are known, the thermal conductivity can be calculated if the measurement time is longer than Δt_i. The coupled values of Θ and κ are first unknown but are calculated through iteration. More in-depth explanations about the calculations can be found in following references: [2], [3].

Anisotropic specimens rely on the same theoretical principles, though the solution for the thermal equation needs to be slightly adjusted [1]:

$$\Delta T_s(\tau_a) = P_0 \left[\pi^{3/2} r (\lambda_a \lambda_c)^{1/2}\right]^{-1} D(\tau_a) \quad \text{A8}$$

with λ_a the thermal conductivity along the *a*-axis, being the main axis (flow direction) so reflecting the in-plane TC under the assumption that the TC in the *b*-axis (transverse direction) is equal to that of the *a*-axis. In other words, the in-plane TC is assumed equal over the whole radial direction in the plane ($\lambda_{ab} = \lambda_a = \lambda_b$) , and λ_c is the TC in the *c*-axis, or through-plane direction. In Equation (A8) τ_a is defined by [1]:

$$\tau_a = (t/\Theta_a)^{1/2} \quad \text{A9}$$

with

$$\Theta_a = r^2/\kappa_a \quad \text{A10}$$

Similar to the isotropic system, this equation needs to be solved for κ_a and Θ_a through iteration noting that [1]:

$$\lambda_a = C\kappa_a \quad \text{A11}$$

with *C* the heat capacity per volume unit. If *C* is known λ_c can be calculated as well from the slope of the resulting curve.

Notably the TPS 2500s includes a software module and sensor for measuring the *c/C* value of a sample as well. The sensor is again there as introduced above, but now with a golden cup attached to one side of the sensor covering the spiral. The gold cup can be closed with a gold lid. During the measurement, the gold cup is insulated so that no (or a negligible amount of) heat is lost to the environment. A sketch of the set-up is given in Figure 5.

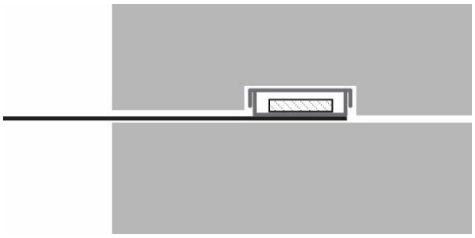

Figure 5: Gold cell set-up to obtain the heat capacity parameter c (and thus C) The sensor as show in Figure 1 is represented as the black line. On the spiral of the sensor, the gold cup with lid is attached. A sample (black dotted lines) can be put in the gold cup. The gold cell is surrounded by insulation to avoid heat escaping to the environment. Missing in this drawing is the cable form the sensor to the machine and the metal cover over the whole system to avoid turbulent air flows from reaching the test set-up.

Measuring the heat capacity requires two steps: a blank run and a sample run. The blank run involves sending power to the sensor for a certain amount of time, heating the empty cup. The time-temperature curve is recorded by measuring the resistance increase of the sensor over time. The second run is done with sample inside the cup. Here, it is of utter most importance that the sample has perfect contact with the bottom of the cup, this in order to easily transfer heat from cup to sample. During the second

run, the power output has to be chosen so that the resulting time-temperature curve approaches that of the blank run as close as possible. Since the system is closed, the extra heat supplied to the system in order to follow the (quasi-)same time-temperature curve can be seen as the heat absorbed by the sample. Provided that the density and mass of the sample are given (required for the test), the heat capacity *C* can be measured.

For this experiment, it is recommended to have a temperature increase between 5-10 K over the measurement time. The time of measurement should be increased for samples with a lower thermal diffusivity. Anisotropic samples should be orientated in the sample holder that the direction with highest thermal conductivity is placed perpendicular to the bottom of the cup. This allows the heat to spread the fastest through the sample. Waiting times in between two measurements should be sufficiently long to allow the sample and sensor to cool to ambient temperature.

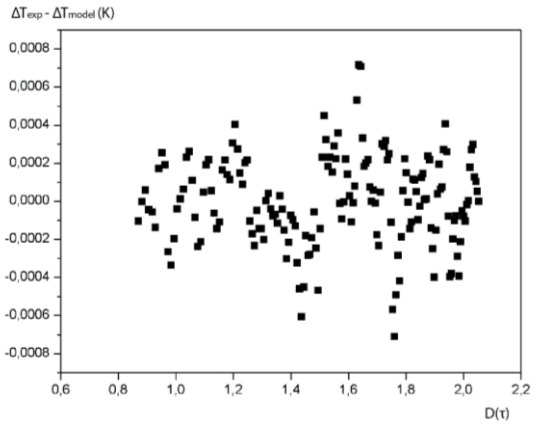

Figure 3: Residual plot of a measurement on an isotropic thermal conductive thermoset. The random pattern indicates the measurement was done correctly. For model use of Equation A4.

A.3 Practical precautions for measurements

To evaluate the reliably of the approaches highlighted above a temperature residual plot should be drawn in which the differences between the experimental and the modeled temperature differences, $\Delta T_{s,\mathrm{exp}} - \Delta T_{s,\mathrm{model}}$, are plotted as function of the specific time function *D*. Ideally, this should show random scattering around a horizontal line, as seen in Figure 3. On the other hand, Figure 4 shows a bad plot of the residuals, meaning that the selected points for the calculation should be adjusted. In Figure 4, more specifically, the first points should be cut out, as these points are likely related to the sensor insulation or sensor-sample interface. The steep increases at the end of the residual plot are related to backscattering of heat waves, which implies a reaching of the sample boundary. Looking at the probing depth of this particular sample, the value indeed exceeds the thickness of the sample.

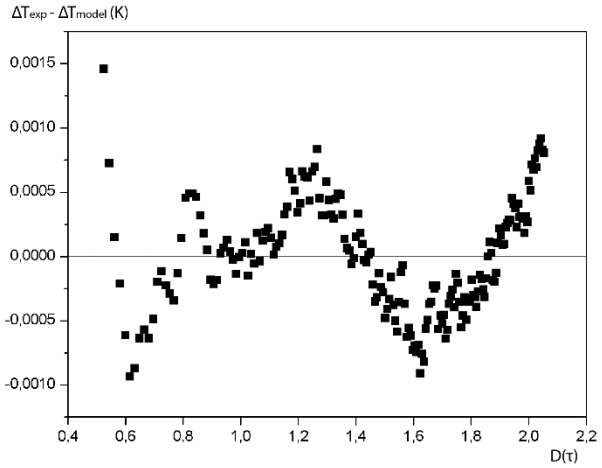

Figure 4: Residual plot of a measurement of a thermal conductive thermoset. Patterns indicate that fewer measurement points near the beginning of the curve should be selected to exclude the effect of the sensor insulation and/or sensor-sample contact. Points from the latter part of the graph should be excluded to prevent the heat wave from traveling beyond the sample dimensions.

Other possible errors that can be seen in the data are related to temperature instabilities that should be visible as a ‘drift’ signal or inhomogeneous materials.

Besides irregularities in the residual plot, it should be checked whether the probing depth of the heat wave during the test did not exceed the sample dimensions, as that could cause false results and conclusions. The probing depth is defined by [1]:

$$d_p = 2\sqrt{\kappa t} \qquad \text{A12}$$

and can be decreased by decreasing the measurement time, or by switching to a smaller sensor. For inhomogeneous materials, it is recommended that the probing depth is at least 20 times the length of the component making up the material [1]. Notice that the scale of the temperature residual of Figure 4, the incorrect residual, is also greater that the scale of a correct measurement, as seen in Figure 3.

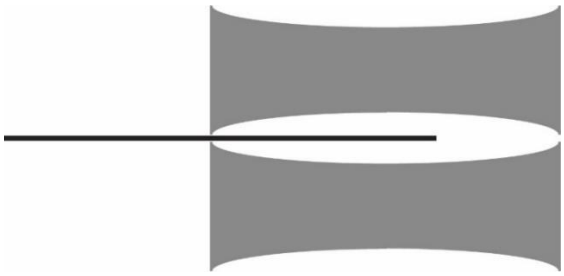

Figure 5: The sensor (black) with its spirals in the middle of the samples (grey), from the outside seemingly sandwiched by the samples. However, because of shrinking, the sensor is in fact trapped by an insulating layer of air.

As highlighted in the PhD thesis, injection moulded polymer shows skin-core with gradually changing filler orientation with increasing probing depth. To measure an average through-plane TC, it is of importance to make sure that the penetration depth

in the through-plane direction is either half the sample thickness or the whole sample thickness.

In addition, as some of the composites might show shrink after injection moulding - even with holding pressure to compensate - pre-treatment of samples can also be important. As two samples have to be placed on top and below the sensor for a measurement, shrinking in these samples could mean that there is an insulating air layer in between the sample and the sensor, as shown in Figure 5. Sanding the samples down to a straight and smooth surface is recommended. Care should be taken not to sand down too much, as this would remove the surface/skin layer, resulting in non-representative measurements, as explained in Chapter 2.

Furthermore, as explained above, for anisotropic measurements, the HotDisk manual recommends the *a* and *b* axis, thus the in-plane (and transversal) directions, to have the same (or similar) properties while the through-plane can differ. Here, the values of the in-plane TC (so a and b axis jointly) are given as following:

$$\lambda_{ab} = \sqrt{\lambda_a \lambda_b} \qquad \text{A13}$$

In some cases with one dimensional fillers, such as carbon fibres, oriented in one direction (*a*-axis), the TC in the *b*-axis can be considered equal to the TC in the *c*-axis, or the through plane, meaning that

$$\lambda_a = \frac{\lambda_{ab}^2}{\lambda_b} = \frac{\lambda_{ab}^2}{\lambda_c} \qquad \text{A14}$$

It is always also good to compare measuring results with other techniques. For example, Miller et. al. [4] performed measurements on injection moulded liquid crystal polymers (LCPs) filled with synthetic graphite, comparing the anisotropic

through-plane values of a hot disk, with the through-plane values of a heat flow meter (TCA-300). As can be seen in Table 1, both techniques show similar results for different amounts of fillers.

Table A.1: Through-plane thermal conductivity results of LCPs with synthetic graphite measured with heat flow meter (TCA-300) and transient plane source (HotDisk). Each sample was measured at least 3 times with each technique [4].

Synthetic graphite (wt%)	Through-plane TCA-300 (W/mK)	st. dev	Through-plane HotDisk (W/mK)	st. dev.
0	0,2169	0,0068	0,220	/
10	0,2935	0,0100	0,284	0,001
15	0,3494	0,0130	0,323	0,001
20	0,3869	0,0120	0,385	0,010
25	0,4699	0,0120	0,459	0,022
30	0,5464	0,0190	0,545	0,015
35	0,6106	0,0210	0,635	0,021
40	0,7064	0,0100	0,702	0,078
45	0,8804	0,0430	0,874	0,005
50	1,1081	0,0310	1,101	0,010
55	1,2851	0,0270	1,265	0,010
60	1,5586	0,0740	1,545	0,044
65	1,9426	0,1130	1,982	0,052
70	2,3225	0,0850	2,318	0,049
75	2,6251	0,0970	2,624	0,076

Finally, stacking of samples is not allowed, should the penetration depth exceed the sample thickness and no smaller sensor or shorter measurement time is available or allowed. Stacking creates extra interfaces between materials, causing backscattering,

insulating pockets and other phenomena that would lead to wrong results. The software does include modules for measuring thin films or one dimensional samples, hence, these are out of scope of this doctoral research.

REFERENCES

[1] International Organization for Standardization, “Plastics - Determination of thermal conductivity and diffusivity - Part 2: Transient plane heat source (hot disk) method,” in *ISO 22007-2:2015(E)*, International Organization for Standardization, Geneva, Switzerland: ISO, 2015.

[2] Y. He, “Rapid thermal conductivity measurement with a hot disk sensor: Part 1. Theoretical considerations,” *Thermochim. Acta*, vol. 436, no. 1–2, pp. 122–129, Oct. 2005.

[3] S. E. Gustafsson, “Transient plane source techniques for thermal conductivity and thermal diffusivity measurements of solid materials,” *Rev. Sci. Instrum.*, vol. 62, no. 3, pp. 797–804, 1991.

[4] M. G. Miller, J. M. Keith, J. A. King, B. J. Edwards, N. Klinkenberg, and D. A. Schiraldi, “Measuring thermal conductivities of anisotropic synthetic graphite-liquid crystal polymer composites,” *Polym. Compos.*, vol. 27, no. 4, pp. 388–394, Aug. 2006.

Appendix B

Principles of the transient plane source to enable an evaluation of isotropic and anisotropic thermal conductivities in a polymeric composite

B. 1 Targeted reaction pathways for four modification routes

A natural question that arises is which functional groups need to be present in the CNTs to enable the desired 3D chemical interaction. It has been opted in the present work to functionalize the CNTs with groups that react quickly and with high yields. Since carbon-carbon bond formation has little possibilities to such a type of modification, specific functional groups such as OH and COOH were first attached to the CNTs. To further improve the reaction rate and yield, long chains with a functional group are recommended over a direct bond of that functional group to the CNT. The resulting macrospecies will contain bonds other than hexagonal C-C bonds, with possibility to graphitize and anneal said bonds in later steps as well. In the long run, this complexity could be turned into an instrument for fine-tuning the final polymer/composite properties bearing in mind that several industries with applications being for instance medicine, electronics, and catalysts see potential in advanced CNTs [1]–[6].

Adjusting the amount, length and type of functional groups or the CNTs themselves could change macroscopic properties such as porosity, hydrophobicity, and chemical reactivity. As adding of functional groups relates to the replacing of sp^2 by sp^3

configurations, electrical conductivity which is dependent on these sp^2 configurations can also be altered, specifically for sufficiently high degrees of functionalization. However, literature has shown that the original structure of the CNT can be partially restored by annealing, possibly further increasing mechanical properties and reclaiming the lost electrical and thermal properties [7]–[10]. Modification of the CTNs can thus be seen in combination with a control of conductivity with limiting cases of a highly insulating or conductive material.

The general synthesis strategy for introducing functional groups in CNTs is by treatment with strong acids [11], [12] or oxidants [12], most of the time aided by ultrasound [13]–[16]. These procedures introduce carboxyl (-COOH), hydroxyl (-OH) and carbonyl (-C=O) groups. Strong basic conditions (combined with H_2O_2 [14]), aided by reflux and/or ultrasound [17], or Fenton reagent [18], [19] have been proven to introduce mainly OH functional groups to CNTs. Functional groups will attach to already existing defects present in the CNTs, resulting in mostly end-cap functionalization [20]. Ultrasonic treatments have shown to introduce new defects in the CNTs [21], that can potentially be used for further functionalization [22]. CNTs can also be chemically 'cut' in smaller pieces by long reaction times under extreme oxidizing conditions [23]–[25], with previously mentioned functional groups on the cut sites. After one or multiple series of these steps, classic organic chemistry can be used to further modify the CNTs.

In the present work, four routes for CNT modification and subsequent 3D network formation have been chosen. As all except one of the used routes are based on a step-growth mechanism, it is of high importance to achieve the correct reaction stoichiometry, as even small deviations could lead to low molar mass specimen and thus poor macroscopic properties [26]. Unfortunately, it still remains difficult to keep

close track of the exact number of functional groups on CNTs, explaining why the reaction techniques have been essentially adjusted based on intuitive insights to try and achieve high average molar masses. In what follows the ideal reaction pathways of the 4 modification routes are discussed.

The first route aims a “Bakelite-CNT”, where the conventional phenol is replaced with a hydroxyl functionalized CNT. This reaction can take place in aqueous environment. Upon using a basic catalyst, an increased temperature and an excess of formaldehyde are sufficient to form a 3D network for the conventional system in conventional Bakelite synthesis. A disadvantage is that the low mobility of the CNTs, especially when the solvent has evaporated, leaves limited option for further crosslinking. The basic reaction path with phenol creates methylene links and ether links. With further heating, the formed ether links are converted to methylene links as well. The same temperatures were used for the synthesis with CNTs (e.g. 80°C + 150°C for further crosslinking). As it was unclear whether reaction had occurred, the reaction mixture was tested in DSC for monitoring exo- or endothermic changes and FTIR to check for ether bonds. The reaction scheme of phenol with formaldehyde is shown in Figure 1 (top). This synthesis of Bakelite-CNT’s relies on the assumption that hydroxylated CNTs can undergo the same reaction steps as phenol (Figure 1; bottom).

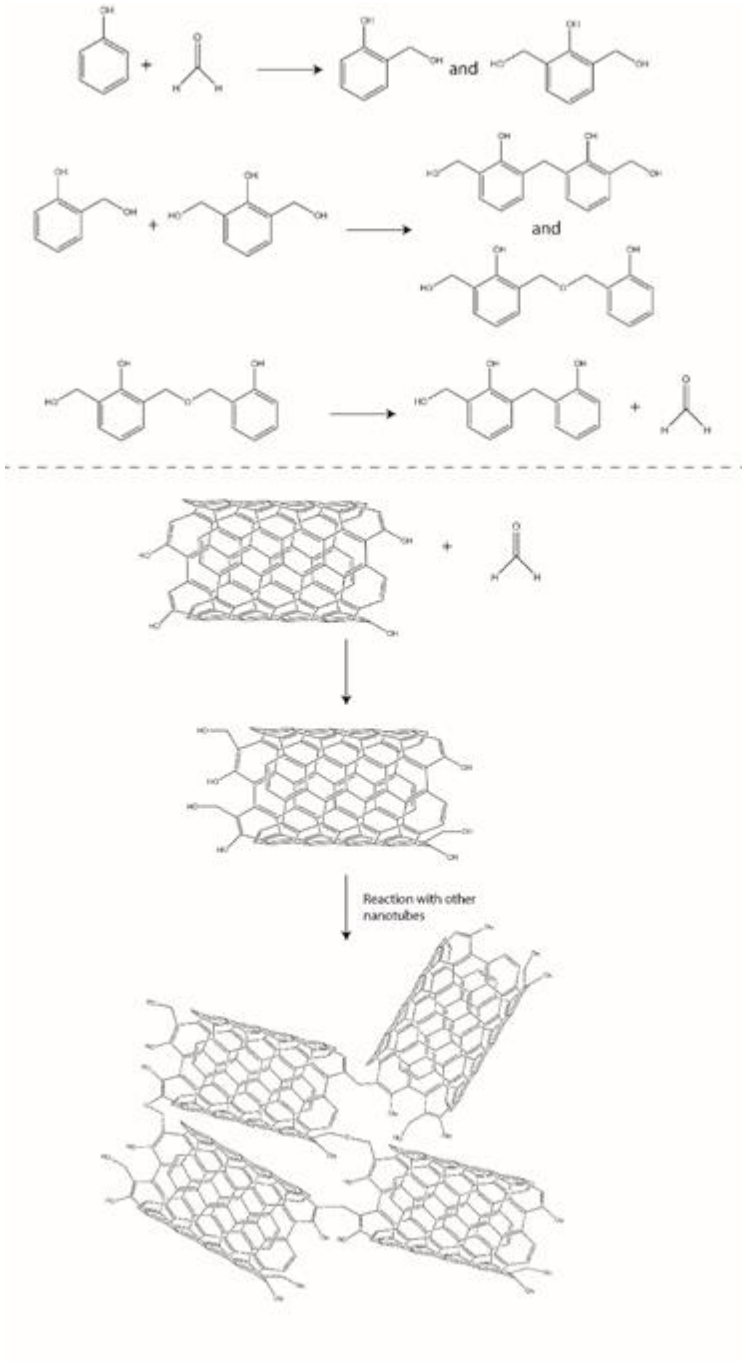

Figure 1: Chemical reactions relevant for modification route 1. Top: overview of three main reactions in phenol-formaldehyde Bakelite synthesis. Bottom: starting molecule in case of CNT precursor, so instead of phenol (also shown further reaction with other CNTs).

The second modification route aims to modify hydroxylated CNTs to epoxy-functionalized CNTs by reaction with epichlorohydrine, as shown in the top part of Figure 2. In a second step, as shown at the bottom of Figure 2, these nanotubes are mixed with a commercially available harder. The harder used contained primary amines as curing agent and tertiary amines as accelerator. As a correct stoichiometry is required for high yields, the obtained epoxy-carbon nanotubes were mixed with the harder in different mass ratios with added *n*-heptane, as the wettability of the nanotubes by the liquid harder was rather low.

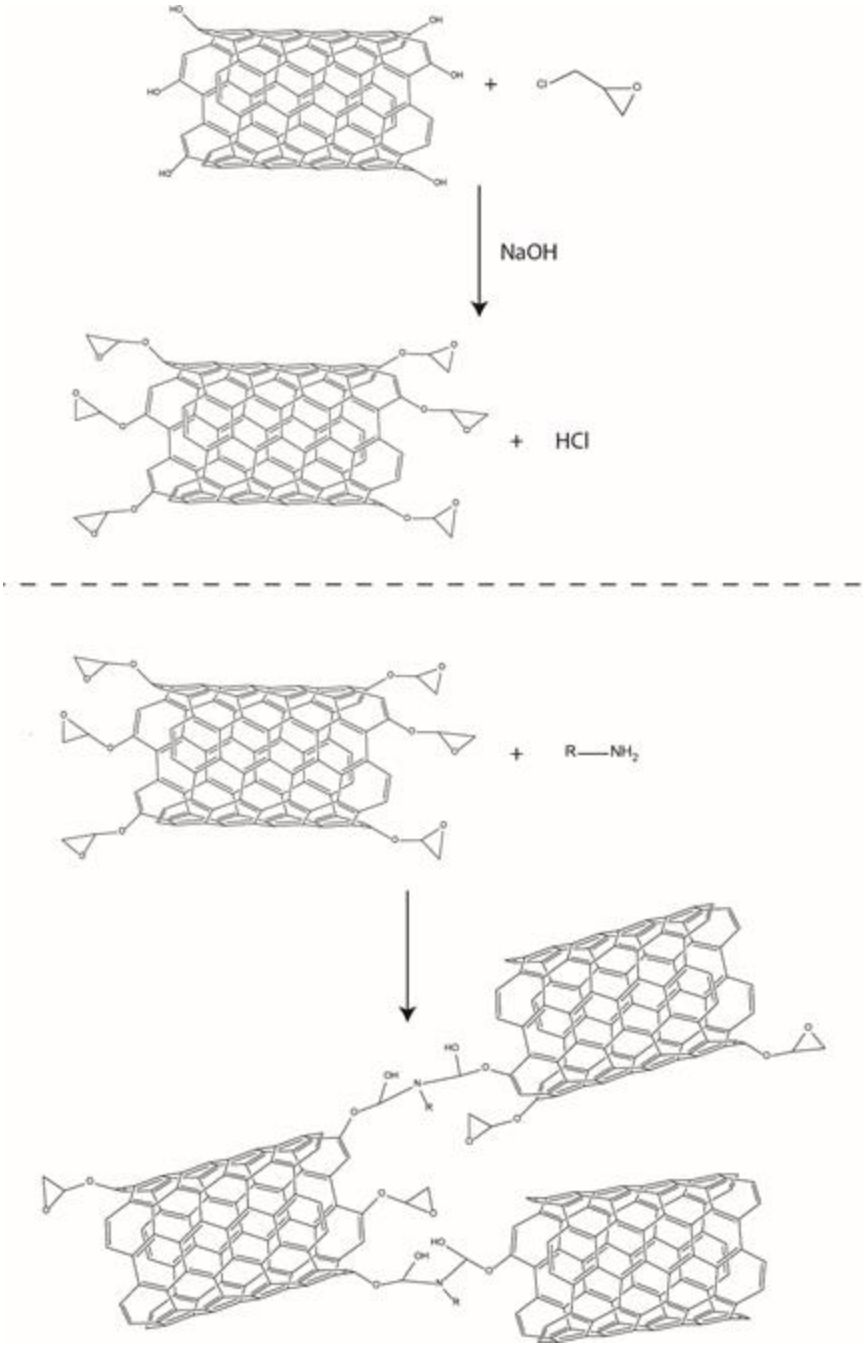

Figure 2: Chemical reactions for modification route 2: top: reaction of hydroxylated carbon nanotubes with epichlorohydrine; bottom: network formation with addition of epoxy hardener. Note that, besides the currently shown primary amine, a wide variety of epoxy hardeners are commercially available

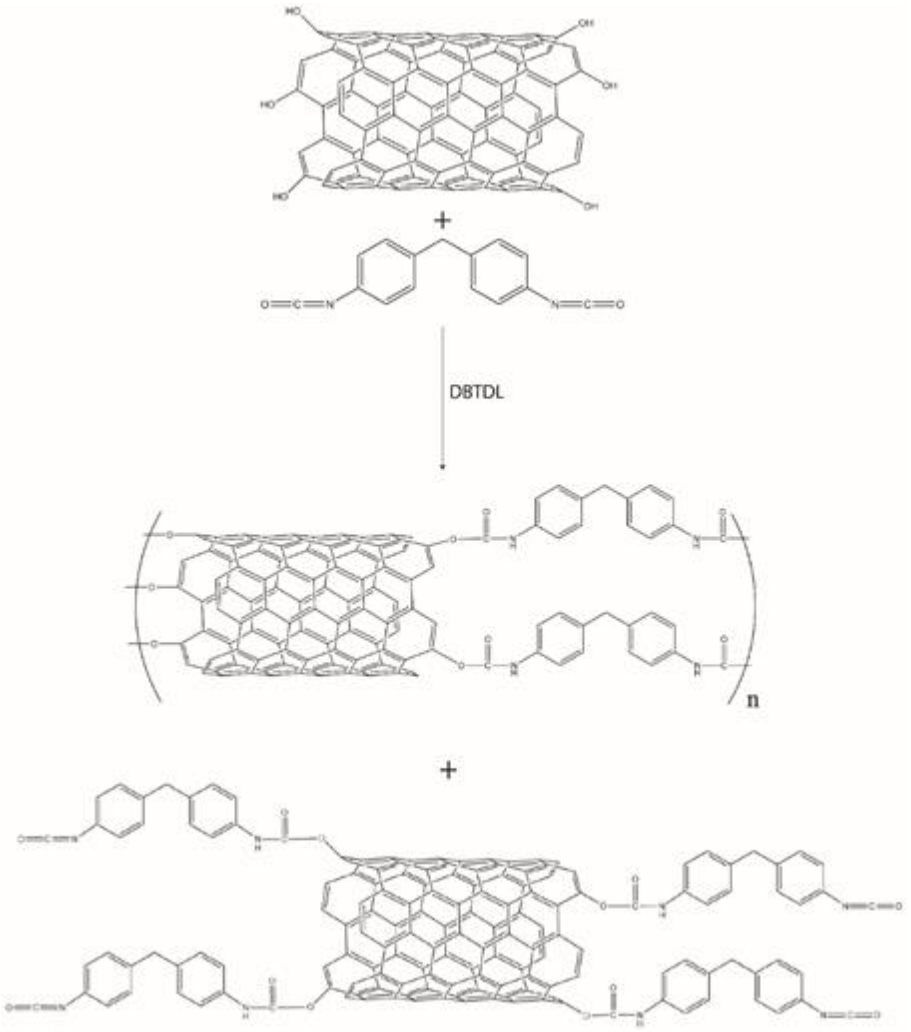

Figure 3: Chemical reactions for modification route 3: Simplified reaction scheme of CNT-OH with excess MDI, potentially forming pre-polymers or isocyanate-functionalized CNT's that can react further with cross linker (see bottom Figure 6).

The third route relates to the synthesis of polyurethane(PUR)-CNT. Here, hydroxyl functionalized CTNs are first reacted with an excess methylene diphenyl diisocyanate (MDI) in the presence of dibutyltin dilaurate (DBTDL) under water-free conditions in THF as solvent (step 1). The reaction is shown in Figure 3, where the possibility of formation of pre-polymer is already shown as well. It is likely that unreacted MDI will be present as well.

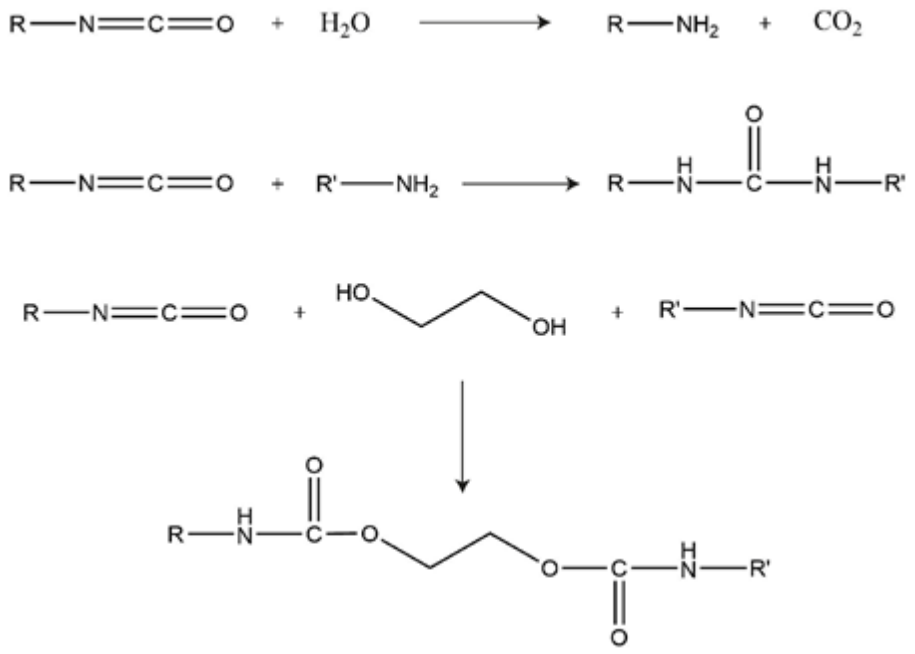

Figure 4: Extra reactions for isocyanate groups with step 1 reaction in Figure 5 with water, forming an amine group. Also shown the reaction of the said amine group with another isocyanate and the reaction of two isocyanate groups with ethylene glycol (cross linker) forming urethane links.

A cross linker (ethylene glycol) is added in a second phase with a small insufficiency (cf. Figure 4). This means that, at the end of the reaction of ethylene glycol with the isocyanates, there will still be isocyanates left to react. The ethylene glycol can react with the isocyanates, both free and coupled to the CNTs. A low average molar mass is still expected at this point since the stoichiometry is still off. As THF shows hygroscopic properties, it is expected that water will slowly enter the solvent [27]. The reaction product of water with isocyanate, an amine, can also react with isocyanate, meaning the crosslinking continues to form urea bridges, as illustrated in Figure 4. Under the premise that water enters the system slow enough, at a certain point, stoichiometric amounts of isocyanate and crosslinker (amine as a reaction

product of water and excess of isocyanate) are expected, allowing to achieve a high average molar mass.

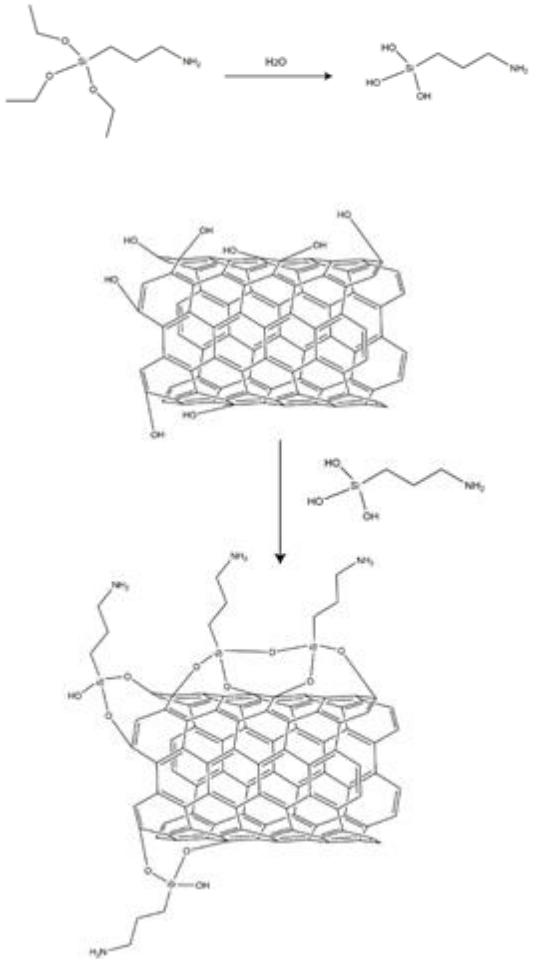

Figure 5: Activation of APTES by water thus hydrolysis; reaction of activated APTES with hydroxyl groups on the CNT. Notice that bridge formation between multiple APTES molecules is possible as well.

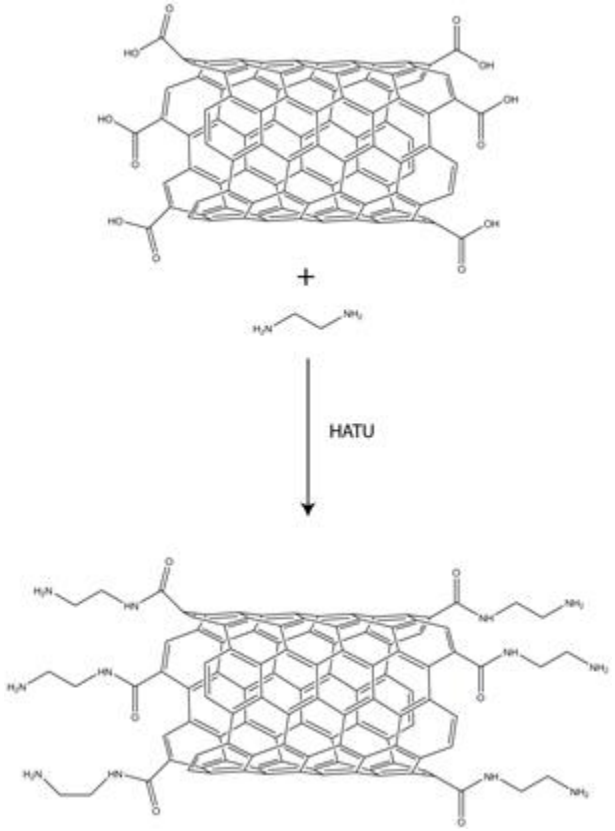

Figure 6: Alternative for Figure 7: reaction of ethylenediamine with carboxyl groups on the carbon nanotubes.

The fourth route aims at polyamide-CNT, where APTES is first linked to hydroxyl functionalized CNT's (Figure 5), or alternatively carbocyclic acid on CNTs is first reacted with diamines to form amide-bonds (Figure 6). The remaining amine-bonds are then reacted with a di-acryl chloride to form a second amide-bond, coupling two CNTs. This final step, as shown in Figure 7, takes place at the separation layer of two fluids, as seen in the popular nylon rope trick [28]. Water is used to disperse the amine-CNTs and hexane (or any other immiscible liquid) is used to dissolve sebacoyl chloride. By adding a few drops of NaOH to the water solution, the HCl molecules released by reaction of the sebacoyl chloride with the amine-functions are neutralized,

effectively making the reaction irreversible. Since the reaction only takes place at the contact surface between the water and the hexane phase, a perfect stoichiometric balance is not required. Sebacoyl chloride was chosen over reactants with shorter carbon chains, as longer carbon chains decrease the reactivity of the chloric acid with water.

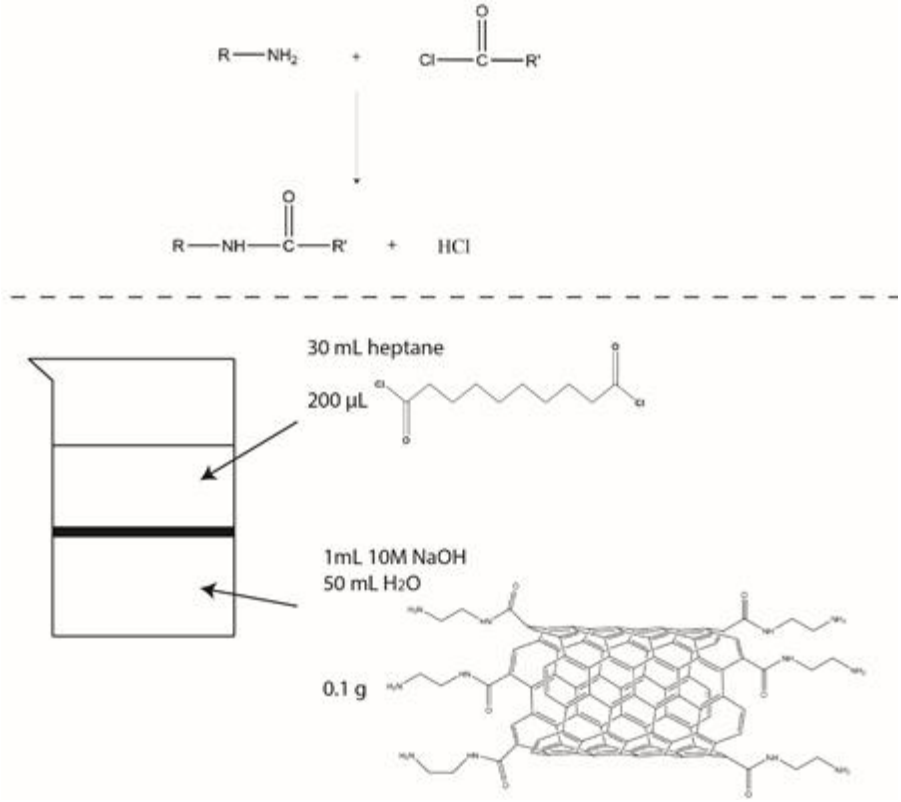

Figure 7: Final step for the CNT-polyamide synthesis, adjusted from 'the nylon rope trick'. Chemical principle at top of figure.

B. 2 Deviations from ideal network formation

It should be stressed that in any modification route different actual executions of the reaction are possible, as visualized in Figure 8 with the polyamide as example. Reactions can take place in a linear fashion, creating long chains with entanglement-possibilities. A reaction with two functional groups of the same carbon nanotube can (partially) eliminate a CNT from polymerizing. This type of reaction is undesired. At last, different groups on a single nanotube can react with multiple nanotubes. This can lead to branching, if other nanotubes keep reacting linearly, or the formation of a 3D network, like thermosetting polymers. It is expected that all three types of reactions will occur during the synthesis.

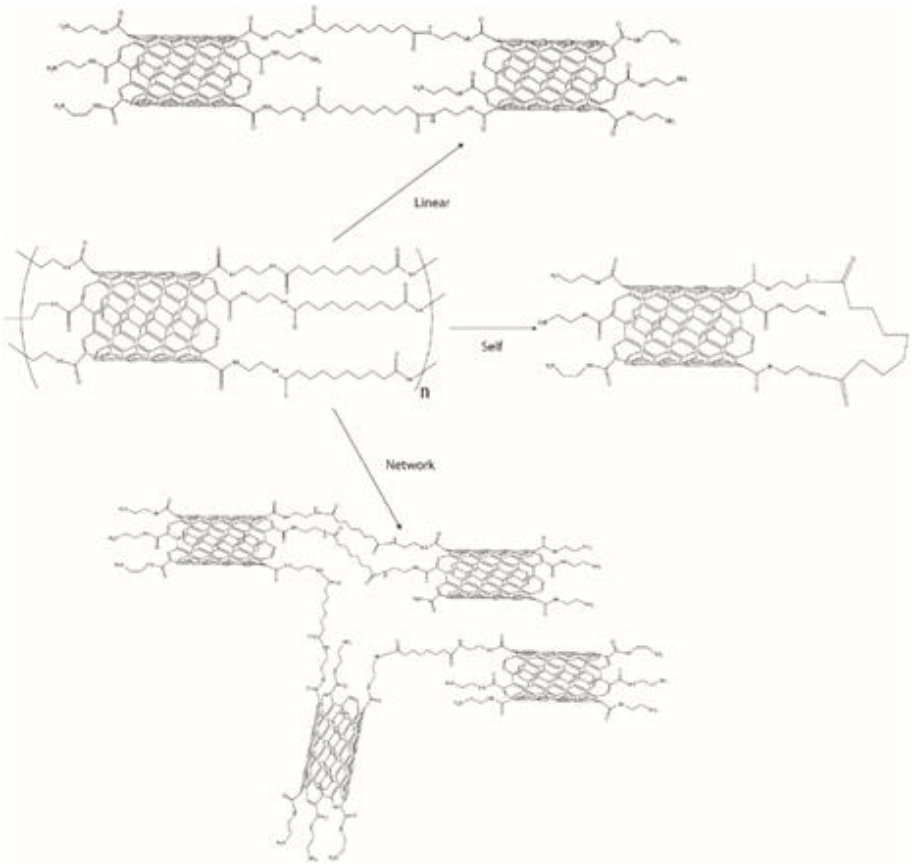

Figure 8: Different ways of linkage of CTNs based on a given chemistry (here example with polyamide).

REFERENCES

[1] R. H. Baughman, A. A. Zakhidov, and W. A. de Heer, "Carbon nanotubes - the route toward applications," *Science (80-.).*, vol. 297, no. 5582, pp. 787–792, Aug. 2002.

[2] M. F. L. De Volder, S. H. Tawfick, R. H. Baughman, and A. J. Hart, "Carbon Nanotubes: Present and Future Commercial Applications," *Science (80-.).*, vol. 339, no. 6119, pp. 535–539, Feb. 2013.

[3] L. Qu, Y. Liu, J.-B. Baek, and L. Dai, "Nitrogen-Doped Graphene as Efficient Metal-Free Electrocatalyst for Oxygen Reduction in Fuel Cells," *ACS Nano*, vol. 4, no. 3, pp. 1321–1326, 2010.

[4] G. L. Che, B. B. Lakshmi, E. R. Fisher, and C. R. Martin, "Carbon nanotubule membranes for electrochemical energy storage and production," *Nature*, vol. 393, no. 6683, pp. 346–349, 1998.

[5] P. Serp, M. Corrias, and P. Kalck, "Carbon nanotubes and nanofibers in catalysis," *Appl. Catal. A-GENERAL*, vol. 253, no. 2, pp. 337–358, 2003.

[6] Z. Liu, S. Tabakman, K. Welsher, and H. Dai, "Carbon Nanotubes in Biology and Medicine: In vitro and in vivo Detection, Imaging and Drug Delivery," *NANO Res.*, vol. 2, no. 2, pp. 85–120, Feb. 2009.

[7] N. Karousis, N. Tagmatarchis, and D. Tasis, "Current progress on the chemical modification of carbon nanotubes," *Chem. Rev.*, vol. 110, no. 9, pp. 5366–5397, 2010.

[8] N. Souza, M. Zeiger, V. Presser, and F. Muecklich, "In situ tracking of defect healing and purification of single-wall carbon nanotubes with laser radiation by time-resolved Raman spectroscopy," *RSC Adv.*, vol. 5, no. 76, pp. 62149–62159, 2015.

[9] E. C. Neyts, K. Ostrikov, Z. J. Han, S. Kumar, A. C. T. van Duin, and A. Bogaerts, "Defect Healing and Enhanced Nucleation of Carbon Nanotubes by Low-Energy Ion Bombardment," *Phys. Rev. Lett.*, vol. 110, no. 6, Feb. 2013.

[10] T. Palucka, "Nano Focus Defects in carbon nanotubes heal themselves under the right conditions," *MRS Bull.*, vol. 37, no. 8, p. 712, Aug. 2012.

[11] V. Datsyuk *et al.*, "Chemical oxidation of multiwalled carbon nanotubes," *Carbon N. Y.*, vol. 46, no. 6, pp. 833–840, 2008.

[12] T. A. Saleh, "The influence of treatment temperature on the acidity of MWCNT oxidized by HNO3 or a mixture of HNO3/H2SO4," *Appl. Surf. Sci.*, vol. 257, no. 17, pp. 7746–7751, 2011.

[13] S. Liang, G. Li, and R. Tian, "Multi-walled carbon nanotubes functionalized with a ultrahigh fraction of carboxyl and hydroxyl groups by ultrasound-assisted oxidation," *J. Mater. Sci.*, vol. 51, no. 7, pp. 3513–3524, Apr. 2016.

[14] R. Das, M. Ali, S. B. Abd Hamid, M. S. Annuar, and S. Ramakrishna, "Common Wet Chemical Agents for Purifying Multiwalled Carbon Nanotubes," *J. Nanomater.*, vol. 2014, pp. 1–9, 2014.

[15] J. Zhang *et al.*, "Effect of chemical oxidation on the structure of single-walled carbon nanotubes," *J. Phys. Chem. B*, vol. 107, no. 16, pp. 3712–3718, 2003.

[16] F. Avilés, J. V. Cauich-Rodríguez, L. Moo-Tah, A. May-Pat, and R. Vargas-Coronado, "Evaluation of mild acid oxidation treatments for MWCNT functionalization," *Carbon N. Y.*, vol. 47, no. 13, pp. 2970–2975, 2009.

[17] X. L. Ling, Y. Z. Wei, L. M. Zou, and S. Xu, "Preparation and characterization of hydroxylated multi-walled carbon nanotubes," *Colloids Surfaces A Physicochem. Eng. Asp.*, vol. 421, pp. 9–15, 2013.

[18] R. H. Bradley *et al.*, "Surface studies of hydroxylated multi-wall carbon nanotubes," *Appl. Surf. Sci.*, vol. 258, no. 11, pp. 4835–4843, 2012.

[19] W. Li *et al.*, "Effect of hydroxyl radical on the structure of multi-walled carbon nanotubes," *Synth. Met.*, vol. 155, no. 3, pp. 509–515, 2005.
[20] N. G. Sahoo, S. Rana, J. W. Cho, L. Li, and S. H. Chan, "Polymer nanocomposites based on functionalized carbon nanotubes," *Prog. Polym. Sci.*, vol. 35, no. 7, pp. 837–867, Jul. 2010.
[21] Q. Cheng, S. Debnath, E. Gregan, and H. J. Byrne, "Ultrasound-Assisted SWNTs Dispersion: Effects of Sonication Parameters and Solvent Properties," *J. Phys. Chem. C*, vol. 114, no. 19, pp. 8821–8827, 2010.
[22] L. Y. Jun, N. M. Mubarak, L. S. Yon, C. H. Bing, M. Khalid, and E. C. Abdullah, "Comparative study of acid functionalization of carbon nanotube via ultrasonic and reflux mechanism," *J. Environ. Chem. Eng.*, vol. 6, no. 5, pp. 5889–5896, 2018.
[23] K. J. Ziegler *et al.*, "Cutting single-walled carbon nanotubes," *Nanotechnology*, vol. 16, no. 7, 2005.
[24] K. J. Ziegler, Z. N. Gu, H. Q. Peng, E. L. Flor, R. H. Hauge, and R. E. Smalley, "Controlled oxidative cutting of single-walled carbon nanotubes," *J. Am. Chem. Soc.*, vol. 127, no. 5, pp. 1541–1547, Feb. 2005.
[25] J. Li and Y. Zhang, "Cutting of multi walled carbon nanotubes," *Appl. Surf. Sci.*, vol. 252, no. 8, pp. 2944–2948, 2006.
[26] J. Asua, *Polymer Reaction Engineering*. Wiley, 2007.
[27] "Drying of Solvents." [Online]. Available: http://www.chem.ucla.edu/~bacher/General/30BL/tips/dryingofsolvents.html.
[28] P. W. Morgan and S. L. Kwolek, "The nylon rope trick: Demonstration of condensation polymerization," *J. Chem. Educ.*, vol. 36, no. 4, p. 182, 1959.